The Graduate University for Advanced Studies

Doctoral Thesis

Comparative study of various probes of CP violation in the Higgs sector

---

Author:
Kai Ma

Supervisor:
Prof. Kaoru Hagiwara

A thesis submitted in fulfilment of the requirements
for the degree of Doctor of Philosophy

in the

KEK Theory Center
Department of Particle and Nuclear Physics
School of High Energy Accelerator Science

December 2015

Contents

Declaration of Authorship

I, Kai Ma, declare that this thesis titled, 'The Graduate University for Advanced Studies' and the work presented in it are my own. I confirm that:

- This work was done wholly or mainly while in candidature for a research degree at this University.
- Where any part of this thesis has previously been submitted for a degree or any other qualification at this University or any other institution, this has been clearly stated.
- Where I have consulted the published work of others, this is always clearly attributed.
- Where I have quoted from the work of others, the source is always given. With the exception of such quotations, this thesis is entirely my own work.
- I have acknowledged all main sources of help.
- Where the thesis is based on work done by myself jointly with others, I have made clear exactly what was done by others and what I have contributed myself.

Signed: Kai Ma

Date: Dec. 17. 2015

The Graduate University for Advanced Studies (Sokendai)

Abstract

KEK Theory Center
Department of Particle and Nuclear Physics
School of High Energy Accelerator Science

Doctor of Philosophy

The Graduate University for Advanced Studies

by Kai Ma

Higgs particle is one of the most important ingredients of the Standard Model. It breaks the electroweak vacuum, and generates the mass of both electroweak bosons and matter particles. A similar scalar particle possessing these physical properties has been observed at about 125GeV by both ATLAS and CMS collaborations at CERN in 2012. However, it has not been so clear that whether the observed particle $h(125)$ is the Higgs boson of Standard Model, or the model needs some extensions. So further investigations on the physical properties of $h(125)$ are crucial for the understanding of physics.

CP symmetry of the $h(125)$ is one of the most important properties that has not been understood well. While only one scalar particle is predicted in the Standard Model, many of its extensions not only modify the Higgs couplings to electroweak bosons and fermions, but additional scalars and pseudo-scalars are also predicted. So CP violation effects could be appear naturally through the mixing among these particles. Even through the experimental results disfavor a pure CP odd particle at about 3σ level, large mixing is still allowed in general. In this thesis we study the CP violation effects in the Higgs sector.

There are many channels in which the CP violation effects could appear. In the process of Higgs decaying into two vector bosons, either Z or photon, the CP violation effects appear in the azimuthal angle correlations. This correlation could be measured by observing the leptons from the subsequent decay of these two gauge bosons. However, the leptons are highly boosted because of the large mass of Higgs, so resolving the correlation in the transverse plane is still challenging, particularly for the electrons coming from the photon conversion. Similar correlation appears in the production channels via the vector bosons fusion. In this case the CP violation effects could be measured by analyzing the tagged jets or leptons in the final states. The main problem is the huge

QCD backgrounds which can completely wash out this correlation. However, by using matching technique, the QCD backgrounds could be well predicted and then significantly enhance the experimental sensitivity.

We investigate CP violation effect in the Higgs sector via $h \to 4l$ channels at the LHC14. Measuring CP violation effect through $h \to ZZ^* \to 4l$ process is completely impossible because of the dominant CP even contributions. In contrast, CP even and odd contributions are at the same level in both $h \to Z\gamma \to 4l$ and $h \to \gamma\gamma \to 4l$ decay channels. In this paper we study to which level the CP violation effect in the spin correlation of final states could be measured via this two processes at the LHC. The polarization of photons from Higgs decay could be measured through the photon conversion and internal splitting processes. However we find the conversion process is completely useless unless the experimental precision could be improved by a factor of 4. On the other hand the internal splitting channels provide a hope even through it is still challenging.

On the other hand, the CP violation effects could be observed in the interactions between the Higgs and fermions, for instances $h \to \tau^+\tau^-$, and $t\bar{t}$ production in associated with a Higgs. In the $h \to \tau^+\tau^-$ channel, observing the CP violation effects is challenging because the neutrinos carry away lots of kinematical informations. However, it is still promising because of the large decay length of τ, by which the decay vertex and impact parameter could be employed to reconstruct the full kinematics. We use the impact parameter and density function of missing transverse energy as well as the density function of the distance between the neutrinos and visible taus decay products to reconstruct the full kinematics event by event. The most likely configuration is obtained by scanning the taus momentums. Within the present experimental resolution, we find very good collinearity between the reconstructed and true kinematics. The experimental sensitivity of is expected to be 0.1 at LHC14 with an integrated luminosity $3\,\mathrm{ab}^{-1}$.

In the $t\bar{t}$ production in associated with a Higgs at the ILC with $\sqrt{s} = 500\mathrm{GeV}$, under the approximation that the production vertex of Higgs and toponia is contact, and neglecting the P-wave toponia, we analytically calculated the density matrix. We find that the production rate of singlet toponium is highly suppressed, which behaves just like the production of a P-wave toponia. This is because in the singlet case the Higgs can not affect anything except for carrying away some energy, and also the specialty of near threshold region. In case of triplet toponium, the CP property of Higgs can affect the physics significantly. This is because the S-wave triplet toponium can contribute even in the pseudo-scalar case, even through the contribution is still small. Three completely independent CP observables, azimuthal angles of lepton and anti-leptons in the toponium rest frame as well as their sum, are predicted based on our analytical results, and checked by using the tree-level event generator. The nontrivial correlations

come from the longitudinal-transverse interference for azimuthal angles of leptons, and transverse-transverse interference for their sum. The azimuthal angle correlation of lepton is related to the azimuthal angle correlation of anti-lepton by CP transformation. Most importantly, the interferences between the transverse and longitudinal component require only either lepton or anti-lepton to be reconstructed. Therefore the number of signal events can be enhanced significantly. These three observables are well defined at the ILC, because the rest frame of toponium can be reconstructed directly. Furthermore, the QCD-strong corrections, which are important at the near threshold region, are also studied with the approximation of spin-independent QCD-Coulomb potential.

Acknowledgements

First and foremost I want to thank my supervisor Kaoru Hagiwara. It has been an honor to be his last Ph.D. student. He has taught me, both consciously and unconsciously, how good elementary particle physics is done, particularly the connection between theories and experiments that is very important for young researcher to be a real physicist. I appreciate all his contributions of time, ideas, and fundings to make my Ph.D. experience productive and stimulating. The joy and enthusiasm he has for his own research was contagious and motivational for me, even during tough times in my Ph.D. pursuit.

The members of the KEK theory center have contributed immensely to my personal and professional time at KEK. The group has been a source of friendships as well as good advices and collaboration. I also would like to acknowledge my friend Satyanarayan Mukhopadhyay who is a postdoc at IPMU. We worked together on an MSSM Dark Matter project. I am very much moved by his enthusiastic explanation of Dark Matter physics, as well as by his intensity, willingness to do the analysis and writing the paper. I also would like to acknowledge my senior Junya Nakamura, and my junior Shingo Mori. We worked together and learned much from them. I would like to acknowledge Prof. Osamu Jinnouchi, from whom I learned details about the ATLAS detector. I would like to acknowledge Dr. Hiroshi Yokoya. We worked together on the toponia project, and I learned much from him on physics of top-anti-top production at electron-positron collider. My time at KEK was made enjoyable in large part due to the many friends that became a part of my life. I am grateful for the time I spent with friends at KEK.

For this dissertation I would like to thank my referees: Keisuke Fujii, Osamu Jinnouchi, Kaoru Hagiwara, Ryuichiro Kitano, Mihoko Nojiri, and Yutaka Sakamura for their time, interest, and helpful comments.

I gratefully acknowledge the China Scholarship Council for the financial support that made my Ph.D. work possible. My work was also supported partially by the Hanjiang Scholar Project of Shaanxi University of Technology, and I am honored to be a Younger Hanjiang Scholar of Shaanxi University of Technology.

Lastly but not least, I would like to thank my family for all their love and encouragement, and to my parents who raised me with a love of science and supported me in all my pursuits.

Kai Ma
KEK Theory Center and Sokendai
August 2015

List of Figures

List of Tables

Chapter 1

Introduction

Symmetry, in the early days of sciences, was just a language of interpretation in the study of simple geometric objects. It has only been last century that the importance of symmetry in complex physical systems was gradually being realized since the pioneering work of Wigner and others in atom and nuclear physics. Now days, almost everybody believe that symmetries are so fundamental that all lows of nature are originate in symmetries. Noether proved that every continuous symmetry implies a conserved quantity[1]. The most powerful theory, Electrodynamics, was found to be a result of (continuous) local gauge symmetry[2]. The profound extrapolation of abelian gauge symmetry by Yang and Mills[3], which was initially treated as a just formal product, was realized in a latter time playing essential role in both weak and strong interactions. Discrete symmetry was also never hanged out. It dominates the structure of crystal. Bose-Einstein and Fermi-Dirac statistics, which are the footstones of modern particle physics, are governed by the permutation symmetries.

Nevertheless, just as people were immersed in the beauty of the symmetry, the came symmetry breaking, shocked everyone. The Cooper electron pair[4–6], which can explain the superconductivity in low temperature, was found to be a result of the spontaneous symmetry breaking of local gauge symmetry. Its generalization in the context of quantum field theory, which is called Higgs mechanism[7–9], has been proved to be the most profound discovery in elementary particle physics. The parity symmetry, which is discrete, is also broken in weak interactions[10, 11]. It was also found that, the classical conservation low from Embedding discrete symmetries into local gauge theories, can be broken at the quantum level[12]. Even through more realistic is the symmetry breaking as it should since we can distinguish one thing from another, nobody ever before recognized that it can have so profound and lasting influences. Now days, nobody talks symmetry without mentioning symmetry breaking. To which degree the symmetry is broken becomes the fundamental question of physics.

Charge conjugate C, parity P, time reversal T symmetries are three of the most fundamental and relevant ones. Among their combinations, CP occupy a very unique place in elementary particle physics. Apart from the CP violation in the Kaon system (and other hadron systems), we have learnt that our universe also breaks the CP symmetry[14]. On the other hand, talking about C alone is somehow ambiguous because the particle moving forward is equivalent to its anti-particle moving backward. Therefore we could not unambiguously distinguish the particle from anti-particle as long as CP is conserved which breaks this equivalency.

On the other hand, the relativistic quantum field theory is naturally CPT invariant[15]. Therefore CP violation implies the breaking of time reversal symmetry. Furthermore, the time reversal symmetry T in the context of quantum mechanics is an anti-Hermite operator which transforms numbers into their complex conjugates. Therefore breaking of T or CP must be related to some complex parameters in the model. According to the principles of quantum mechanics, any observable in a quantum process, for instance the transition probability, is invariant under a global phase rotation on the transition amplitudes. Therefore only the relative phase among different transition amplitudes can affect the measurements, which is called quantum interference in general. This is similar to the classical phenomena of Young's double-slit interference where the two slits generate two different path (mimic to different quantum amplitudes) to the detector.

There are three kinds of relative phases that can arise in the quantum amplitudes: 1) strong phase, that is defined to be one which has same signs in the transition amplitude for a quantum process and in the transition amplitude for its CP conjugate quantum process; 2) weak phase, that has the same sign in the transition amplitudes for the two CP conjugated quantum processes; 3) spurious phase, which are purely conventional relative phases between an amplitude and the amplitude for CP conjugate process. They just come from the assumed CP transformation of the related quantum states and field operators, and usually are related the some kinematical variables.

The strong, weak phase and spurious phases (here and below we always talk about relative phase) can affect the quantum measurements in different ways. The spurious phase can always be measured because it is related to the kinematical variables that are measured directly. This is not true for the strong and weak phases. Without loss of generality, we assume there are two transition amplitudes, which is the minimal condition to observe quantum interference. Let i and f are the initial and final quantum states, and $\mathcal{M}_1(i \to f)$ and $\mathcal{M}_2(i \to f)$ are the two amplitudes which cause the transition $i \to f$. According to the principles of quantum mechanics, the total transition amplitude is the sum of these two,

$$\mathcal{M}(i \to f) = \mathcal{M}_1(i \to f) + \mathcal{M}_2(i \to f)\,. \tag{1.1}$$

Then the total transition probability is

$$\begin{aligned} P(i \to f) &\propto |\mathcal{M}(i \to f)|^2 \\ = \sum_{k=1,2} &|\mathcal{M}_k(i \to f)|^2 + 2|\mathcal{M}_1(i \to f)||\mathcal{M}_2(i \to f)|\cos(\xi_1 - \xi_2 + \delta_1 - \delta_2)\,, \end{aligned} \tag{1.2}$$

where ξ_k and δ_k are the weak and strong phases of the two transition amplitudes. On the other hand, the conjugated filed operators can cause quantum transition $\bar{i} \to \bar{f}$ with a transition probability

$$\begin{aligned} P(\bar{i} \to \bar{f}) &\propto |\mathcal{M}(\bar{i} \to \bar{f})|^2 \\ = \sum_{k=1,2} &|\mathcal{M}_k(\bar{i} \to \bar{f})|^2 + 2|\mathcal{M}_1(\bar{i} \to \bar{f})||\mathcal{M}_2(\bar{i} \to \bar{f})|\cos(-\xi_1 + \delta_1 + \xi_2 - \delta_2)\,. \end{aligned} \tag{1.3}$$

Then the CP asymmetry is given by

$$\frac{P(i \to f) - P(\bar{i} \to \bar{f})}{P(i \to f) + P(\bar{i} \to \bar{f})} = \frac{2|\mathcal{M}_1||\mathcal{M}_2|\sin(\xi_1 - \xi_2)\sin(\delta_1 - \delta_2)}{|\mathcal{M}_1|^2 + |\mathcal{M}_2|^2 + 2|\mathcal{M}_1||\mathcal{M}_2|\cos(\xi_1 - \xi_2)\cos(\delta_1 - \delta_2)}\,. \tag{1.4}$$

Therefore in the case of we are measuring only the total transition rate, observing either one of them requires another one must be non-zero. On the other hand, if we can relate the strong/weak phase to a certain spurious phase which has to a CP-even/odd, then the strong/weak phase can be observed by investigating the distribution of the transition rate with respect to the corresponding kinematical observable of this spurious phase.

Chapter 2

Probing CP violation in $h \to (\ell\bar{\ell})(\ell'\bar{\ell}')$ at the LHC

The $h \to VV' \to 4\ell$ channels, which are called the golden channels, are promising to measuring the CP violation. The $V \to \ell\bar{\ell}$ transition can happen via the internal splitting, and photon conversion if $V = \gamma$. In Ref. [23], a maximum likelihood analysis on the $h \to VV' \to 4\ell$ was performed for the internal splitting processes. By assuming an overall uniform efficiency 60%, they found the golden channel has the potential to probe both the CP nature as well as the overall sign of the Higgs coupling to photons well before the end of high-luminosity LHC running. However, the most important effects because of the experimental angular resolution, particularly for the internal splitting process of virtual photon, were not analyzed carefully. For the photon conversion process, the CP sensitivity was analyzed with the assumption that Higgs is at rest in the lab frame in Ref. [36].

We study sensitivity of the $h(125) \to 4\ell$ decay distributions to the CP-odd component of the Higgs boson in various kinematical configurations. The dominant $h \to ZZ^\star \to 4\ell$ process are found to be least sensitive because of the overwhelmingly large tree-level CP-even amplitudes. Since both CP-even and -odd amplitudes appear in the one-loop order for the $h \to Z\gamma$ and $h \to \gamma\gamma$ decay channels, we examine carefully the kinematical region where one or both pair of $\ell\bar{\ell}$ is near the photon mass shell, in particular the $\gamma \to e^+e^-$ conversion process. For the photon conversion process, we include the non-trivial p_T and η distribution of the Higgs by convoluting the production rate and BH conversion probability in the p_T and η plane (because of the symmetry of detector, the azimuthal angle direction is trivial and have been integrated). Once typical angular resolution of e^+e^- in the LHC detectors is taken into account, the conversion processes are strongly suppressed and found to be useless unless the experimental angular resolution can be improved by a factor of 4. Without takeing into account of the background, we find the experimental sensitivity is about $\Delta\xi_{h\gamma\gamma} = 0.33$ for $pp \to \gamma^*\gamma^* \to 4\ell$, and $\Delta\xi_{hZ\gamma} = 0.25$ for $pp \to Z\gamma^* \to 4\ell$, with an integrated luminosity $3\,\mathrm{ab}^{-1}$.

2.1 CP violation in the di-vector bosons decay of Higgs

Both the ATLAS and CMS have studied the CP property of the new scalar boson in the $h \to ZZ^\star$ decay channel[19–21], and the pure pseudo-scalar assumption is disfavored at more than 3σ. However, if the mass eigenstate $h(125)$ does not have a definite CP, the fraction of its CP-odd component is not constrained effectively effectively because of the smallness of the CP-odd coupling to Z pair, which is loop suppressed, as compared to the CP-even coupling that appear in the tree-level. In this section we first give our parameterization of the couplings and the mixing parameters, and then discuss how to measure the CP violation effects appearing in the $h \to 4\ell$ decay channels.

2.1.1 Parameterization

There is a wide variety of BSMs that could lead to relatively large CP violation in the Higgs sector, such as the Type-I and Type-II 2HDMs, the MSSM and its extensions with or without R-parity violation. In models with two Higgs doublets, we have three neutral real scalar bosons, two of which have CP-even and one CP-odd couplings to quarks and leptons. The observed boson $h(125)$ can be a mixture of the CP-even and CP-odd states in the presence of CP violation, which can be significant in models with CP violating Higgs potential in the tree-level or through large radiative effects.

Motived by the observation that the $h(125)$ couplings do not deviate much from the SM predictions, we introduce the following simple parameterization of the Higgs mixing,

$$h = \frac{1}{\sqrt{1+|\epsilon|^2}}(H + \epsilon A), \tag{2.1}$$

where H has the CP-even couplings to the weak bosons and the fermions, just like the SM Higgs boson, and A has the CP-odd couplings to quarks and leptons. This is an approximation in generic two Higgs doublet models, where $h(125)$ is a mixture of three real scalars, H, H', A:

$$h = U_{hH}H + U_{hH'}H' + U_{hA}A\,. \tag{2.2}$$

In the current basis, where H has the SM Higgs boson couplings, the state H' has no tree-level couplings to quarks, leptons and weak bosons. We therefore find that all the results for CP-odd observables presented in this paper are valid in generic 2HDM's with the identification

$$\epsilon = \frac{U_{hA}}{U_{hH}} \tag{2.3}$$

whereas the normalization of the couplings should be replaced by the parameter

$$\frac{1}{\sqrt{1+|\epsilon|^2}} \to |U_{hH}| \tag{2.4}$$

We nevertheless adopt a single parameterization Eq. (2.1), since it allows us to parametrize the CP-violating effects in the Higgs mixing by a single complex parameter ϵ, just like in the neutral K system.

By including the mixing Eq. (2.1), the effective Lagrangian relevant for the $h \to 4\ell$ process can be expressed as

$$\begin{aligned}-\mathcal{L} \;=\; h\Bigg\{ & \frac{m_Z^2}{2v\sqrt{1+|\epsilon|^2}}Z^\mu Z_\mu + \bar{g}_{hZ\gamma}\frac{\alpha}{4\pi v}Z^{\mu\nu}F_{\mu\nu} + \bar{\epsilon}_{hZ\gamma}\frac{\alpha}{4\pi v}Z^{\mu\nu}\widetilde{F}_{\mu\nu} \\ & + \bar{g}_{h\gamma\gamma}\frac{\alpha}{8\pi v}F^{\mu\nu}F_{\mu\nu} + \bar{\epsilon}_{h\gamma\gamma}\frac{\alpha}{8\pi v}F^{\mu\nu}\widetilde{F}_{\mu\nu}\Bigg\}\,.\end{aligned} \tag{2.5}$$

where $v = 256\text{GeV}$ is the vacuum expectation value of the SM Higgs boson (H), and

$$\bar{g}_{hVV'} = \frac{g_{HVV'}}{\sqrt{1+|\epsilon|^2}} \quad , \quad \bar{\epsilon}_{hVV'} = \frac{\epsilon g_{AVV'}}{\sqrt{1+|\epsilon|^2}}\,. \tag{2.6}$$

Here the couplings $\bar{g}_{hVV'}$ and $\bar{\epsilon}_{hVV'}$ are typically induced in the one-loop order for $VV' = \gamma\gamma$ and $Z\gamma$, and we normalized to the factor $\alpha/(4\pi)$. Note that we do not examine the CP-odd operator for the ZZ channel,

$$\bar{\epsilon}_{hZZ} = \frac{\alpha}{8\pi v}Z^{\mu\nu}\widetilde{Z}_{\mu\nu}\,, \tag{2.7}$$

since it is obvious that the tree-level mediated $h \to ZZ$ channel has little sensitivity to the loop induced physics. In the $\gamma\gamma$ and $Z\gamma$ channels, on the other hand, both the CP-even and CP-odd interactions are mediated in the loop-level, and there is a possibility that the CP-even and CP-odd amplitudes have the same order of magnitudes, which is a necessary condition to observe CP violation in the $h(125)$ couplings, even if it has a significant mixture of CP-odd component.

All the measurements of the $h(125)$ couplings are so far consistent with the predictions of the SM Higgs boson, and in particular the $h\gamma\gamma$ (hZZ and hWW) coupling strength are even constrained as $\mu_{hVV} = 1.04 \pm 0.13$ [29]. In the effective Lagrangian Eq. (2.5), this implies the constraint

$$\frac{1}{\sqrt{1+|\epsilon|^2}} = 1.04 \pm 0.13\,, \tag{2.8}$$

which implies $|\epsilon| < 0.7$ at the 95% CL. Although the allowed region of $|\epsilon|$ depends on our assumptions, we note here that relatively large mixture of CP-odd component in $h(125)$ is not ruled out by the present measurements, and that there is still a possibility of discovering CP violation in the h coupling.

2.1.2 CP observables

It has been well know that the CP property of the two photon (or two transversely polarized vector boson) system in zero angular momentum (J=0) can be studied by suing their spin correlation, which can *e.g.* be measured through the vector boson decay (or conversion) into a lepton pair. Historically, the pseudo-scalar nature of π^0 meson was established by the e^+e^- plane correlation in the leptonic conversion process.

The helicity amplitude for the decay process $h \to Z\gamma$ ($h \to \gamma\gamma$) is (hear and after we will suppress an overall factor $\alpha/(2\pi v)$)

$$\mathcal{M}^{\lambda_1\lambda_2} = \bar{g}_{hVV'}[(k_1\cdot\varepsilon_2^*)(k_2\cdot\varepsilon_1^*) - (k_1\cdot k_2)(\varepsilon_1^*\cdot\varepsilon_2^*)] + \bar{\epsilon}_{hVV'}\epsilon^{\mu\nu\alpha\beta}k_{1\mu}k_{2\nu}\varepsilon^*_{1\alpha}\varepsilon^*_{2\beta}\ , \tag{2.9}$$

where $k^\mu_{1,2}$ and $\varepsilon^\alpha_{1,2}$ are the momenta and polarization vector of the two vector bosons, see Fig. 2.1. We observe that the CP even interaction makes the polarization vectors of the two vector boson parallel, while the CP odd interaction makes them perpendicular to each other. So in order to observe the CP violation effects, coherent superposition of the two transverse polarization states is necessary.

In the $h(125)$ rest frame we choose the VV' momentum directions along the z-axis,

$$k_1 = \frac{1}{2}m_h\left(1+\frac{s_1-s_2}{m_h^2},\, 0,\, 0,\, \beta\right), \tag{2.10a}$$

$$k_2 = \frac{1}{2}m_h\left(1-\frac{s_1-s_2}{m_h^2},\, 0,\, 0,\, -\beta\right), \tag{2.10b}$$

$$\beta = \left(1+\frac{(s_1-s_2)^2}{m_h^4}-\frac{2(s_1+s_2)}{m_h^2}\right)^{1/2}, \tag{2.10c}$$

where $\sqrt{s_1} = \sqrt{k_1^2}$ and $\sqrt{s_2} = \sqrt{k_2^2}$ are the virtual mass of the two photons that are measured by the invariant mass of the lepton pair. The polarization vectors are

$$\varepsilon_1^{\mu}(k_1,\lambda_1) = \frac{1}{\sqrt{2}}(0,\, -\lambda_1,\, -i,\, 0)\,, \tag{2.11a}$$

$$\varepsilon_2^{\mu}(k_2,\lambda_2) = \frac{1}{\sqrt{2}}(0,\, \lambda_2,\, -i,\, 0)\,. \tag{2.11b}$$

For definition, we define $s_2 > s_1$, for both $Z\gamma$ ($k_2^2 = m_Z^2 \gg k_1^2$) and $\gamma\gamma(k_2^2 \gg k_1^2)$. The helicity amplitude of Eq. (2.9) are then

$$\mathcal{M}^{\pm\pm} = -(k_1\cdot k_2)\bar{g}_{hVV'} \pm \frac{i}{2}m_h^2\beta\bar{\epsilon}_{hVV'}\,. \tag{2.12}$$

We find it is convenient to parameterize the amplitude in terms of the magnitudes, $g^{\pm}_{hVV'}$, and the phases, $\xi^{\pm}_{hVV'}$

$$\mathcal{M}^{\pm\pm} = -(k_1\cdot k_2)\cdot g^{\pm}_{hVV'}\cdot e^{\mp i\xi^{\pm}_{hVV'}}\,. \tag{2.13}$$

By noting that the effective couplings $\bar{g}_{hVV'}$ and $\bar{\epsilon}_{hVV'}$ in the Lagrangian Eq. (2.5) can have complex phase due to the loops of the light particles, such as τ-lepton and b-quark, we find

$$g^{\pm}_{hVV'} = \sqrt{|\bar{g}_{hVV'} \mp i\kappa\bar{\epsilon}_{hVV'}|^2}\,, \tag{2.14a}$$

$$\xi^{\pm}_{hVV'} = \arg\{\bar{g}_{hVV'} \mp i\kappa\bar{\epsilon}_{hVV'}\}\,, \tag{2.14b}$$

with

$$\kappa = \frac{m_h^2\beta}{2k_1\cdot k_2} = \sqrt{1-2\frac{s_1+s_2}{s}+\left(\frac{s_1-s_2}{s}\right)^2}\Big/\left(1-\frac{s_1+s_2}{s}\right). \tag{2.15}$$

In the limit when we can neglect the complex phase of $g_{HVV'}$ and $g_{AVV'}$, as well as in the CP mixing parameter ϵ, the magnitude and the phase of the helicity amplitude imply

$$g^{\pm}_{hVV'} = \sqrt{(\bar{g}_{hVV'})^2 + (\kappa\bar{\epsilon}_{hVV'})^2}\,, \tag{2.16a}$$

$$\xi^{\pm}_{hVV'} = \tan^{-1}\frac{\kappa\bar{\epsilon}_{hVV'}}{\bar{g}_{hVV'}} = \tan^{-1}\left(\frac{\kappa g_{AVV'}}{g_{HVV'}}\epsilon\right). \tag{2.16b}$$

In order to study CP violation effects in the spin correlation, without loss of generality, let us define the x-axis along the linear polarization direction of the second vector boson, and the first vector boson is also linearly polarized but with an azimuthal angle ϕ, the corresponding wave functions are

$$|V_2\rangle = |\hat{x}\rangle_2 = \frac{1}{\sqrt{2}}\big(|+\rangle_2 - |-\rangle_2\big)\ , \tag{2.17a}$$

$$|V_1\rangle = |\phi\rangle_1 = \frac{1}{\sqrt{2}}\big(e^{i\phi}|-\rangle_1 - e^{-i\phi}|+\rangle_1\big)\ . \tag{2.17b}$$

The amplitude of the transition from Higgs to these two photon state is

$$\mathcal{M} = \langle V_1 V_2|\mathcal{L}|h\rangle = \sum_{\lambda_1,\lambda_2=\pm1}\langle V_1V_2|\lambda_1\lambda_2\rangle\langle\lambda_1\lambda_2|\mathcal{L}|h\rangle \tag{2.18}$$

By inserting the helicity amplitudes Eq. (2.13) we get

$$\mathcal{M} = -\frac{1}{2}\Big\{e^{i\phi}\mathcal{M}^{++} + e^{-i\phi}\mathcal{M}^{--}\Big\} = -\frac{1}{2}(k_1\cdot k_2)\Big\{g^{+}_{hVV'}e^{i(\phi-\xi^{+}_{hVV'})} + g^{-}_{hVV'}e^{-i(\phi-\xi^{-}_{hVV'})}\Big\}\,. \tag{2.19}$$

Then the transition probability behaves like

$$|\mathcal{M}|^2 = (k_1\cdot k_2)\Big\{(g^{+}_{hVV'})^2 + (g^{-}_{hVV'})^2 + 2(g^{+}_{hVV'})(g^{-}_{hVV'})\cos(2\phi - \xi^{+}_{hVV'} - \xi^{-}_{hVV'})\Big\}\,. \tag{2.20}$$

The effect of CP odd operator is to rotate the polarization direction of the second photon from ϕ to $\phi - \Delta\phi$ with the phase shift

$$\Delta\phi = \frac{\xi^{+}_{hVV'} + \xi^{-}_{hVV'}}{2}\,. \tag{2.21}$$

Although in general the phases $\xi^{\pm}_{hVV'}$ depend on complex phases of the effective couplings $g_{HVV'}$ and $g_{AVV'}$, as well as of the mixing parameter ϵ, in the approximation above these couplings and the mixing parameters are real, we find

$$\Delta\phi = \tan^{-1}\left(\frac{\kappa g_{AVV'}}{g_{HVV'}}\epsilon\right), \tag{2.22}$$

according to eq.Eq. (2.16b). If we know the magnitudes and the signs of the effective couplings $g_{HVV'}$ and $g_{AVV'}$, then from the phase shift measurement we can determine both the magnitude and the sign of the mixing parameter ϵ, or that of $\mathrm{Re}\epsilon$ when $\mathrm{Im}\epsilon \ll \mathrm{Re}\epsilon$. In particular, if the state $h(125)$ is a pure pseudo-scalar, $|\epsilon| = \infty$, then $\Delta\phi = \pm\pi/2$ and the amplitude angular dependence reverses the sign

$$\cos(2(\phi - \Delta\phi)) = \cos(2\phi \mp \pi) = -\cos(2\phi)\,. \tag{2.23}$$

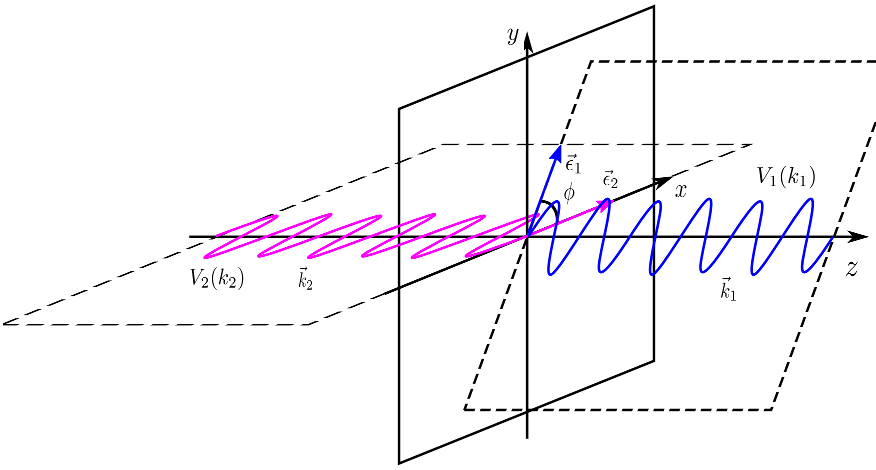

Figure 2.1: Definitions of the momenta and polarizations of the two vector bosons. Without loss of generality, the polarization vector of the first vector bosons (with larger virtual mass) is defined to lie on the $\hat{x}$ direction.

2.2 Helicity amplitudes of $h \to V_1V_2 \to (\ell_1\bar{\ell}_1)(\ell_2\bar{\ell}_2)$

In this section we study the spin correlation of photons via the internal splitting mechanism. Because both the kinematics and dynamics are very similar between $h \to V_1V_2 \to (\ell^+\ell^-)(\ell^+\ell^-)$ with $V_i = Z, \gamma$, we will give the helicity amplitude formulas generally. The kinematical variables are defined as follows (see also the Fig.2.2)

$$h(m_h) \;\to\; V_1(q_1,\lambda_1) + V_2(q_2,\lambda_2) \tag{2.24a}$$

$$\to\; \ell_1(p_1,\sigma_1) + \bar{\ell}_1(\bar{p}_1,\bar{\sigma}_1) + \ell_2(p_2,\sigma_2) + \bar{\ell}_2(\bar{p}_2,\bar{\sigma}_2), \tag{2.24b}$$

where $\ell_i, \bar{\ell}_i$ stand for leptons and anti-leptons, and the momentum and the helicity of

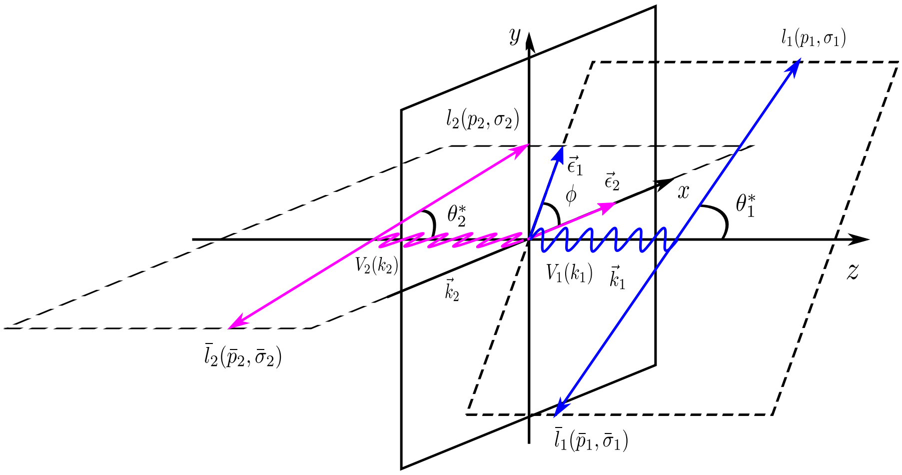

FIGURE 2.2: Definitions of the momenta and polarizations of the two vector bosons. Without loss of generality, the polarization vector of the first vector bosons (with heavy mass) is defined to lie on the $\hat{x}$ direction.

each particle are shown in parentheses. The lepton helicity take the values $\sigma_i/2$ with $\sigma_i = \pm 1$, while the helicity of the off-shell vector bosons take $\lambda_1 = \lambda_2 = \pm 1, 0$. The helicity amplitudes can generally be expressed as

$$\mathcal{M}(\sigma_1, \bar{\sigma}_1; \sigma_2, \bar{\sigma}_2) = J_{V_1}^{\mu_1}(p_1, \sigma_1; \bar{p}_1, \bar{\sigma}_1) J_{V_2}^{\mu_2}(p_2, \sigma_2; \bar{p}_2, \bar{\sigma}_2) D^{V_1}_{\mu_1\nu_1}(q_1) D^{V_2}_{\mu_2\nu_2}(q_2) \Gamma^{\nu_1\nu_2}_{V_1V_2}(q_1, q_2), \tag{2.25}$$

where $J_{V_i}^{\mu_i}$ are the external fermion currents, and the vector boson propagators are

$$D^{V_i}_{\mu_i\nu_i}(q_i) = \begin{cases} \left(-g_{\mu_i\nu_i} + \dfrac{q_{i\mu_i} q_{i\nu_i}}{m_Z^2}\right) D_Z(q_i^2) & \text{for } V_i = Z, \\ -g_{\mu_i\nu_i} D_\gamma(q_i^2) & \text{for } V_i = \gamma\,. \end{cases} \tag{2.26}$$

with the propagator factor $D_V(q_i^2) = (q_i^2 - m_V^2 + i m_V \Gamma_V)^{-1}$. Using the completeness relation and neglecting the terms which vanish due to current conservation, the Higgs decay helicity amplitudes can be rewritten as the product of the two outcoming current amplitudes and the off-shell V_1V_2 production amplitudes summed over the polarization of the intermediate vector bosons

$$\mathcal{M}(\sigma_1,\bar{\sigma}_1;\sigma_2,\bar{\sigma}_2) = D_{V_1}(q_1^2)D_{V_2}(q_2^2)\sum_{\lambda_1,\lambda_2}\mathcal{J}_{V_1}^{\lambda_1}(p_1,\sigma_1;\bar{p}_1,\bar{\sigma}_1)\mathcal{J}_{V_2}^{\lambda_2}(p_2,\sigma_2;\bar{p}_2,\bar{\sigma}_2)\mathcal{M}_{V_1V_2}^{\lambda_1\lambda_2}(q_1,q_2), \tag{2.27}$$

where

$$\mathcal{J}_{V_i}^{\lambda_i}(p_i,\sigma_i;\bar{p}_i,\bar{\sigma}_i) = J_{V_i}^{\mu_i}(p_i,\sigma_i;\bar{p}_i,\bar{\sigma}_i)\epsilon_{\mu_i}(q_i,\lambda_i)\,, \tag{2.28}$$

$$\mathcal{M}_{V_1V_2}^{\lambda_1\lambda_2}(q_1,q_2) = \Gamma_{V_1V_2}^{\nu_1\nu_2}(q_1,q_2)\epsilon^{\star}_{\nu_1}(q_1,\lambda_1)\epsilon^{\star}_{\nu_2}(q_2,\lambda_2)\,. \tag{2.29}$$

The angular momentum conservation tells $\lambda_1 = \lambda_2$. Although on numerical studies we account for the lepton helicity flip contributions $\bar{\sigma}_i = \sigma_i$, which can be relevant near the lepton pair production threshold, $m(\ell\bar{\ell}) \approx 2m_\ell$, we give only the dominant helicity conserving $\bar{\sigma}_i = -\sigma_i$ component in the following analytical expressions. The helicity amplitudes are then determined by the ℓ_1 and ℓ_2 helicity,

$$\mathcal{M}(\sigma_1;\sigma_2) = D_{V_1}(q_1^2)D_{V_2}(q_2^2)\sum_{\lambda}\mathcal{J}_{V_1}^{\lambda}(p_1,\bar{p}_1,\sigma_1)\mathcal{J}_{V_2}^{\lambda}(p_2,\bar{p}_2,\sigma_2)\mathcal{M}_{V_1V_2}^{\lambda}(q_1,q_2)\,. \tag{2.30}$$

Because $\mathcal{J}_{V_i}^{\lambda}(p_i,\bar{p}_i,\sigma_i)$ and $\mathcal{M}_{V_1V_2}^{\lambda}$ are separately invariant under the boost along the momentum direction (the z-axis), we calculate $\mathcal{J}_{V_i}^{\lambda}(p_i,\bar{p}_i,\sigma_i)$ in the rest frame of the corresponding virtual vector boson with invariant mass $s_i = q_i^2$, and $\mathcal{M}_{V_1V_2}^{\lambda}$ is calculated in the $h(125)$ rest frame. The angular configuration of the particles is summarized in Fig. 2.2. In the rest frame of q_i^μ, we have

$$q_i^\mu = (\sqrt{s_i},0,0,0)\,, \tag{2.31a}$$

$$p_i^\mu = \frac{\sqrt{s_i}}{2}(1\,,\ \beta_i^\star\sin\theta_i^\star\cos\phi_i^\star\,,\ \beta_i^\star\sin\theta_i^\star\sin\phi_i^\star\,,\ \beta_i^\star\cos\theta_i^\star)\,, \tag{2.31b}$$

$$\bar{p}_i^\mu = \frac{\sqrt{s_i}}{2}(1\,,-\beta_i^\star\sin\theta_i^\star\cos\phi_i^\star\,,-\beta_i^\star\sin\theta_i^\star\sin\phi_i^\star\,,-\beta_i^\star\cos\theta_i^\star)\,. \tag{2.31c}$$

Without loss of generality, we set $\phi_2^\star = 0$ and denote

$$\phi = \phi_1^\star - \phi_2^\star = \phi_1^\star\,. \tag{2.32}$$

Because of the isotropic property of the Higgs decay, we can always chose the out-going vector bosons to have momenta along the z-axis, and

$$q_1^\mu = \frac{\sqrt{s}}{2}(1+(s_1-s_2)/s,\, 0,\, 0, \quad \beta)\,, \tag{2.33a}$$

$$q_2^\mu = \frac{\sqrt{s}}{2}(1+(s_2-s_1)/s,\, 0,\, 0,\, -\beta)\,, \tag{2.33b}$$

in the rest frame of the Higgs boson. Using the kinematical variables defined above and the wave functions in HELAS [46] convention we can obtain the helicity amplitude,

$$\begin{aligned}\mathcal{M}(\sigma_1,\sigma_2) \;\propto\; & \sqrt{s_1}\sqrt{s_2}D_{V_1}D_{V_2}(g_V^{V_1}+\sigma_1 g_A^{V_1})(g_V^{V_2}+\sigma_2 g_A^{V_2})(\sigma_1\sigma_2) \\ & \times\Big(g^+_{hV_1V_2}(1+\sigma_1\cos\theta_1^\star)(1+\sigma_2\cos\theta_2^\star)e^{i(\phi-\xi^+_{hV_1V_2})} \\ & \quad + g^-_{hV_1V_2}(1-\sigma_1\cos\theta_1^\star)(1-\sigma_2\cos\theta_2^\star)e^{-i(\phi-\xi^-_{hV_1V_2})}\Big)\,,\end{aligned} \tag{2.34}$$

The squared matrix elements are

$$\begin{aligned} & |\mathcal{M}(\sigma_1,\sigma_2)|^2 \\ = \; & \mathcal{N}_{V_1V_2}s_1s_2D^2_{V_1}D^2_{V_2}(g_V^{V_1}+\sigma_1 g_A^{V_1})^2(g_V^{V_2}+\sigma_2 g_A^{V_2})^2 \\ & \times\Big((g^+_{hV_1V_2})^2(1+\sigma_1\cos\theta_1^\star)^2(1+\sigma_2\cos\theta_2^\star)^2+(g^-_{hV_1V_2})^2(1-\sigma_1\cos\theta_1^\star)^2(1-\sigma_2\cos\theta_2^\star)^2 \\ & \quad + 2g^+_{hV_1V_2}g^-_{hV_1V_2}\sin^2\theta_1^\star\sin^2\theta_2^\star\cos(2\phi-\xi^+_{hV_1V_2}-\xi^-_{hV_1V_2})\Big)\,,\end{aligned} \tag{2.35}$$

where the normalization constant is

$$\mathcal{N}_{V_1V_2} = \alpha^2 m_h^2\frac{m_Z^2\beta}{2v^2\kappa}\,. \tag{2.36}$$

It's clear that the interference between the transverse V_1V_2 contributions exhibit the $\cos(2\phi)$ azimuthal angle correlation, with exactly the same phase shift, $\phi \to \phi - \Delta\phi$, in the presence of CP violation, as the correlation between the linear polarization planes of $h \to Z\gamma$ and $h \to \gamma\gamma$ decay amplitudes. This is simply a consquence of the linear polarization dependence of the $\gamma \to \ell\bar{\ell}$, and the transverse polarized $Z \to \ell\bar{\ell}$, helicity amplitudes. In the case of real couplings, the squared helicity amplitudes for $h \to \gamma\gamma \to$

4ℓ become very simple,

$$\begin{aligned}
& |\mathcal{M}(\sigma_1, \sigma_2)|^2 \\
= \; & \mathcal{N}_{V_1V_2} s_1 s_2 D_{V_1}^2 D_{V_2}^2 (g_{hV_1V_2})^2 (g_V^{V_1} + \sigma_1 g_A^{V_1})^2 (g_V^{V_2} + \sigma_2 g_A^{V_2})^2 \\
& \times \Big((1 + \sigma_1 \cos\theta_1^\star)^2 (1 + \sigma_2 \cos\theta_2^\star)^2 + (1 - \sigma_1 \cos\theta_1^\star)^2 (1 - \sigma_2 \cos\theta_2^\star)^2 \\
& \quad + 2 \sin^2\theta_1^\star \sin^2\theta_2^\star \cos(2\phi - \xi_{hV_1V_2}^+ - \xi_{hV_1V_2}^-) \Big) \,. \qquad (2.37)
\end{aligned}$$

after summing over the lepton helicities, we find

$$|\mathcal{M}(h \to \gamma\gamma \to 4\ell)|^2 \propto (1+\cos^2\theta_1^\star)(1+\cos^2\theta_2^\star) + \sin^2\theta_1^\star \sin^2\theta_2^\star \cos(2\phi - 2\xi_{hV_1V_2}) \,. \qquad (2.38)$$

which is relevant in the measurements at the LHC experiments, which have no capability of measuring the lepton (e and μ) helicities. It is worth noting that the phase shift measurement power is proportional to the kinematical factor $\sin^2\theta_1^\star \sin^2\theta_2^\star$ in the $V_{1,2} \to \ell\bar{\ell}$ rest frame decay angular distributions, since they are proportional to the interference between the helicity $+1$ and -1 vector boson decay amplitudes.

2.3 Helicity amplitudes of photon conversion

We now study the conversion process of a single isolated photon into lepton pair. Photon conversion is proceed by Bethe-Heitler (BH) mechanism on atomic nuclei [51]. Both ATLAS and CMS pixel detectors contain a significant amount of material, most of the photons are converted inside the detectors. For ATLAS, on average about 30 % of the photons can convert into an electron-positron pair before reaching the face of the calorimeter [53]. The reconstruction efficiency (including the single track reconstruction) is about 80%for a tight reconstruction condition, and is about 90% for a loose one in the whole η_γ region [54]. In this paper, the reconstruction efficiency is estimated by using the $\chi^2_{\min}$ function defined in Eq. (2.67) with the condition Eq. (2.68). Although the detectors are consist of many kinds of materials, we study only the ^{28}Si for illustration as the main component of the vertex detectors. The groundstate of ^{28}Si is spin-0, so we neglect the effects of target polarization in the BH process [52].

The kinematics of the conversion process

$$\gamma(k,\lambda) + \mathrm{Si}(p) \quad \to \quad \mathrm{Si}(p') + \ell^-(k_1,\sigma_1) + \ell^+(k_2,\sigma_2) \tag{2.39}$$

are defined as in Fig.2.3. Without loss of generality we will study the case of a photon linearly polarized along the x-axis where the photon momentum (k) direction is chosen along the z-axis. The matrix element can be written as

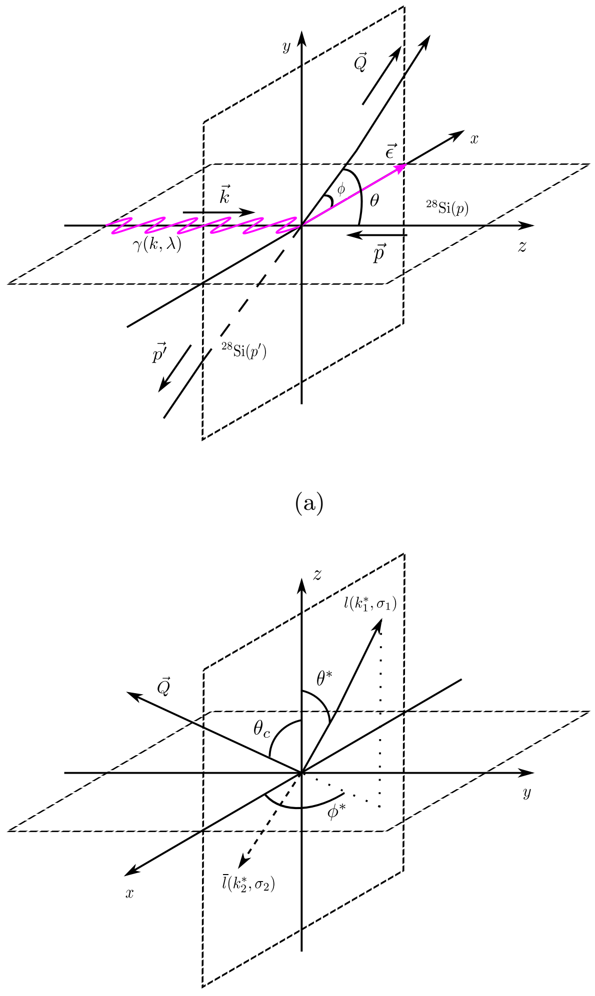

(a)

(b)

FIGURE 2.3: Definitions of the momenta and polarizations of the particles. Without loss of generality, the $\hat{z}$-axis is defined along the momentum direction of in-coming photon, $\hat{x}$-axis is defined as the polarization direction of the same photon.

$$\mathcal{M} = \frac{g_{\mu\nu}}{t}\langle \ell^-\ell^+|\mathcal{T}^\mu_\ell|\gamma\rangle\langle N'|\mathcal{T}^\nu_N|N\rangle\,, \tag{2.40}$$

where $\langle \ell^- \ell^+ | \mathcal{T}_\ell^\mu | \gamma \rangle$ denote the amplitude for $\gamma\gamma^* \to \ell^+\ell^-$ and $\langle N' | \mathcal{T}_N^\nu | N \rangle$ denote the Si$\gamma^* \to$ Si$'$ transition, and $g_{\mu\nu}/t$ with

$$t = -(p - p')^2 \tag{2.41}$$

denote the γ^* propagator. The squared amplitude can be written as

$$|\mathcal{M}|^2 = \frac{1}{t^2} L^{\mu\nu} W_{\mu\nu} \,, \tag{2.42}$$

where

$$L^{\mu\nu} = \langle \gamma | (\mathcal{T}_\ell^\mu)^\dagger | \ell^- \ell^+ \rangle \langle \ell^- \ell^+ | \mathcal{T}_\ell^\nu | \gamma \rangle \,, \tag{2.43a}$$

$$W^{\mu\nu} = \langle N | (\mathcal{T}_N^\mu)^\dagger | N' \rangle \langle N' | \mathcal{T}_N^\nu | N \rangle \,. \tag{2.43b}$$

For inclusive measurements we can sum over the final state of ^{28}Si, and we define further the nucleus form factor as follows

$$\begin{aligned} \mathcal{W}_{\mu\nu} &= \int \frac{d^3p'}{(2\pi)^3 2E'_p} (2\pi)^4 \delta^4(k + p - Q - p') W_{\mu\nu} \\ &= 2\pi\delta(p'^2 - m_{\rm Si}^2) \langle N | (\mathcal{T}_{N\mu})^\dagger \mathcal{T}_{N\nu} | N \rangle \\ &= W_1(q^2)\Big(- g_{\mu\nu} + \frac{q_\mu q_\nu}{q^2} \Big) + W_2(q^2) \frac{1}{m_S^2} \Big(p_\mu - \frac{p \cdot q}{q^2} q_\mu \Big) \Big(p_\nu - \frac{p \cdot q}{q^2} q_\nu \Big) \end{aligned} \tag{2.44}$$

Then the total cross section can be written as

$$d\sigma = \frac{1}{4 m_{\rm Si} E_\gamma} \frac{dQ}{2\pi} \frac{\bar{\beta}}{8\pi} \frac{d\cos\bar{\theta} d\bar{\phi}}{4\pi} \frac{\beta^\star}{8\pi} \frac{d\cos\theta^\star d\phi^\star}{4\pi} \frac{1}{t^2} L^{\mu\nu} \mathcal{W}_{\mu\nu} \,. \tag{2.45}$$

Here $\bar{\theta}$ and $\bar{\phi}$ are measured in the γSi collision rest frame (see Fig.2.3) where $\bar{\beta} = |\vec{Q}|/\sqrt{s}$ with

$$s = (k + p)^2 = m_{\rm Si}(2E_\gamma + m_{\rm Si}) \,. \tag{2.46}$$

Both the BH conversion and the opening angle of the subsequent lepton pair depend strongly on the momentum transfer $t = -q^2$ of the target nucleus. There are two typical energy scales that are important for the elastic scattering. One is the atomic scale Λ_a, below which the atom virtual photon probes the whole neutral atom where the electron clouds screen the nuclear charge. Another one is the nuclear scale Λ_n, above which the virtual photon probes individual the protons and neutrons, broking the nucleus and the inelastic scattering comes into play. We consider only the elastic scattering, where amplitude are coherently multiplied by the nucleon number (28 for ^{28}Si). Because the scattering region of $t > \Lambda_n^2$ is irrelevant for the conversion process, we introduce a single elastic nuclear form factor $G_2^e(t)$,

$$G_2^e(t) = \begin{cases} \dfrac{t/\Lambda_a^2}{(1+t/\Lambda_a^2)} & \text{for}\, t < \Lambda_n \\ \\ 0 & \text{for}\, t \geq \Lambda_n \end{cases} \tag{2.47}$$

with the relation

$$W_1(q^2) = 0 \ , \ W_2 = 2\pi\delta(p'^2 - m_S^2)(G_2^e(t))^2. \tag{2.48}$$

Here we use an atomic scale $\Lambda_a = 6.05 \times 10^{-10}\text{GeV}^2$, and nuclear scale $\Lambda_n = 1.75 \times 10^{-2}\text{GeV}^2$. The atomic form factor plays an important role of suppressing scattering at low t region. The t threshold of the conversion is about $4Q_{min}^2/E_\gamma$. For $E_\gamma = m_h/2 = 62.5\text{GeV}$, it is about $(10^{-9}\text{GeV})^2$ for $Q_{\min} = 2m_e$. The atomic form factor strongly suppresses the contributions near photon pole, and significantly alters the important regions of the phase space, particularly the invariant mass of the lepton pair and then the opening angle between them in the laboratory frame.

The leptonic matrix elements are

$$\mathcal{M}^\nu(\sigma_1,\sigma_2) = -e^2\bar{u}(k_1,\sigma_1)\left\{\frac{\gamma^\mu(\not{\ell}_1 + m_\ell)\gamma^\nu}{\ell_1^2 - m_\ell^2} + \frac{\gamma^\nu(\not{\ell}_2 + m_\ell)\gamma^\mu}{\ell_2^2 - m_\ell^2}\right\}v(k_2,\sigma_2)\epsilon_\mu(\vec{k},\hat{x})\,, \tag{2.49}$$

where $\ell_1 = k_1 - k$ and $\ell_2 = k - k_2$ are the momentum transfer in the photon-lepton system. With the application of equation of motion the helicity amplitude is simplified as

$$\mathcal{M}^\nu(\sigma_1,\sigma_2) = e^2\left\{\frac{2J_{V1}^\nu - J_{T1}^\nu}{2k\cdot k_1} - \frac{2J_{V2}^\nu - J_{T2}^\nu}{2k\cdot k_2}\right\}, \tag{2.50}$$

where we have defined four kinds of leptonic currents as follows

$$J_{V1}^\nu(\sigma_1,\sigma_2) = \bar{u}(k_1,\sigma_1)\gamma^\nu v(k_2,\sigma_2)k_1\cdot\epsilon(k,x)\,, \tag{2.51a}$$

$$J_{V2}^\nu(\sigma_1,\sigma_2) = \bar{u}(k_1,\sigma_1)\gamma^\nu v(k_2,\sigma_2)k_2\cdot\epsilon(k,x)\,, \tag{2.51b}$$

$$J_{T1}^\nu(\sigma_1,\sigma_2) = \bar{u}(k_1,\sigma_1)\gamma^\mu\not{k}\gamma^\nu v(k_2,\sigma_2)\epsilon_\mu(k,x)\,, \tag{2.51c}$$

$$J_{T2}^\nu(\sigma_1,\sigma_2) = \bar{u}(k_1,\sigma_1)\gamma^\nu\not{k}\gamma^\mu v(k_2,\sigma_2)\epsilon_\mu(k,x)\,. \tag{2.51d}$$

The kinematical variables are specified as in Fig. 2.3. In the rest frame of photon-Silicon system, the kinematical variables are given by

$$k^\mu = (\bar{E}_\gamma, 0, 0, \bar{E}_\gamma)\,, \tag{2.52a}$$

$$p^\mu = (\bar{E}_S, 0, 0, -\bar{E}_\gamma)\,, \tag{2.52b}$$

$$Q^\mu = (\bar{E}_Q, \quad |\vec{Q}|\sin\bar{\theta}\cos\bar{\phi}, \quad |\vec{Q}|\sin\bar{\theta}\sin\bar{\phi}, \quad |\vec{Q}|\cos\bar{\theta})\,, \tag{2.52c}$$

$$p'^\mu = (\bar{E}'_p, -|\vec{Q}|\sin\bar{\theta}\cos\bar{\phi}, -|\vec{Q}|\sin\bar{\theta}\sin\bar{\phi}, -|\vec{Q}|\cos\bar{\theta})\,, \tag{2.52d}$$

$$\epsilon^\mu = (0, 1, 0, 0)\,, \tag{2.52e}$$

where

$$\bar{\beta} = \frac{2|\vec{\bar{Q}}|}{\sqrt{s}} = \left(1 - \frac{2(m_{\rm Si}^2 + Q^2)}{s} + \frac{(m_{\rm Si}^2 - Q^2)^2}{s^2}\right)^{1/2}. \tag{2.53}$$

The rest frame of the lepton pair $Q^\mu = k_1^\mu + k_2^\mu$, can be obtained from the c.m. frame by the Lorentz transformation,

$$L(\bar{\beta}_Q, \bar{\theta}, \bar{\phi}) = K_{\bar{z}}^{-1}(\bar{\beta}_Q) R_{\bar{y}}^{-1}(\bar{\theta}) R_{\bar{z}}^{-1}(\bar{\phi})\,. \tag{2.54}$$

The incident momentum k^μ is transformed to

$$k^\mu = \bar{E}_\gamma(\bar{\gamma}_Q(1 - \bar{\beta}_Q\cos\bar{\theta}),\ \sin\bar{\theta},\ 0,\ \bar{\gamma}_Q(\cos\bar{\theta} - \bar{\beta}_Q))\,. \tag{2.55}$$

In order to make the calculation simple we make a further rotation $R_{\bar{y}}^{-1}(\bar{\theta}_c)$ about the $\bar{y}$-axis with

$$\sin\bar{\theta}_c = \frac{\bar{E}_\gamma}{E_\gamma^\star}\sin\bar{\theta}\,, \quad \cos\bar{\theta}_c = \frac{\bar{E}_\gamma}{E_\gamma^\star}\bar{\gamma}_Q(\cos\bar{\theta} - \bar{\beta}_Q)\,, \tag{2.56}$$

which makes the $z^\star$-axis along the photon momentum direction. The $\ell\bar{\ell}$ rest frame (the $R^\star$ frame) then gives

$$Q^\mu = (\sqrt{Q}, 0, 0, 0)\,, \tag{2.57a}$$

$$k^\mu = E_\gamma^\star(1,\ 0,\ 0, 1)\,, \quad E_\gamma = \bar{E}_\gamma\bar{\gamma}_Q(1 - \bar{\beta}_Q\cos\bar{\theta})\,, \tag{2.57b}$$

$$k_1 = \sqrt{Q}/2(1, \beta^\star\sin\theta^\star\cos\phi^\star, \beta^\star\sin\theta^\star\sin\phi^\star, \beta^\star\cos\theta^\star) \tag{2.57c}$$

$$k_2 = \sqrt{Q}/2(1, -\beta^\star\sin\theta^\star\cos\phi^\star, -\beta^\star\sin\theta^\star\sin\phi^\star, -\beta^\star\cos\theta^\star)\,, \tag{2.57d}$$

$$\epsilon^\mu = (-|\vec{Q}|/\sqrt{Q}\sin\bar{\theta}\cos\bar{\phi},\ \cos\bar{\phi},\ -\sin\bar{\phi},\ -|\vec{Q}|/\sqrt{Q}\sin\bar{\theta}\cos\bar{\phi})\,. \tag{2.57e}$$

However, the correlation is remained for small momentum transfer t which means $\sin\bar{\theta} \approx$

0. With the definitions of kinematical variables above we get following results for the leptonic currents in the $R^\star$ frame,

$$J^\nu_{V_1}(\sigma_1 - \sigma_2 = 1) = C_1 E^\star_\ell (1+\beta^\star)(0, \cos\theta^\star \cos\phi^\star + i\sin\phi^\star, \cos\theta^\star \sin\phi^\star - i\cos\phi^\star, -\sin\theta^\star) \tag{2.58a}$$

$$J^\nu_{V_1}(\sigma_1 - \sigma_2 = 1) = C_2 E^\star_\ell (1+\beta^\star)(0, \cos\theta^\star \cos\phi^\star + i\sin\phi^\star, \cos\theta^\star \sin\phi^\star - i\cos\phi^\star, -\sin\theta^\star) \tag{2.58b}$$

$$J^\nu_{T_1}(\sigma_1 - \sigma_2 = 1) = 2E^\star_\gamma E^\star_\ell (1+\beta^\star) e^{-i\bar{\phi}} (e^{-i\phi^\star} \sin^2\frac{\theta^\star}{2},\ -\frac{1}{2}\sin\theta^\star,\ \frac{i}{2}\sin\theta^\star,\ e^{-i\phi^\star}\sin^2\frac{\theta^\star}{2}) \tag{2.58c}$$

$$J^\nu_{T_2}(\sigma_1 - \sigma_2 = 1) = 2E^\star_\gamma E^*_\ell (1+\beta^*) e^{i\bar{\phi}} \left(-e^{i\phi^\star} \cos^2\frac{\theta^\star}{2},\ -\frac{1}{2}\sin\theta^\star,\ -i\frac{1}{2}\sin\theta^\star,\ -e^{i\phi^\star}\cos^2\frac{\theta^\star}{2}\right) \tag{2.58d}$$

where

$$C_1 = k_1 \cdot \epsilon = E^\star_\ell \left(-\frac{|\vec{Q}|}{\sqrt{Q}} \sin\bar{\theta}\cos\bar{\phi}(1 - \beta^\star_\ell \cos\theta^\star) - \beta^\star_\ell \sin\theta^\star \cos(\phi^\star + \bar{\phi}) \right), \tag{2.59a}$$

$$C_2 = k_2 \cdot \epsilon = E^\star_\ell \left(-\frac{|\vec{Q}|}{\sqrt{Q}} \sin\bar{\theta}\cos\bar{\phi}(1 + \beta^\star_\ell \cos\theta^\star) + \beta^\star_\ell \sin\theta^\star \cos(\phi^\star + \bar{\phi}) \right). \tag{2.59b}$$

The currents with $\sigma_1 - \sigma_2 = -1$ could be obtained by complex conjugations,

$$J^\nu_{V_i}(\sigma_1 - \sigma_2 = -1) = [J^\nu_{V_i}(\sigma_1 - \sigma_2 = 1)]^*\ , \quad J^\nu_{T_i}(\sigma_1 - \sigma_2 = -1) = [J^\nu_{T_i}(\sigma_1 - \sigma_2 = 1)]^*\,. \tag{2.60}$$

We find that the chirality flip contribution for $\sigma_1 + \sigma_2 = 0$ are proportional to m_ℓ, and are very relevant when we neglect the of the ℓ and $\bar{\ell}$ opening angle and the LHC detector.

Inserting these results into Eq. (2.50) and contract with the nuclear form factor we can obtain the total Helicity amplitudes,

$$\mathcal{M}^\nu(\sigma_1, \sigma_2) = -e^2 \bar{u}(k_1, \sigma_1) \left\{ \frac{\gamma^\mu(\ell_1 + m_\ell)\gamma^\nu}{\ell_1^2 - m_\ell^2} + \frac{\gamma^\nu(\ell_2 + m_\ell)\gamma^\mu}{\ell_2^2 - m_\ell^2} \right\} v(k_2, \sigma_2) \epsilon_\mu(\vec{k}, \hat{x})\,. \tag{2.61}$$

Fig. 2.4 shows the differential cross section of the BH conversion process with respect to the invariant mass of the electron pair, $m_{e\bar{e}} = \sqrt{Q^2}$. The blue-solid line gives the distribution for a bare ^{28}Si without any form factor, the cross section grows with $m_{e\bar{e}}^{-3}$ at small $m_{e\bar{e}}$ as the total cross section is proportional to $1/m_{e\bar{e}}^2$. The red-dashed line is the distribution for a ^{28}Si with the form factor of Eq. (2.47). The small $m_{e\bar{e}}$ singularity is taned by the atomic shielding effects, making the total conversion cross section 2.62b, consistent with the observation.

The black-dotted line is the cross section after an additional cut on the opening angle between the ℓ and $\bar{\ell}$ momenta, $\theta(\ell, \bar{\ell}) \geq 0.001$ and a momentum cut $p_{\ell,\bar{\ell}} > 2\text{GeV}$. As we study in the next section, ℓ and $\bar{\ell}$ momenta should have the opening angle greater than about $\theta_{\text{cut}} = 0.001$ in order for the LHC detectors to reconstruct the $\gamma \to \ell\bar{\ell}$ splitting correlation, the azimuthal angle $\phi^\star$, that measure the linear polarization of γ. The black-solid line shows the distributions with the same opening angle cut and a momentum cut $p_{\ell,\bar{\ell}} > 10\text{GeV}$. The opening angle cut hugely reduces the cross section, more than a factor of 10^{10} in the low invariant mass region.

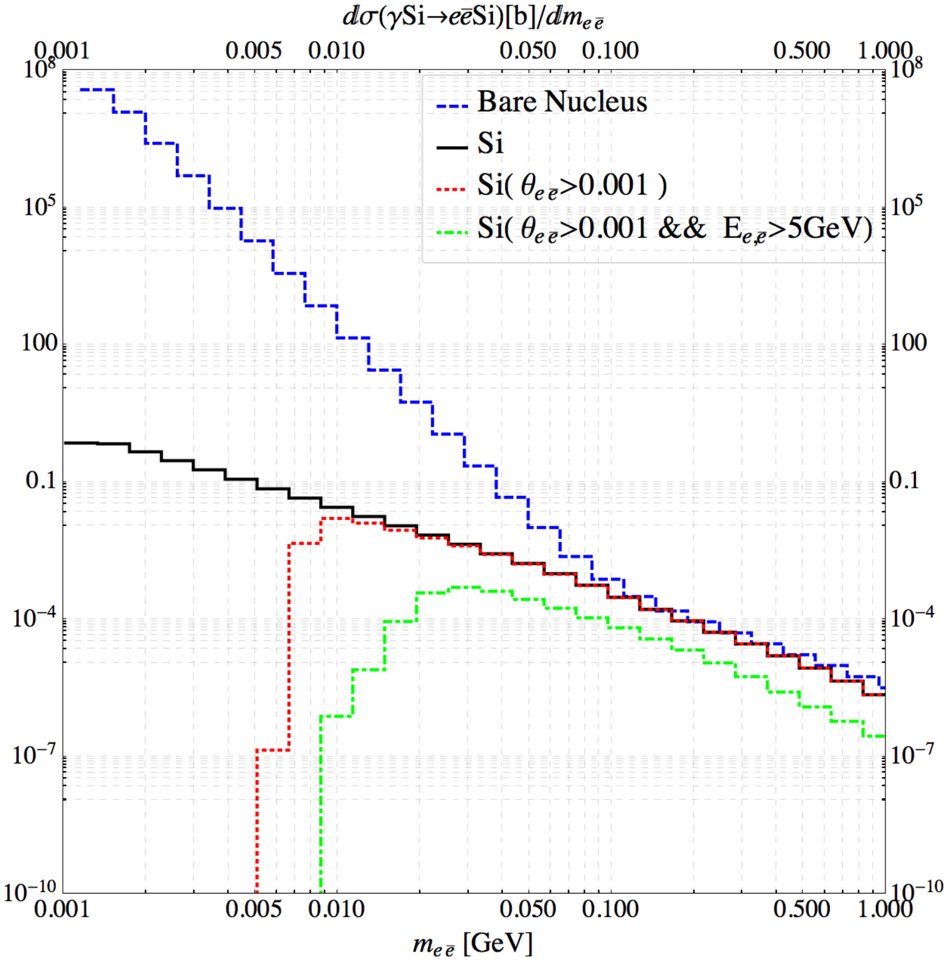

FIGURE 2.4: The blue-dashed line is the distribution for a bare ^{28}Si without any form factor. The black-solid line is the distribution for a ^{28}Si with the form factor Eq. (2.47). The red-dotted line shows the distribution with additional cut on the opening angle $\theta_{cut}(e^-, e^+) = 0.001$. The green-dotdashed line is the distribution cut on the opening angle $\theta_{cut}(e^-, e^+) = 0.001$, and cut on the lepton energy $E(e^-), E(e^+) > 5\text{GeV}$.

Fig. 2.5 shows the distributions of the lepton azimuthal angle measured in the Lab frame where the momentum of incident photon is in the positive $x - z$ plane.

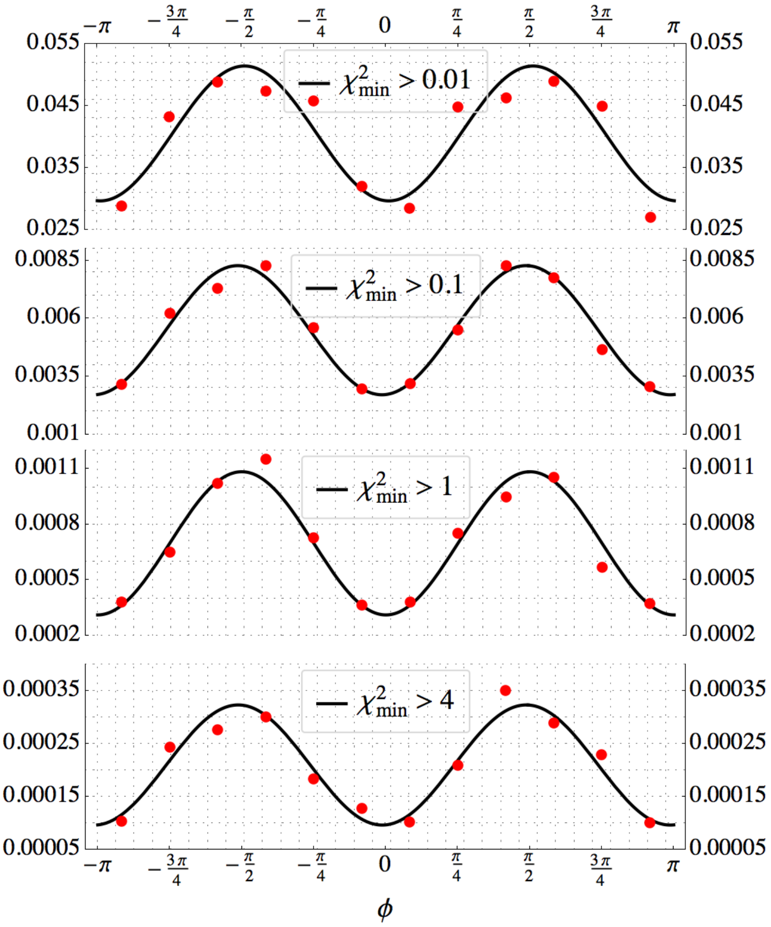

FIGURE 2.5: Distributions of the azimuthal angle of leptons which is measured in the Lab frame.

2.4 Angular resolution

In order to measure the azimuthal angle ($\phi^\star$) that determine the orientation of the $\gamma \to \ell\bar{\ell}$ conversion plane, the spatial momenta of e and $\bar{e}$ should be measured precisely. Such measurements require exquisitely precise tracking. Both ATLAS and CMS have very good granularity in the azimuthal and polar angle directions. However, we will show it is still challenging to have a good measurement on the CP violation. We choose the ATLAS detector as an example for illustration of the tracking resolution. We use the data in Ref. [61] and obtain the following fits for the resolutions in azimuthal and polar angle directions,

$$\sigma_\phi(\eta, p_T) = 0.0002 + 0.0031 p_T^{-1} - 0.0006 p_T^{-2} \ , \tag{2.62a}$$

$$\sigma_\theta(\eta, p_T) = 0.0008 + 0.0009 p_T^{-1} + 0.0043 p_T^{-2} \ , \tag{2.62b}$$

where p_T is measured in GeV unite. Fig. 2.6 shows the experimental data [61] and our fits, Eq. (2.62a) and Eq. (2.62b). They are perfectly consistent. The resolution of

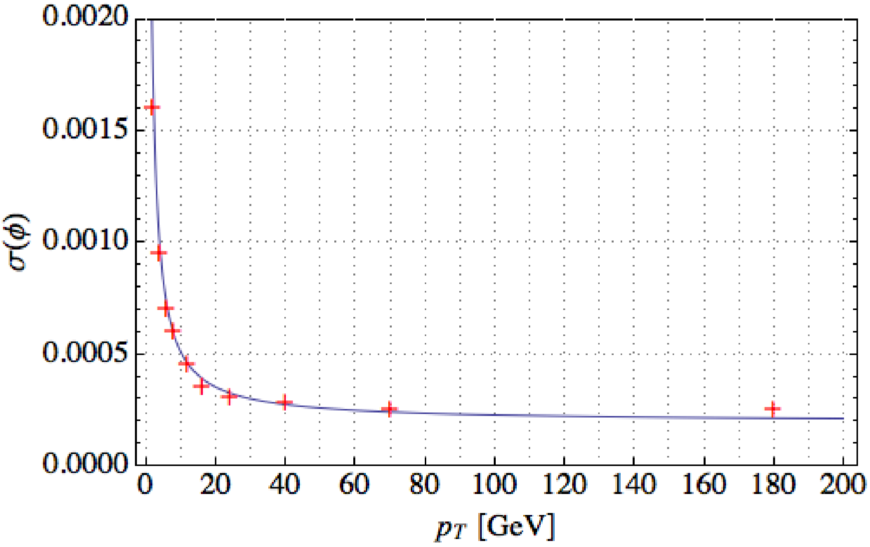

(a)

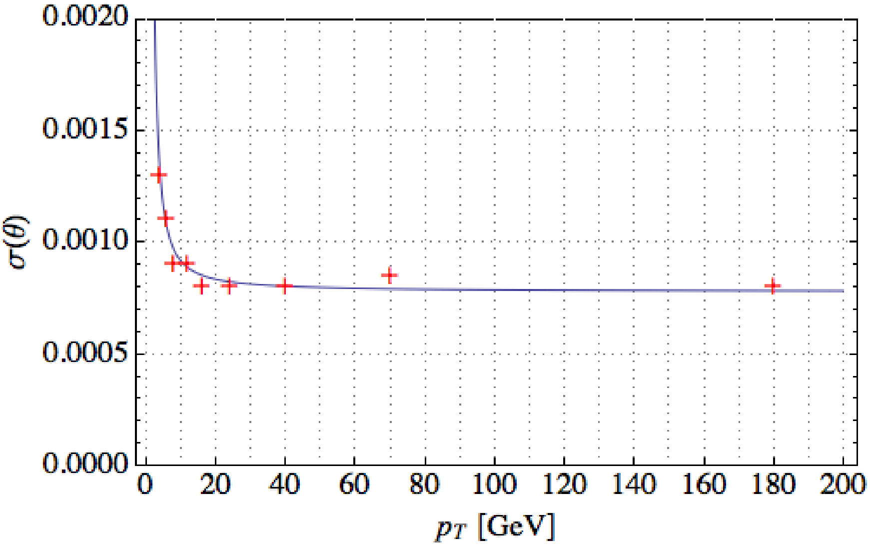

(b)

FIGURE 2.6: p_T dependence of the experimental resolution in azimuthal and polar angle directions. The red cross points are experimental data taken from Ref. [61]. The solid-blue line is our result by fitting the data.

pseudo-rapidity is related to $\sigma_\theta(\eta, p_T)$ by

$$\sigma_\eta(\eta, p_T) = \cosh(\eta)\sigma_\theta(\eta, p_T) \ . \tag{2.63}$$

Fig.2.7 shows the 1σ contours for different combinations of p_T and η.

Assuming that the observed pseudo-rapidity η_{obs} and azimuthal angle ϕ_{obs} follow the Gaussian distribution, we define the χ^2 function for true value (η, ϕ) as follows,

$$\chi^2(\eta_{obs}, \phi_{obs}; \eta, \phi, p_T) = \frac{(\eta_{obs} - \eta)^2}{\sigma_\eta^2(\eta, p_T)} + \frac{(\phi_{obs} - \phi)^2}{\sigma_\phi^2(\eta, p_T)} \ . \tag{2.64}$$

Given a set of two momenta

$$(\eta_\ell, \phi_\ell, p_{T\ell}) \ \text{ and } \ (\eta_{\bar{\ell}}, \phi_{\bar{\ell}}, p_{T\bar{\ell}}) \ , \tag{2.65}$$

and a possible common orientation (η, ϕ) of the two momenta, then the total χ^2 function is

$$\chi^2(\eta, \phi; \eta_\ell, \phi_\ell, p_{T\ell}; \eta_{\bar{\ell}}, \phi_{\bar{\ell}}, p_{T\bar{\ell}}) = \chi^2_\ell(\eta, \phi; \eta_\ell, \phi_\ell, p_{T\ell}) + \chi^2_{\bar{\ell}}(\eta, \phi; \eta_{\bar{\ell}}, \phi_{\bar{\ell}}, p_{T\bar{\ell}}) \ . \tag{2.66}$$

If the minimum of this χ^2 function is high, then the two momenta are well resolved. The probability that this interpretation is valid is dictated by the χ^2 function. By minimizing χ^2 function we find

$$\chi^2_{\min}(\eta_\ell, \phi_\ell, p_{T\ell}; \eta_{\bar{\ell}}, \phi_{\bar{\ell}}, p_{T\bar{\ell}}) = \frac{(\eta_\ell - \eta_{\bar{\ell}})^2}{\sigma^2_{\eta_\ell}(\eta_\ell, p_{T\ell}) + \sigma^2_{\eta_{\bar{\ell}}}(\eta_{\bar{\ell}}, p_{T\bar{\ell}})} + \frac{(\phi_\ell - \phi_{\bar{\ell}})^2}{\sigma^2_{\phi_\ell}(\eta_\ell, p_{T\ell}) + \sigma^2_{\phi_{\bar{\ell}}}(\eta_{\bar{\ell}}, p_{T\bar{\ell}})} \ . \tag{2.67}$$

For the above form, it is clear that the two angles are consistent with being one, if $\chi^2_{\min} \lesssim 2$. We will use a conservative cut

$$\chi^2_{\min}(\eta_\ell, \phi_\ell, p_{T\ell}; \eta_{\bar{\ell}}, \phi_{\bar{\ell}}, p_{T\bar{\ell}}) > 4 \ , \tag{2.68}$$

as the necessary condition that the ℓ and $\bar{\ell}$ momenta ($\vec{p}_\ell$ and $\vec{p}_{\bar{\ell}}$) can be resolved to be non-collinear.

TABLE 2.1: Number of events for the process $pp \to h \to Z\gamma \to 4\ell$ after the kinematical cuts. The total number of events are normalized to the SM values with $1\,\mathrm{ab}^{-1}$ of luminosity at HL-LHC(14TeV).

$\sigma(pp \to h) = 54\,\mathrm{pb}$	$\mathrm{R}_e^\gamma = \dfrac{\Gamma(h \to e^+e^-\gamma)}{2\Gamma(h \to \gamma\gamma)} = 1.77\%$
$\mathrm{Br}(h \to \gamma\gamma) = 0.23\%$	$\mathrm{R}_\mu^\gamma = \dfrac{\Gamma(h \to \mu^+\mu^-\gamma)}{2\Gamma(h \to \gamma\gamma)} = 0.86\%$
$\mathrm{Br}(h \to Z\gamma) = 0.15\%$	$\mathrm{R}_e^Z = \dfrac{\Gamma(h \to e^+e^-Z)}{\Gamma(h \to Z\gamma)} = 1.64\%$
$\mathrm{Br}(Z \to \ell\ell) = 6.73\%$	$\mathrm{R}_\mu^Z = \dfrac{\Gamma(h \to \mu^+\mu^-Z)}{\Gamma(h \to Z\gamma)} = 0.77\%$

2.5 Numerical results

In this section we give our numerical results, and show how the finite angular resolution of the LHC detectors affects our CP violation measurements in the $h \to 4\ell$ processes. The signal events are generated at tree level by using MadGraph5 [62] with model HC[*] [63]. Only the gluon fusion production mechanism is included. Events are generated at $\sqrt{s} = 14\mathrm{TeV}$ with the cteq6l1 PDF set [64]. The parton level events are then showered by using Pythia 6 [65]. Below we use following values for overall normalization

2.5.1 $h \to \gamma^\star\gamma^\star \to (\ell^+\ell^-)(\ell^+\ell^-)$ via internal splitting

Fig. 2.8 shows the p_T distributions of the intermediate photons and electrons in the final states. The distributions are normalized to 1, *i.e.* half of the number of γ in $h \to \gamma\gamma$ and half of the number of ℓ in $h \to (\ell\bar{\ell})^2$. The transverse momentum of virtual photons have a peak around 60GeV as expected. However, the electrons from virtual photons have soft transverse momentum, and about 25% of them have $p_T < 10\mathrm{GeV}$. This means about 30% of the events survive after the transverse momentum cut $p_T > 10\mathrm{GeV}$ for all the 4 leptons.

Fig. 2.9 shows the probability of the $\ell\bar{\ell}$ pair that satisfy the angular resolution condition $\chi^2_{\rm min} > \bar{\chi}^2_{\rm min}$. The angular resolution cut has negligible effects on muons, but it strongly

---

[*] We have revised the HS model file so that complex couplings are allowed.

TABLE 2.2: Number of events for the process $pp \to h \to \gamma\gamma \to 4\ell$ after the kinematical cuts. The total number of events are normalized to the SM values with $1\,\mathrm{ab}^{-1}$ of luminosity at HL-LHC(14TeV).

	$N(\gamma^\star_{e\bar{e}}\gamma^\star_{e\bar{e}})$	$N(\gamma^\star_{\mu\bar{\mu}}\gamma^\star_{\mu\bar{\mu}})$	$N(\gamma^\star_{e\bar{e}}\gamma^\star_{\mu\bar{\mu}})$
Total #	35	10	38
for $p_T(\ell), p_T(\bar{\ell}) > 10\mathrm{GeV}$, $\lvert\eta(\ell)\rvert, \lvert\eta(\bar{\ell})\rvert < 2.5$	7	2	8
and $\chi^2_{\mathrm{min}} > 4$	3	2	5
for $p_T(\ell), p_T(\bar{\ell}) > 5\mathrm{GeV}$, $\lvert\eta(\ell)\rvert, \lvert\eta(\bar{\ell})\rvert < 2.5$	14	4	15
and $\chi^2_{min} > 4$	6	4	10

affects the $\gamma^\star \to e^- e^+$ splitting. For our default cut of $\bar{\chi}^2_{min} = 4$, almost all the $\gamma^\star \to \mu^-\mu^+$ events survive, but about 70% of the $\gamma^\star \to e^- e^+$ events survive.

Table 2.2 shows the number of events after the kinematical cuts for three difference final states. We can see that the angular resolution cut doesn't affect the muons as we have shown above. For a transverse momentum cut $p_T(\ell), p_T(\bar{\ell}) > 5\mathrm{GeV}$ there are 20 events in total with an integrated luminosity $1\mathrm{ab}^{-1}$. Only 10 event survives if we use a transverse momentum cut $p_T(\ell), p_T(\bar{\ell}) > 10\mathrm{GeV}$. For experiments with significantly lower statistics, we should make use of all the kinematical informations of the $h \to \gamma^\star\gamma^\star \to 4\ell$ candidate events. The relevant distributions is

$$\frac{dN}{dz_1 d_{z_2} \mathrm{d}\phi} = N_{4\ell}\frac{9}{8\pi}\left([z_1^2 + (1-z_1)^2][z_2^2 + (1-z_2)^2] + z_1(1-z_1)z_2(1-z_2)\cos(2\phi - 2\xi)\right), \tag{2.69}$$

where $z_k = E_{\ell k}/E_{\gamma k}, (k = 1, 2)$ are the energy fraction of the leptons in the $\gamma^\star_k$ rest frames with small ($k = 1$) and larger ($k = 2$) invariant mass ($s_1 < s_2$). Although not all the regions of z_k ($0 < z_k < 1$) survive the $p_T(\ell), p_T(\bar{\ell}) > 10\mathrm{GeV}$ (or 5GeV) events, we can normalize the statistics by giving $N_{4\ell}$ as the total number of events. As an illustration, we show the azimuthal angle correlation in Fig. 2.10 for the $h \to \gamma\gamma \to 4\ell$ events that satisfy $\chi^2_{\mathrm{min}} > 4$, $p_T(\ell), p_T(\bar{\ell}) > 5\mathrm{GeV}$, $|\eta(\ell)|, |\eta(\bar{\ell})| < 2.5$ at $\sqrt{s} = 14\mathrm{TeV}$ with $100\mathrm{ab}^{-1}$. As a references, the prediction of the CP-conserving case (the SM Higgs

TABLE 2.3: Number of events for the process $pp \to h \to Z\gamma \to 4\ell$ after the kinematical cuts. The total number of events are normalized to the SM values with $1\,\mathrm{ab}^{-1}$ of luminosity at HL-LHC(14TeV).

	$N(Z\gamma^\star \to Ze^+e^-)$	$N(Z\gamma^\star \to Z\mu^+\mu^-)$
Total #	1360	639
$Z \to \ell\bar{\ell}, (\ell = e, \mu)$	92	43
$p_T(\ell), p_T(\bar{\ell}) > 5\mathrm{GeV}$, $\lvert\eta(\ell)\rvert, \lvert\eta(\bar{\ell})\rvert < 2.5$	31	16
$\chi^2_{min} > 4$	21	16

boson) is give by the black-solid line. The blue-dashed line and red-dotted line are the distributions for $\xi = \pi/4$ and $\xi = -\pi/4$, respectively. CP violation is clearly seen. A simple χ^2 fit gives $\xi = 0.81 \pm 0.02$ and $\xi = -0.82 \pm 0.03$.

2.5.2 $h \to Z\gamma^\star \to (\ell^+\ell^-)(\ell^+\ell^-)$

Fig.2.11 shows the p_T distributions of the intermediate Z, $\gamma^\star$ as well as μ for $Z \to \mu^-\mu^+$ and e^- for $\gamma^\star \to e^-e^+$. All the distributions are normalized to unity. For the process $pp \to h \to Z\gamma$, the virtual photon has a peak at around 30GeV. The leptons from Z decay have hard transverse momentum, and more than 90% have $p_T > 10\mathrm{GeV}$. However, the leptons from virtual photons are very soft, and nearly 50% of them have $p_T < 10\mathrm{GeV}$. Because lower p_T leptons from $\gamma^\star$ splitting always accompany high p_T leptons, we accept events with $p_T(\ell), p_T(\bar{\ell}) > 5\mathrm{GeV}$ in the $Z\gamma^\star$ channel.

Fig. 2.12 shows the probability of the $\ell\bar{\ell}$ pair that satisfy the angular resolution condition $\chi^2_{\mathrm{min}} > \bar{\chi}^2_{\mathrm{min}}$. The angular resolution cut has negligible effects on muons, but it strongly affects the $\gamma^\star \to e^-e^+$ splitting. Almost all the $Z \to \mu^-\mu^+$ events can be resolved, while about 70% of the $\gamma^\star \to e^-e^+$ events can be resolved at $\bar{\chi}^2_{min} = 4$.

Table 2.3 shows the number of events after the kinematical cuts for three difference final states. We can see that the angular resolution cut doesn't affect the muons as we have shown above. For a transverse momentum cut $p_T(\ell), p_T(\bar{\ell}) > 5\mathrm{GeV}$ there are 37 events in total with an integrated luminosity $1\mathrm{ab}^{-1}$.

Fig. 2.13 shows the azimuthal angle correction for the $h \to Z\gamma \to 4\ell$ events that satisfy $\chi^2_{\min} > 4$, $p_T(\ell), p_T(\bar{\ell}) > 5\text{GeV}$, $|\eta(\ell)|, |\eta(\bar{\ell})| < 2.5$ at $\sqrt{s} = 14\text{TeV}$ with 100ab^{-1}. As a references, the prediction of the CP-conserving case (the SM Higgs boson) is give by the black-solid line. The blue-dashed line and red-dotted line are the distributions for $\xi = \pi/4$ and $\xi = -\pi/4$, respectively. A simple χ^2 fit gives $\xi = 0.62 \pm 0.16$ and $\xi = -0.78 \pm 0.002$.

2.5.3 $h \to \gamma\gamma$ and $h \to Z\gamma$ via $\gamma \to e^+e^-$ conversion

Shown in Fig. 2.14 and Fig. 2.15 are the contour plots of the normalized production cross section (in unite of 10^-3) in the $p_T(\gamma) - \eta(\gamma)$ plane for the process $pp \to h \to \gamma\gamma$ and $pp \to h \to Z\gamma$ at $\sqrt{s} = 14\text{TeV}$, respectively. The bin size is 10GeV for $p_T(\gamma)$ and 0.2 for $\eta(\gamma)$. The BH conversion cross section is nearly constant over the interesting energy region of incident photons: $\sigma_{\text{BH}} = (2.64, 2.63, 2.62)\text{b}$ at $E_\gamma = (20, 30, 60)\text{GeV}$. However the probability of the converted e^+e^- can be resolved by the LHC detectors is not high. Because the detector is symmetric in the azimuthal angle direction in the laboratory frame, therefore the probability of resolved e^+e^- pair can be obtained by choosing the incident photon is in the $x - z$ plane in the laboratory frame. On the other hand $p_T(\gamma)$ and $\eta(\gamma)$ can affect the probability through the $\chi^2_{\min}$. Fig. 2.16 shows the probability of the conversion events when e^+e^- pair can be resolved by the condition $\chi^2_{\min} > \bar{\chi}^2_{\min}$, as a function of $\bar{\chi}^2_{\min}$ for $\eta_\gamma = 0$ and $E_\gamma = 30, 60\text{GeV}$ in Fig. 2.16. The typical conversion probability is only about 0.001. For $\bar{\chi}^2_{\min} \sim \mathcal{O}(1)$, the probability distribution has a very weak dependence on $\eta(\gamma)$, while a strong $\eta(\gamma)$ dependence appears in the low $\bar{\chi}^2_{\min}$ region because of the high sensitivity to angular resolution of the detector. Furthermore the high $p_T(\gamma)$ events have lower probabilities because the e^+e^- pair become more collinear. Compared to the internal splitting process, that the efficiency is about 70% for $\gamma^* \to e^-e^+$, and about 95% for $\gamma^* \to \mu^-\mu^+$, the photon conversion process can become compatible if the the current angular resolution can be improved by a factor of 4.

Fig. 2.17 shows the contour lines of the probability of the e^-e^+ pair that satisfy the angular resolution condition $\chi^2_{\min} > 4$ in the $p_T(\gamma) - \eta(\gamma)$ plane with $p_T(e^-), p_T(e^+) > 5\text{GeV}$. The probability decreases a little for increasing $|\eta(\gamma)|$ and $p_T(\gamma)$, and is at an order of $\sim 10^{-4}$ in almost all the interesting phase space.

In Ref. [36], the CP sensitivity is analyzed with the assumption that Higgs is at rest in the lab frame. Here we include the non-trivial p_T and η distribution of the Higgs by convoluting the production rate and BH conversion probability in the p_T and η plane (because of the symmetry of detector, the azimuthal angle direction is trivial and have been integrated). The probability of the e^-e^+ pair that satisfy the angular resolution condition $\chi^2_{\rm min} > 4$ for the process $pp \to \gamma\gamma$ is obtained by convoluting the probability of BH conversion process in the $p_T(\gamma) - \eta(\gamma)$ plane (see Fig. 2.17) and the probability (for single photon) of the photon production in the process $pp \to h \to \gamma\gamma$ (see Fig. 2.14). The contour plot is shown in Fig. 2.18. The probability roughly follows the distribution of the $pp \to h \to \gamma\gamma$ process. By summing over the phase space we find following total efficiencies

$$c_{\hat{\gamma}\hat{\gamma}} \approx 1.78 \times 10^{-4} \ . \tag{2.70}$$

The production cross section of $pp \to h \to \gamma\gamma$ at $\sqrt{s} = 14$TeV is about 123 fb. For an integrated luminosity 3 ab^{-1}, only about 5×10^{-4} events can be observed, assuming the photon conversion rate is 60%[53].

The probability of the e^-e^+ pair that satisfy the angular resolution condition $\chi^2_{\rm min} > 4$ for the process $pp \to Z(\ell\bar{\ell})\gamma$ can be obtained in the same way by convoluting the probability of BH conversion process in the $p_T(\gamma) - \eta(\gamma)$ plane (see Fig. 2.17) and the probability of the photon production in the process $pp \to h \to Z(\ell\bar{\ell})\gamma$ (see Fig. 2.15). The contour plot is shown in Fig. 2.19. The probability roughly follows the distribution of the $pp \to h \to Z(\ell\bar{\ell})\gamma$ process. By summing over the phase space we find following total efficiencies

$$c_{Z\hat{\gamma}} \approx 1.66 \times 10^{-4} \ . \tag{2.71}$$

The production cross section of $pp \to h \to Z(\ell\bar{\ell})\gamma$ at $\sqrt{s} = 14$TeV is about 5.7 fb. For an integrated luminosity 3 ab^{-1}, about 1 event can be observed, assuming the photon conversion rate is 60%[53].

2.5.4 Interference betwwen $h \to ZZ^\star$ and $h \to Z\gamma$

Recently it is pointed out in Ref.[24] that the interferences between tree level $h \to ZZ^*$ and loop level $h \to Z(\gamma)\gamma$ could enhance the experimental sensitivity. In this section we study the possible enhancement because of the interference. We will neglect the interference between $h \to ZZ^*$ and $h \to \gamma\gamma$ since the phase spaces of these two channels are populated completely different. The helicity amplitudes of the transverse contribution for the $h \to ZZ^*$ process has the same structure with the one for $h \to Z\gamma^*$ except some different coupling constants. The squared helicity amplitudes of the longitudinal contributions (including the interferences) are

$$|\mathcal{M}(\sigma_1,\sigma_2)|^2 \propto \omega^2 + g_{hV_1V_2}\omega(1+\sigma_1\sigma_2\cos\theta_1^*\cos\theta_2^*)\cos(\phi-\xi_{hV_1V_2})\,, \tag{2.72}$$

where

$$\omega = \frac{8\pi m_Z^2 \overline{v}_{HZZ}}{\alpha m_h^2 \kappa}\frac{s^2\kappa}{4s_1s_2}\left(1-\frac{(s_2-s_1)^2}{s^2}\right)\sin\theta_1^*\sin\theta_2^*\,. \tag{2.73}$$

We can see that there is an azimuthal angle correlation.

Fig. 2.20 shows the contributions of transverse and longitudinal contributions from $h \to ZZ^*$ and $h \to Z\gamma$ as well as their interferences with respect to the invariant mass m_2. For the longitudinal interference, since it is zero after the integral, therefore we integrate the azimuthal angle only in the range $(0,\pi/2)$. We can see that only in a small window $m_2 \in (1\text{GeV}, 5\text{GeV})$, the contributions is enhanced since interference, and the dominate contribution comes from the interference between longitudinal polarized $h \to ZZ^*$ and $h \to Z\gamma$. About 0.5% events of $h \to ZZ^*$ are in this window. So, the interference could not enhance the sensitivity.

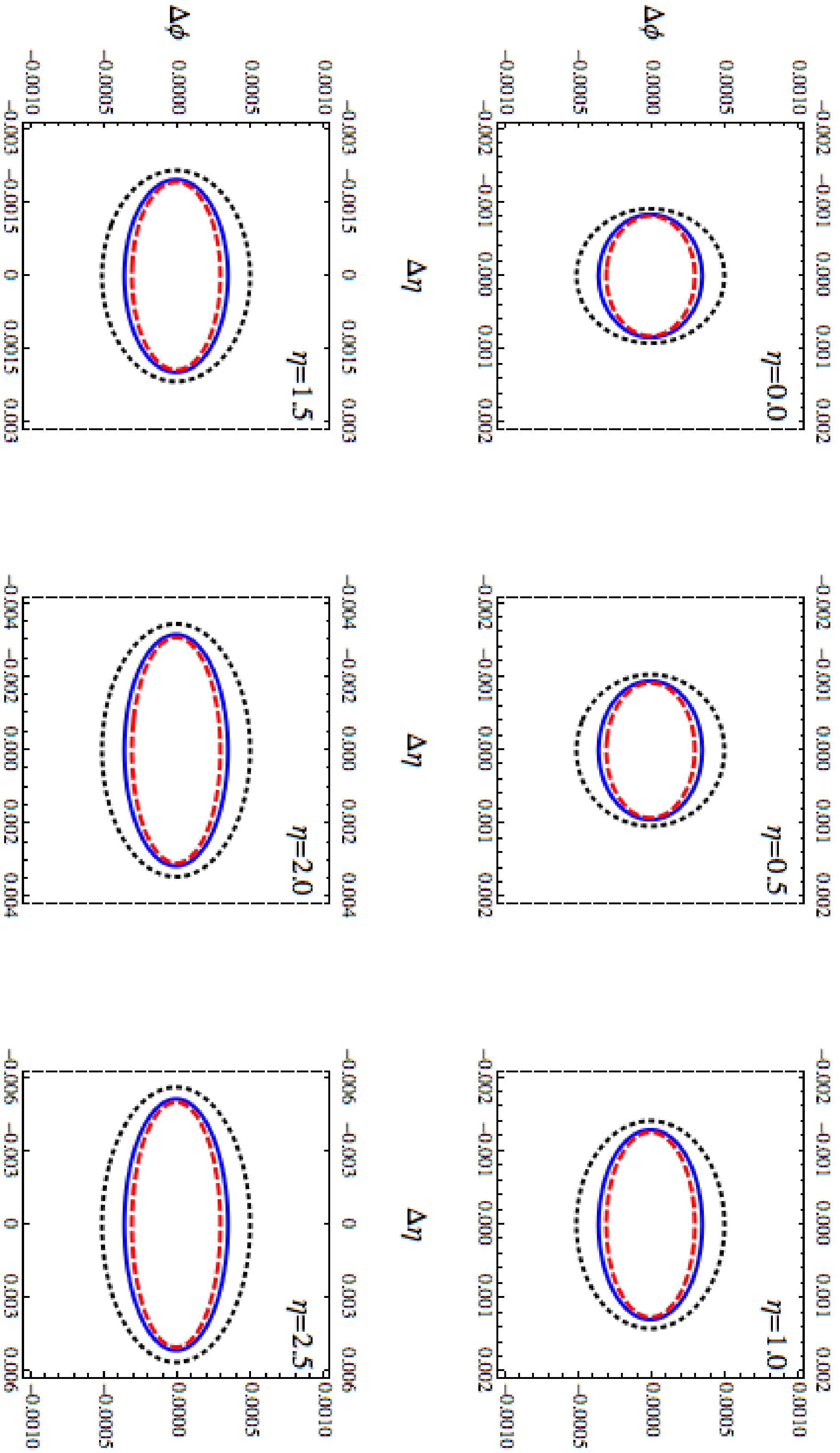

FIGURE 2.7: 1σ contour plots of the resolution for $\phi = 0$ and several $\eta = 0.0$, 0.5, 1.0, 1.5, 2.0, 2.5. In every plots, dotted-black line is for $p_T = 10$GeV, solid-blue line is for $p_T = 20$GeV and dashed-red line is for $p_T = 30$GeV.

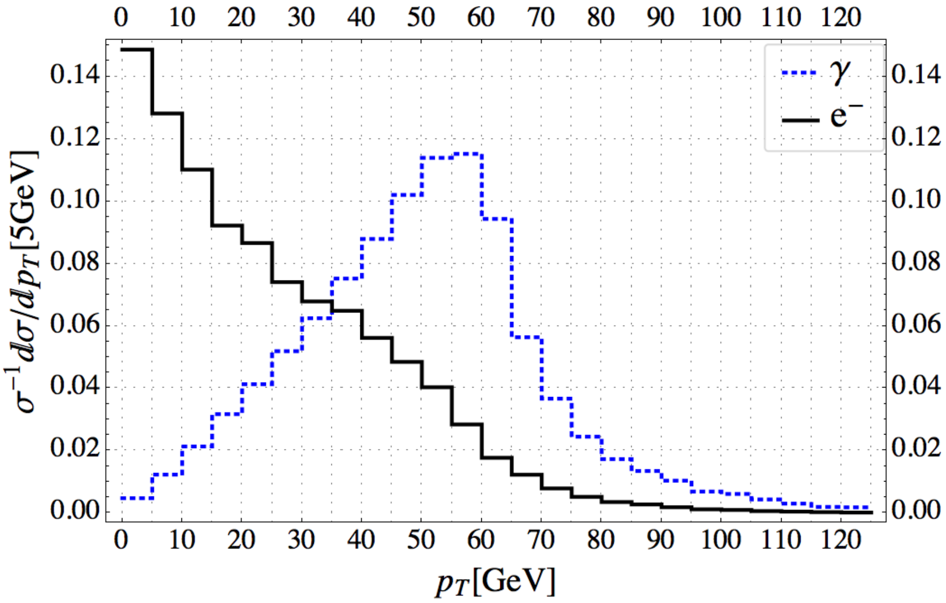

FIGURE 2.8: Transverse momentum distributions for process $pp \to h \to \gamma(e^-e^+)\gamma(e^-e^+)$. The distributions have been normalized to 1, *i.e.* half of the number of γ in $h \to \gamma\gamma$ and half of the number of ℓ in $h \to (\ell\bar{\ell})^2$. The blue-dotted line shows the p_T distribution of virtual photon and the black-solid line shows the p_T distribution of electron from virtual photon.

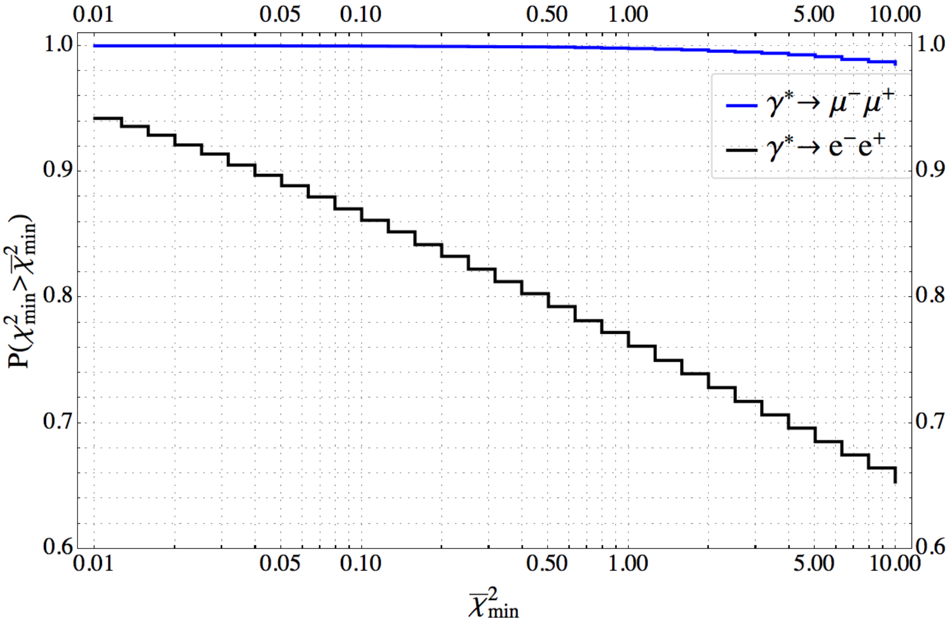

FIGURE 2.9: The probability of the $\gamma \to \ell\bar{\ell}$ splitting events that satisfy the angular resolution condition $\chi^2_{\min} > \bar{\chi}^2_{\min}$ for the process $pp \to h \to \gamma\gamma$. The blue-solid and the black-solid lines show the probabilities of the cut-off value $\bar{\chi}^2_{\min}$, respectively, for the $\gamma^\star \to \mu^-\mu^+$ and $\gamma^\star \to e^-e^+$ splitting events.

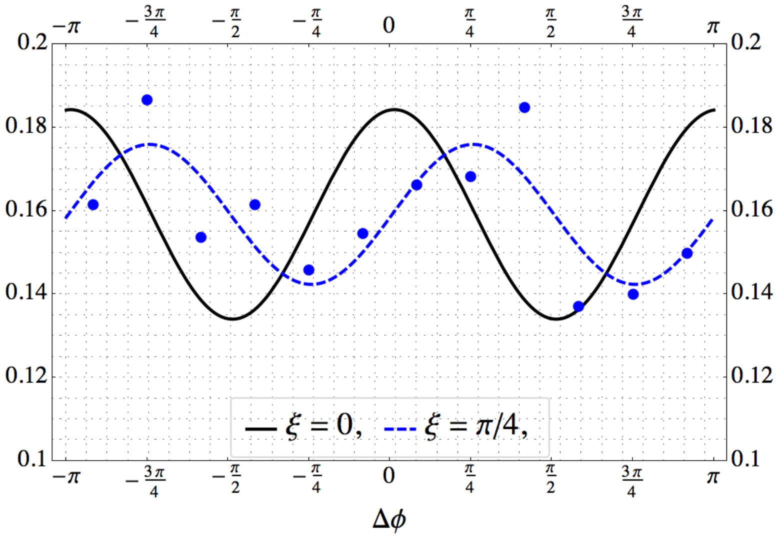

(a)

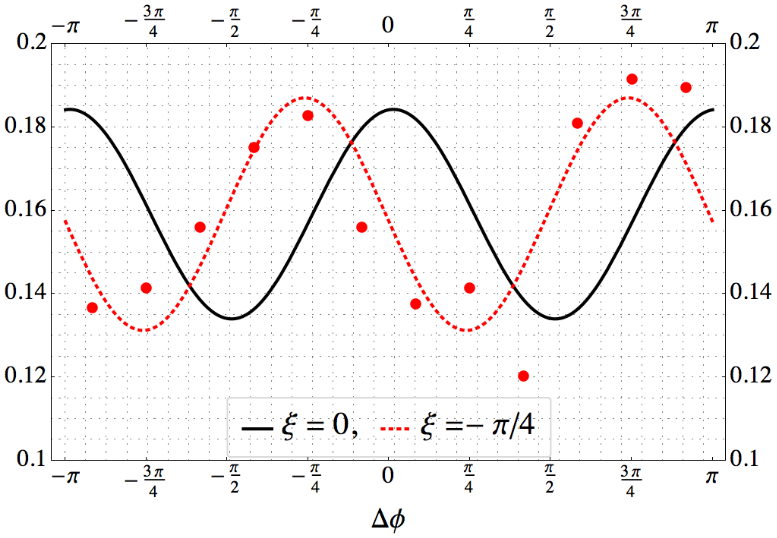

(b)

FIGURE 2.10: Azimuthal angle correlations for the process $pp \to h \to \gamma\gamma \to 4\ell$ with (a) $\xi = \pi/4$ and (b) $\xi = -\pi/4$. As a reference the prediction for the SM Higgs boson is shown by the black dots (and line). The data points correspond to an integrated luminosity $100\,\mathrm{ab}^{-1}$.

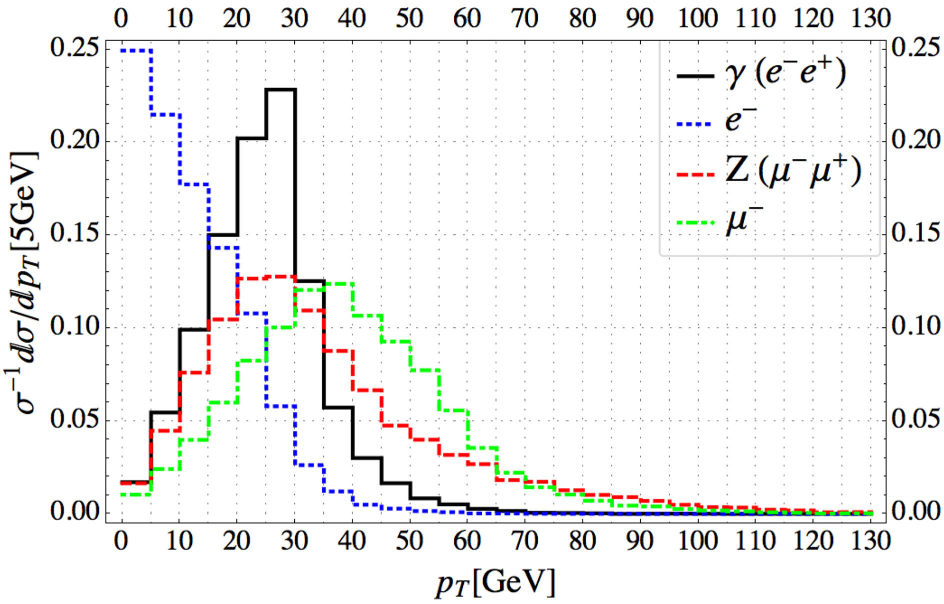

FIGURE 2.11: Transverse momentum distributions for process $pp \to h \to Z\gamma$. The solid-green line shows the $p_T$distribution of Z, the dashed-red line shows the $p_T$distribution of μ from Z decay, the dotted-blue line shows the $p_T$distribution of γ and the solid-black line shows the $p_T$distribution of e from virtual photon.

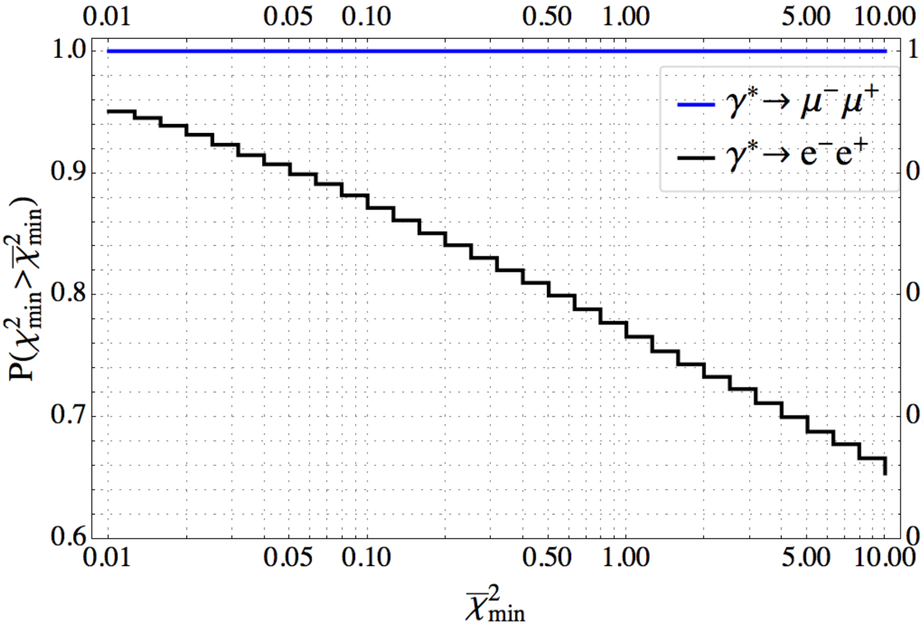

FIGURE 2.12: The probability of the $\gamma \to \ell\bar{\ell}$ splitting events that satisfy the angular resolution condition $\chi^2_{\min} > \bar{\chi}^2_{\min}$ for the process $pp \to h \to Z\gamma$. The blue-solid and the black-solid lines show the probabilities of the cut-off value $\bar{\chi}^2_{\min}$, respectively, for the $\gamma^\star \to \mu^-\mu^+$ and $\gamma^\star \to e^-e^+$ splitting events.

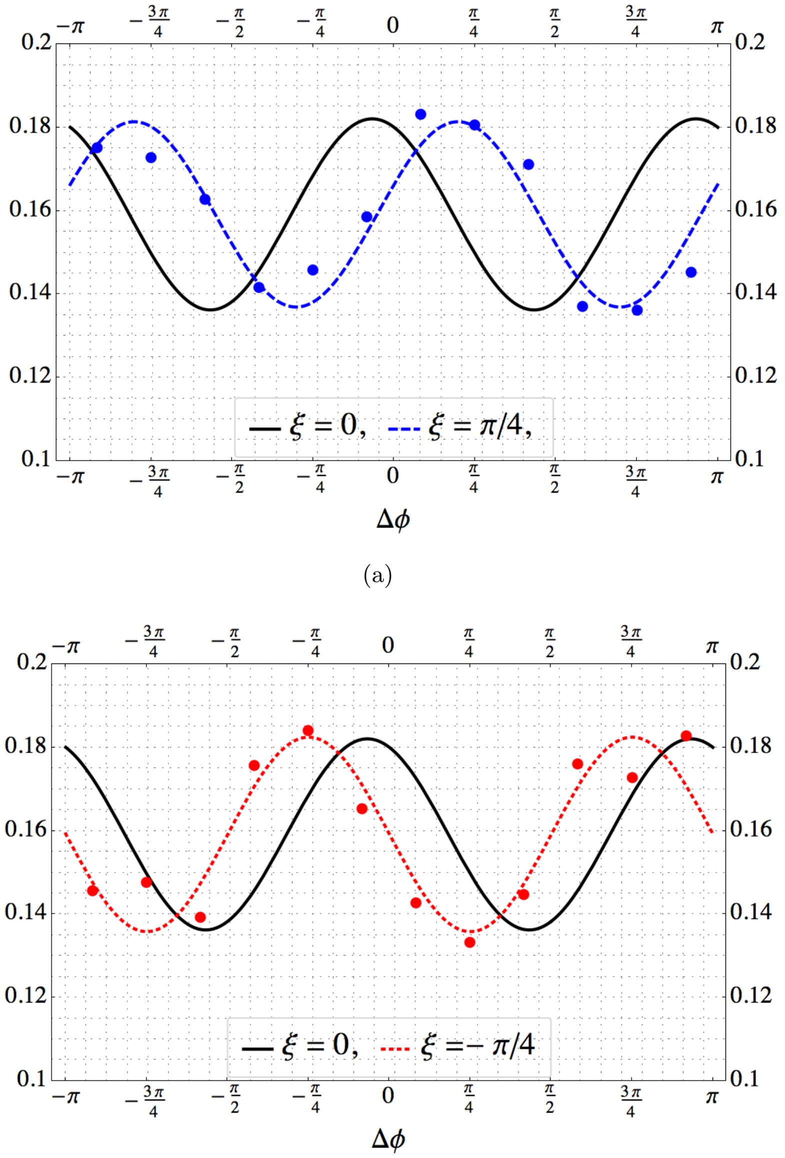

(a)

(b)

FIGURE 2.13: Azimuthal angle correlations for the process $pp \to h \to Z\gamma \to 4\ell$ with (a) $\xi = \pi/4$ (blue points and blue-dashed line) and (b) $\xi = -\pi/4$ (red points and red-dashed line). As a reference the prediction for the SM Higgs boson is shown by the black-solid line. The data points correspond to an integrated luminosity $100\,\mathrm{ab}^{-1}$.

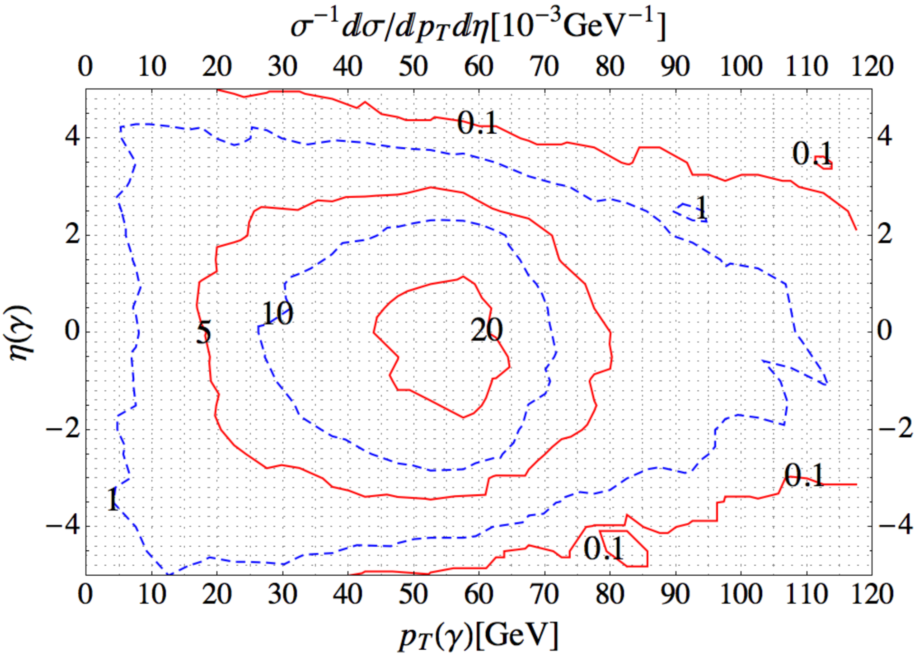

FIGURE 2.14: Contour plot of the normalized production cross section (in unite of 10^-3) in the $p_T(\gamma) - \eta(\gamma)$ plane for the process $pp \to h \to \gamma\gamma$. The bin size is 5GeV for $p_T(\gamma)$ and 0.2 for $\eta(\gamma)$.

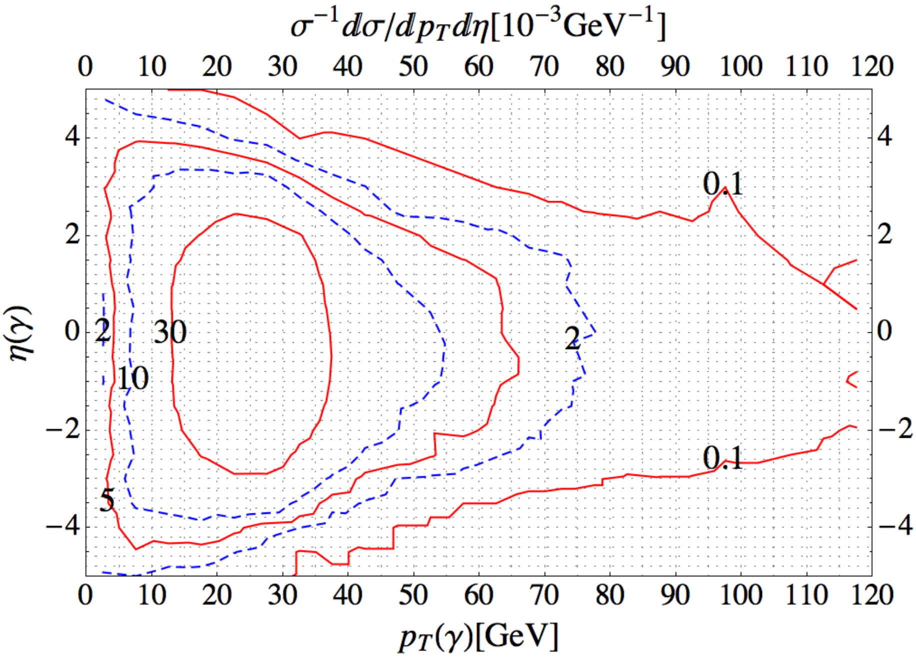

FIGURE 2.15: Contour plot of the normalized production cross section (in unite of 10^-3) in the $p_T(\gamma) - \eta(\gamma)$ plane for the process $pp \to h \to Z\gamma$. The bin size is 5GeV for $p_T(\gamma)$ and 0.2 for $\eta(\gamma)$.

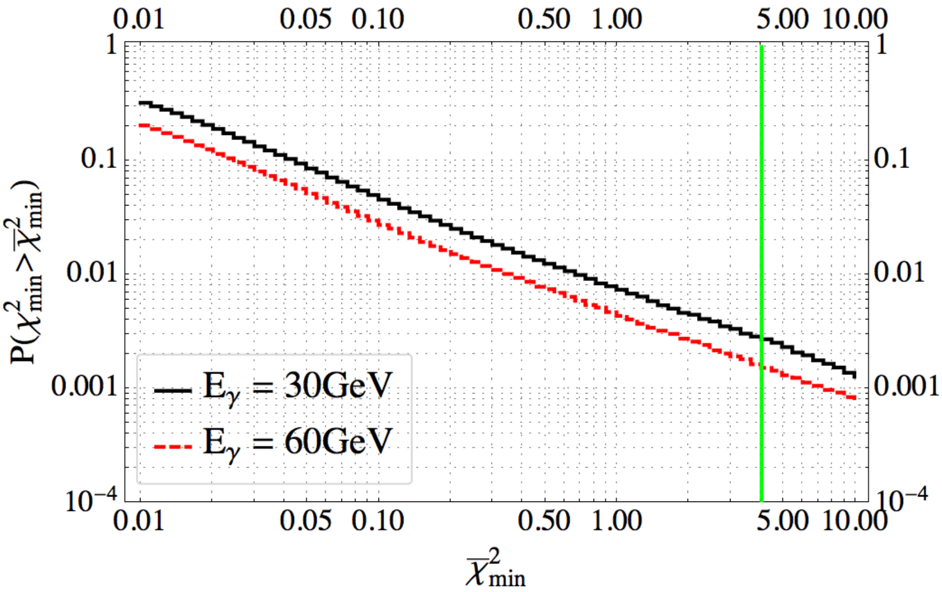

FIGURE 2.16: The probability of the $\hat{\gamma} \to e^-e^+$ that satisfy the angular resolution condition $\chi^2_{\rm min} > \bar{\chi}^2_{\rm min}$ for the BH conversion process $\gamma{\rm Si} \to \ell\bar{\ell}{\rm Si}$. The pseudo-rapidity of incident photon has been chosen as $\eta(\gamma) = 0$. The black-solid and the red-dashed lines show the probabilities for $p_T(\gamma) = E_\gamma = 30$GeV and $p_T(\gamma) = E_\gamma = 60$GeV, respectively.

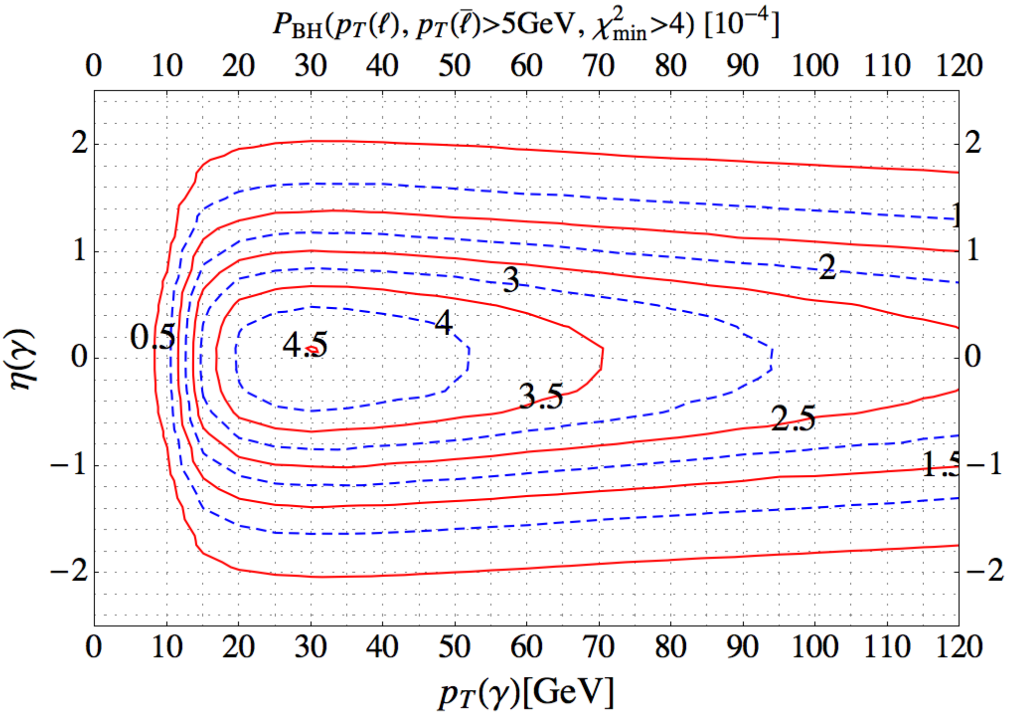

FIGURE 2.17: Contour plot of the probability of e^+e^- pair satisfying the angular resolution condition $\chi^2_{\rm min} > 4$, as well as $p_T(e^-), p_T(e^+) > 5$GeV for the BH conversion process. For convenience, the values have been enlarged by 10^4 times.

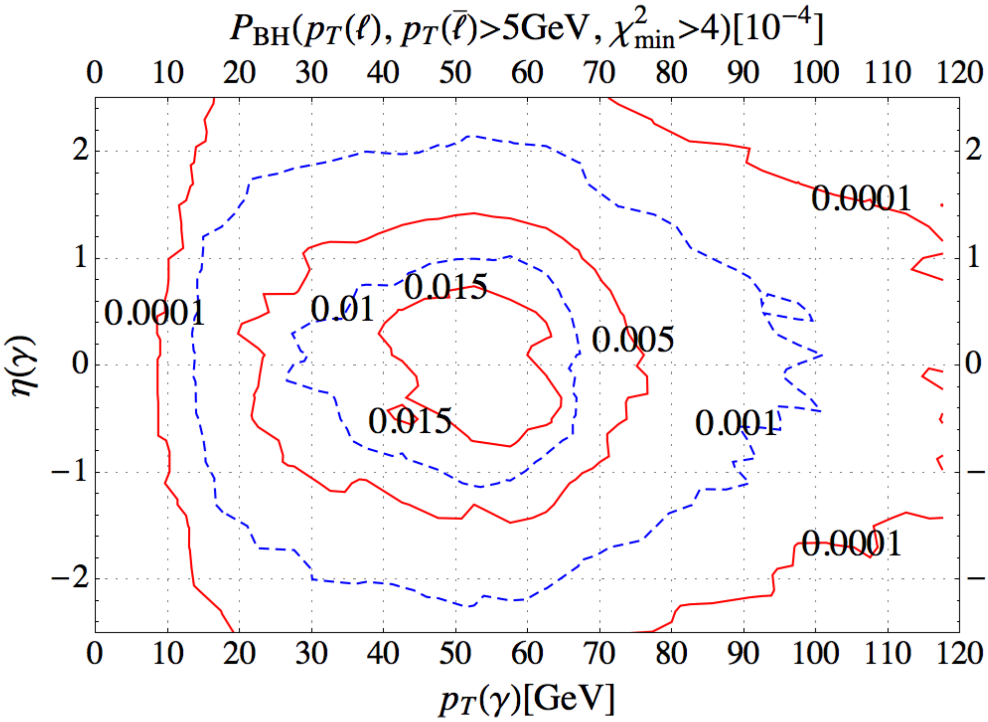

FIGURE 2.18: Contour plot of the probability of e^+e^- pair satisfying the angular resolution condition $\chi^2_{\rm min} > 4$, as well as $p_T(e^-), p_T(e^+) > 5$GeV for the process $pp \to h \to \gamma\gamma$. For convenience, the values have been enlarged by 10^4 times.

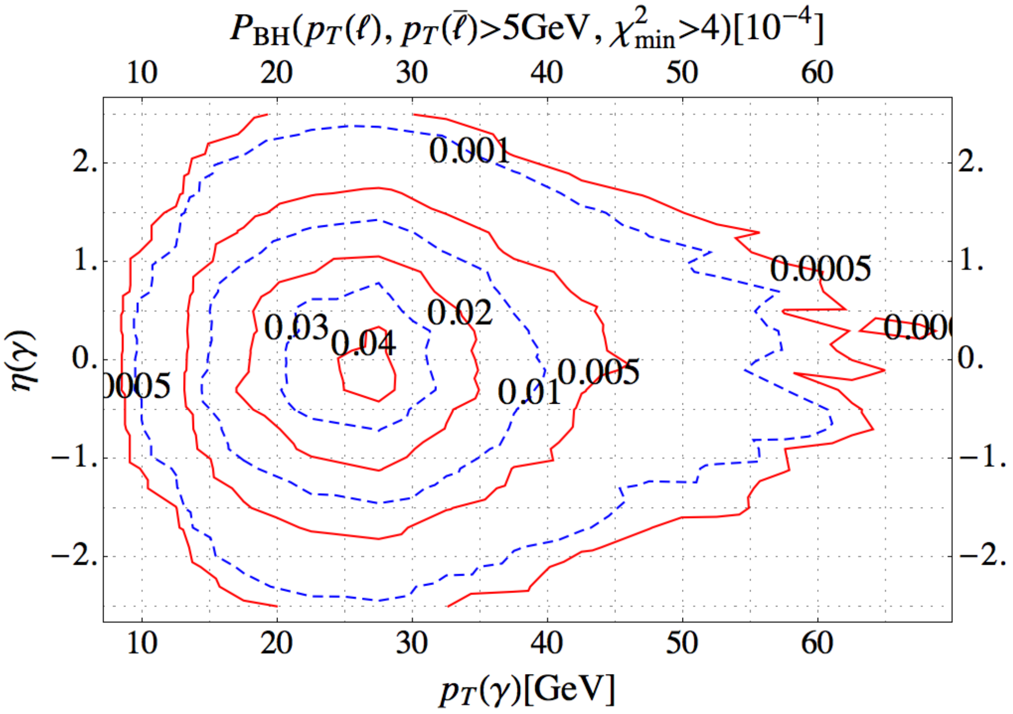

FIGURE 2.19: Contour plot of the probability of e^+e^- pair satisfying the angular resolution condition $\chi^2_{\rm min} > 4$, as well as $p_T(e^-), p_T(e^+) > 5$GeV for the process $pp \to h \to Z\gamma$. For convenience, the values have been enlarged by 10^4 times.

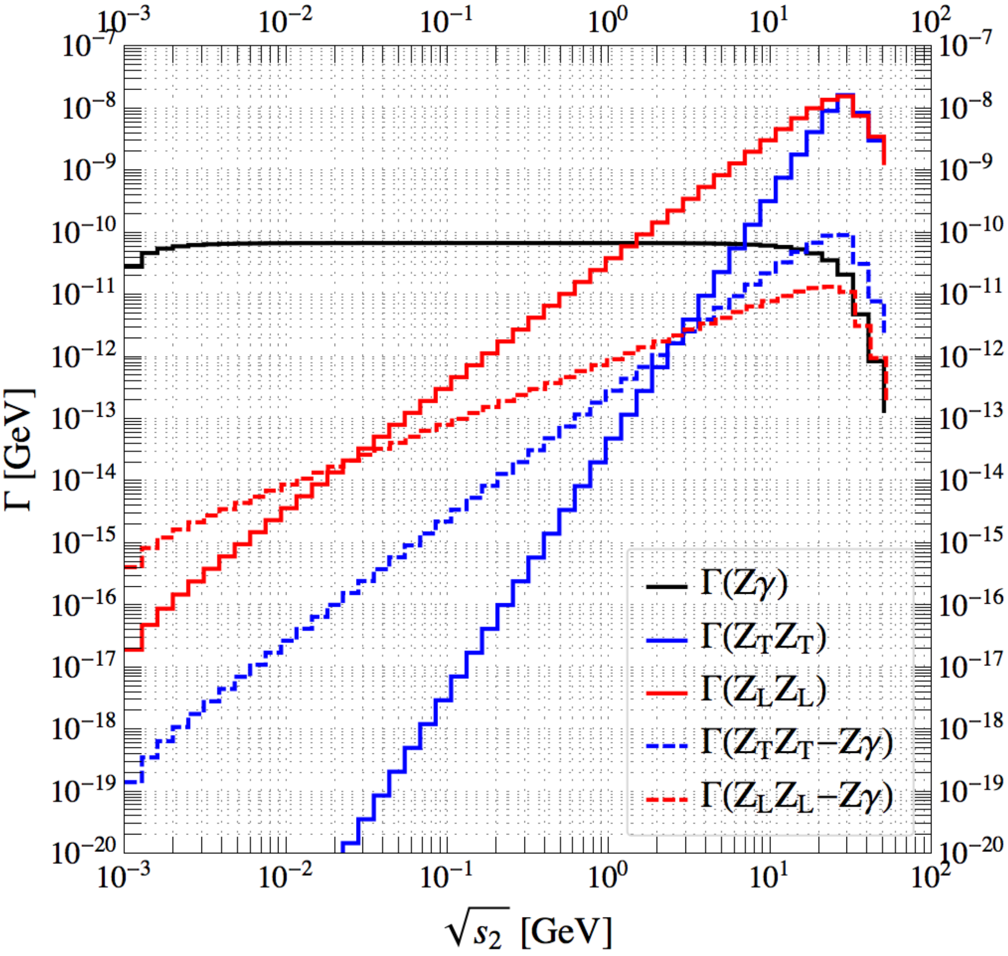

FIGURE 2.20: The black-solid, blue-solid, red-solid lines show the decay width distributions with respect to the invariant mass m_2 for $h \to Z\gamma$, and the longitudinal and transverse contributions of $h \to ZZ^*$. The dashed-blue line shows the interference between $h \to Z\gamma$ and the transverse part of $h \to ZZ^*$. The dashed-red line shows the interference between $h \to Z\gamma$ and the longitudinal part of $h \to ZZ^*$. For the longitudinal interference, since it is zero after the integral, therefore we integrate the azimuthal angle only in the range $(0, \pi/2)$.

Chapter 3

Probing CP violation in $h \to \tau^-\tau^+$ at the LHC

The spin correlation in the $h \to \tau^+\tau^-$ decay is an ideal observable of measuring the CP composition of the Higgs particle [70–78]. However the presence of at least two neutrinos in the final state makes the measurement challenging. In Ref. [72], it was pointed out that the plane spent by $\pi^\pm$ and π^0 from the $\tau \to \rho\nu$ decay can be used to measure the CP violation. However, because the large error in the reconstruction of π^0 momentum, the experimental sensitivity is low. This method was improved by using the impact parameters in [73]. However, because of the lack of the neutrino momentum, there is still a type of twofold ambiguity in reconstructing the τ momentum. Therefore the improvement factor is only about 1.5. In Ref.[74], a similar observable was proposed and they found the experimental sensitivity is $\sim 11^\circ$(or 0.19 in radian) for LHC14 with an integrated luminosity $3\,\mathrm{ab}^{-1}$.

In Ref. [75], the 3-prong decay mode of tau was proposed to measure the CP violation. The advantage is the tau momentum direction can be reconstructed directly. However, sensitivity is very low, because first the branching ratio of 3-prong decay mode is relatively low, second the longitudinal polarized state of a meson has to be selected out for measuring the nontrivial spin correlation. In Ref. [76–78], a new observable defined by using impact parameter and the momentum of charged decay products of tau was proposed to measure the CP violation. However, since the impact parameter carries only part of the spin correlation information, therefore the asymmetry gets diluted, and hence the signal strength is reduced. By combine all the channels, it was found that the experimental sensitivity is $\Delta\xi_{h\tau\tau}$ 0.05 at ILC with $\sqrt{s} = 500$GeV with an integrated luminosity $1\,\text{ab}^{-1}$[78].

We propose a novel method to reconstruct event by event the full kinematics of the $h \to \tau^+(\pi^+\bar{\nu}_\tau)\tau^-(\pi^-\nu_\tau)$ decay process, that makes use of the impact parameter vectors of the τ^+ and τ^- decay pions and the probability distribution functions of the missing p_T vector and the angular separation ΔR between the charged π's. and the neutrinos. We find an excellent agreement between the reconstructed and true kinematics in both the $\tau^+\tau^-(h)$ rest frame and also in the $\pi^+\pi^-$ rest frames, by using the typical experimental resolutions of the LHC detectors. By including the major $Z \to \tau^+\tau^-$ background, the experimental sensitivity to the mixing angle can reach $\Delta\xi_{h\tau\tau}0.10$ with an integrated luminosity 3ab^{-1}, which is better than the result in Ref. [74] by a factor of two. Furthermore, in Ref. [74], they didn't study the detector effects on neutral pion π^0 momentum measurement, which has very large uncertainty and hence can reduce significantly their estimation of experimental sensitivity.

3.1 Parameterization of the $h\tau\tau$ interactions

In the analysis below we assume for simplicity the measured scalar particle is a mixture of CP-even and CP-odd scalars, denoted by H and A respectively.

$$h = \cos\xi\, H + \sin\xi\, A = \frac{1}{\sqrt{1+|\epsilon|^2}}(H + \epsilon A)\,. \tag{3.1}$$

We also assume the Yukawa interactions of H and A with tau-lepton pair are separately CP conserving separately,

$$\mathcal{L} = -g_{H\tau\tau} H\bar{\tau}\tau - i g_{A\tau\tau} A\bar{\tau}\gamma^5\tau\,, \tag{3.2}$$

such that the only source of CP violation is because of mixing (3.1). The interactions between the mass eigenstate $h(125)$ and the tau-lepton pair is then described by

$$\mathcal{L} = -g_{h\tau\tau} h\big(\bar{\tau}\tau + i\epsilon_{h\tau\tau}\bar{\tau}\gamma^5\tau\big)\,, \tag{3.3}$$

where

$$\begin{aligned} g_{h\tau\tau} &= g_{H\tau\tau}\cos\xi && (3.4)\\ \epsilon_{h\tau\tau} &= \tan\xi_{h\tau\tau} = \frac{g_{A\tau\tau}}{g_{H\tau\tau}}\tan\xi\,. && (3.5)\end{aligned}$$

It is worth noting that the effective strengths of the CP-violating hff couplings can be different for each fermion, so that the partial decay width could be significantly different from the SM value. However, here and after, we will use the SM branching ratio of $h \to \tau^-\tau^+$, $R_\tau = 6.1\%$ [94] to estimate the experimental sensitivity.

3.2 Helicity Amplitude in the Higgs rest frame

In this section we give the helicity amplitudes of Higgs decay in the Higgs rest frame. The momenta and the helicities are defined as follows

$$\begin{aligned} h(q) &\to \tau^-(q_1,\lambda_1) + \tau^+(q_2,\lambda_2) && (3.6)\\ &\to \pi^-(k_1) + \nu_\tau(k_3,-) + \pi^+(k_2) + \bar{\nu}_\tau(k_4,+) && (3.7)\end{aligned}$$

The helicities take the values $\lambda_i/2$ for leptons and with $\lambda_i = \pm 1$. The total decay helicity amplitudes can be expressed in terms of the τ-pair production amplitude and the τ decay amplitudes, which can give us better understanding of the distributions. Using the completeness relations

$$\not{q}_1 + m = \sum_{\lambda_1} u(q_1,\lambda_1)\bar{u}(q_1,\lambda_1), \quad (3.8a)$$

$$\not{q}_2 - m = \sum_{\lambda_2} v(q_2,\lambda_2)\bar{v}(q_2,\lambda_2), \quad (3.8b)$$

the full amplitude can be expressed as the product of the tau-pair production amplitude ($\mathcal{M}_P$) and two $\tau \to \pi\nu$ decay amplitudes ($\mathcal{M}_{1,2}$):

$$\mathcal{M} = D(q_1^2)D(q_2^2)\sum_{\lambda_{1,2}} \mathcal{M}_P(q_1,\lambda_1;q_2,\lambda_2)\,\mathcal{M}_1(q_1,\lambda_1;k_1;k_3)\,\mathcal{M}_2(q_2,\lambda_2;k_2;k_4) \quad (3.9)$$

with the τ propagator factor $D(q^2) = (q^2 - m^2 + im\Gamma)^{-1}$. It is straightforward to obtain the squared matrix elements of the full production plus decay amplitudes,

$$\sum |\mathcal{M}|^2 = \left|D(q_1^2)D(q_2^2)\right|^2 \sum_{\lambda_1,\lambda_2} \sum_{\bar\lambda_1,\bar\lambda_2} \mathcal{P}^{\lambda_1\lambda_2}_{\bar\lambda_1\bar\lambda_2}\, \mathcal{D}_1{}^{\lambda_1}_{\bar\lambda_1} \mathcal{D}_2{}^{\lambda_2}_{\bar\lambda_2} \tag{3.10}$$

in terms of the production density matrix $\mathcal{P}^{\lambda_1\lambda_2}_{\bar\lambda_1\bar\lambda_2}$ and the decay density matrices $\mathcal{D}_{1,2}{}^{\lambda_{1,2}}_{\bar\lambda_{1,2}}$;

$$\mathcal{P}^{\lambda_1\lambda_2}_{\bar\lambda_1\bar\lambda_2} = \sum_\sigma \mathcal{M}^{\lambda_1\lambda_2}_\sigma \big(\mathcal{M}^{\bar\lambda_1\bar\lambda_2}_\sigma\big)^*, \tag{3.11}$$

$$\mathcal{D}_1{}^{\lambda_1}_{\bar\lambda_1} = \mathcal{M}_{\lambda_1}\big(\mathcal{M}_{\bar\lambda_1}\big)^*, \tag{3.12}$$

$$\mathcal{D}_2{}^{\lambda_2}_{\bar\lambda_2} = \mathcal{M}_{\lambda_2}\big(\mathcal{M}_{\bar\lambda_2}\big)^*. \tag{3.13}$$

In the narrow width limit the propagator factor becomes

$$|D(q^2)|^2 \to \frac{\pi}{m\Gamma}\,\delta(q^2 - m^2). \tag{3.14}$$

In the Higgs rest frame, we choose the τ^- momentum direction as the z-axis,

$$q_1^\mu = \frac{\sqrt{s}}{2}\big(1 + \frac{q_1^2 - q_2^2}{s}, 0, 0, \beta\big), \tag{3.15}$$

$$q_2^\mu = \frac{\sqrt{s}}{2}\big(1 + \frac{q_2^2 - q_1^2}{s}, 0, 0, -\beta\big), \tag{3.16}$$

where $s = m_h^2$, $\beta = \bar\beta\big(\frac{q_1^2}{\hat s}, \frac{q_2^2}{\hat s}\big)$ with $\bar\beta(a,b)$ defined as follows

$$\bar\beta(a,b) \equiv (1 + a^2 + b^2 - 2a - 2b - 2ab)^{1/2}. \tag{3.17}$$

The momenta of the τ^- decay products are parametrized in the τ^- rest frame,

$$k_1 = \frac{\sqrt{q_1^2}}{2}(1 + \frac{m_\pi^2}{q_1^2}, \beta_1\sin\theta_1\cos\phi_1, \beta_1\sin\theta_1\sin\phi_1, \beta_1\cos\theta_1), \tag{3.18}$$

$$k_3 = \frac{\sqrt{q_1^2}}{2}(1 - \frac{m_\pi^2}{q_1^2}, -\beta_1\sin\theta_1\cos\phi_1, -\beta_1\sin\theta_1\sin\phi_1, -\beta_1\cos\theta_1), \tag{3.19}$$

with $\beta_1 = 1 - m_\pi^2/q_1^2$. Similarly, the momenta of the τ^+ decay products are defined as follows

$$k_2 = \frac{\sqrt{q_2^2}}{2}(1 + \frac{m_\pi^2}{q_2^2}, \beta_2 \sin\theta_2 \cos\phi_2, \beta_2 \sin\theta_2 \sin\phi_2, \beta_2 \cos\theta_2), \tag{3.20}$$

$$k_4 = \frac{\sqrt{q_2^2}}{2}(1 - \frac{m_\pi^2}{q_2^2}, -\beta_2 \sin\theta_2 \cos\phi_2, -\beta_2 \sin\theta_2 \sin\phi_2, -\beta_2 \cos\theta_2), \tag{3.21}$$

with $\beta_2 = 1 - m_\pi^2/q_2^2$. The z-axis and the y-axis normal to the scattering plane are chosen common to all the three frames, and the two decay frames differ only by the boost along the τ^- moving direction. The τ decay width is very narrow, $\Gamma \sim \mathcal{O}(10^{-12}\,\text{GeV})$, and hence we take the narrow width limit, $q_1^2 = q_2^2 = m^2$, in the following analytic amplitudes.

The amplitude for the Higgs decay to tau-lepton pair is

$$\mathcal{M}_P = \frac{\lambda}{2}\tilde{g}_{h\tau\tau}\sqrt{s}\,\beta e^{i\lambda\tilde{\xi}_{h\tau\tau}}, \tag{3.22}$$

where $\lambda = \lambda_1 = \lambda_2$,

$$\tilde{\xi}_{h\tau\tau} = \frac{\xi_{h\tau\tau}}{\beta}. \tag{3.23}$$

Because $\beta \approx 1$, here and after we will always neglect this kinematical factor. The production density matrix elements are

$$\mathcal{P}_{++}^{++} = \frac{1}{4}\tilde{g}_{h\tau\tau}^2 s\,\beta^2\,, \tag{3.24}$$

$$\mathcal{P}_{--}^{--} = \frac{1}{4}\tilde{g}_{h\tau\tau}^2 s\,\beta^2\,, \tag{3.25}$$

$$\mathcal{P}_{--}^{++} = -\frac{1}{4}\tilde{g}_{h\tau\tau}^2 s\,\beta^2 e^{2i\xi_{h\tau\tau}}\,, \tag{3.26}$$

The τ-ν_τ-π vertex can be parameterized by the effective interaction Lagrangian:

$$\mathcal{L}_\pi = \sqrt{2}G_F f_1\, \bar{\tau}\gamma^\mu P_L \nu_\tau\, \partial_\mu\pi^- + \bar{\nu}_\tau\gamma^\mu P_L \tau\, \partial_\mu\pi^+ \tag{3.27}$$

with the chiral projection operator $P_L = (1-\gamma^5)/2$, and the constant form factor

$$f_1 = f_\pi \cos\theta_C, \tag{3.28}$$

where the pion decay constant $f_1 = 0.13041\text{GeV}$ and $\cos\theta_C = 0.97418$. The $\tau \to \pi\nu$ decay amplitudes in the τ rest frame are

$$\mathcal{M}_{1,2} = -G_F f_\pi m^2 \sqrt{\beta_{1,2}}\, \hat{\mathcal{M}}_{\lambda_{1,2}}, \tag{3.29}$$

where

$$\hat{\mathcal{M}}_{\lambda_1} = \sqrt{1+\lambda_1 \cos\theta_1}\, e^{i\lambda_1\phi_1/2}, \tag{3.30a}$$

$$\hat{\mathcal{M}}_{\lambda_2} = \sqrt{1+\lambda_2 \cos\theta_2}\, e^{-i\lambda_2\phi_2/2}\,. \tag{3.30b}$$

Then the decay density matrix is

$$\mathcal{D}^{++}_{++} = (G_F f_\pi m^2)^4 \beta_1\beta_2 (1+\cos\theta_1)(1+\cos\theta_2)\,, \tag{3.31}$$

$$\mathcal{D}^{--}_{--} = (G_F f_\pi m^2)^4 \beta_1\beta_2 (1-\cos\theta_1)(1-\cos\theta_2)\,, \tag{3.32}$$

$$\mathcal{D}^{++}_{--} = (G_F f_\pi m^2)^4 \beta_1\beta_2 \sin\theta_1 \sin\theta_2 e^{i(\phi_1-\phi_2)}\,. \tag{3.33}$$

We can see that there are spin correlations. Define the energy fractions of pions in the Higgs rest frame as $z_1 = E_{\pi^-}/E_{\tau^-}$ and $z_2 = E_{\pi^+}/E_{\tau^+}$ which can be written as

$$z_1 = (1+\cos\theta_1)/2 \quad \text{and} \quad z_2 = (1-\cos\theta_2)/2, \tag{3.34}$$

in the massless limit, the spin correlation can be written as

$$|\mathcal{M}|^2 \propto 4z_1(1-z_2) + 4(1-z_1)z_2 + 8\sqrt{z_1(1-z_1)}\sqrt{z_2(1-z_2)}\cos(\phi_1-\phi_2+2\xi_{h\tau\tau}) \tag{3.35}$$

3.3 Helicity amplitudes in the $\pi^+\pi^-$ rest frame

In this section we give the helicity amplitudes of Higgs decaying to tau pair with subsequent decays of tau in pion mode. Again the total helicity amplitude can be written as the product of production and decay helicity amplitudes,

$$\widehat{\mathcal{M}} = D(q_1^2)D(q_2^2) \sum_{\lambda_1,\lambda_1} \widehat{\mathcal{M}}_P(q_1,\lambda_1;q_2,\lambda_2)\, \widehat{\mathcal{M}}_{D1}(q_1,\lambda_1)\, \widehat{\mathcal{M}}_{D2}(q_2,\lambda_2)\,. \tag{3.36}$$

We have used "$\widehat{\ }$" to distinguish the helicity amplitudes defined here from those given in last section. Because the production and decay helicity amplitudes are Lorentz invariant separately, so we can calculate them in different reference frame, as long as the helicities are preserved. Let us first define the momenta of every particles in the $\pi^+\pi^-$ rest frame as follows

$$\begin{aligned}
k_1^\mu &= E_\pi(1,0,0,\beta_\pi) && \text{(3.37a)}\\
k_2^\mu &= E_\pi(1,0,0,-\beta_\pi) && \text{(3.37b)}\\
q_1^\mu &= E_1(1,\beta_1\sin\theta_1\cos\phi_1,\beta_1\sin\theta_1\sin\phi_1,\beta_1\cos\theta_1) && \text{(3.37c)}\\
q_2^\mu &= E_2(1,\beta_2\sin\theta_2\cos\phi_2,\beta_2\sin\theta_2\sin\phi_2,\beta_2\cos\theta_2) && \text{(3.37d)}\\
k_3^\mu &= E_1(1-x_1,\beta_1\sin\theta_1\cos\phi_1,\beta_1\sin\theta_1\sin\phi_1,\beta_1\cos\theta_1-x_1\beta_\pi) && \text{(3.37e)}\\
k_4^\mu &= E_2(1-x_2,\beta_2\sin\theta_2\cos\phi_2,\beta_2\sin\theta_2\sin\phi_2,\beta_2\cos\theta_2-x_2\beta_\pi) && \text{(3.37f)}
\end{aligned}$$

where $x_i = E_\pi/E_i$ are the energy fractions of π^- and π^+ with respect to τ^- and τ^+ in the $\pi^+\pi^-$ rest frame. In the calculations of the helicity amplitudes we neglect the mass of pion and tau, which is a good approximation because in the event selection we will require the pions have large transverse momenta so that the mass effects are negligible.

Since the usefulness of spin conservation along the z-axis in the Higgs rest frame, the production helicity amplitude $\widehat{\mathcal{M}}_P(q_1,\lambda_1;q_2,\lambda_2)$ is again calculated in the Higgs rest frame that has been given in last section, therefore

$$\widehat{\mathcal{M}}_P(q_1,\lambda_1;q_2,\lambda_2) = \mathcal{M}_P(q_1,\lambda_1;q_2,\lambda_2)\,, \tag{3.38}$$

where the helicities λ_i are quantized along the z-axis in the Higgs rest frame. The $\pi^+\pi^-$ rest frame is related to the Higgs rest frame by the Lorentz transformation $\Lambda^{-1}(\vec{p}_h)$ where $\vec{p}_h$ is the Higgs momentum in the $\pi^+\pi^-$ rest frame. Therefore the helicities λ_i of the spins of $\tau^\mp$ in the Higgs rest frame equal to the helicities λ_i' of the spins of $\tau^\mp$ quantized along the z-axis in the $\pi^+\pi^-$ rest frame. Therefore once we know the decay helicity amplitudes quantized along the z-axis in the $\pi^+\pi^-$ rest frame, then we can obtain the full helicity amplitudes.

The decay helicity amplitudes quantized along the z-axis in the $\pi^+\pi^-$ rest frame are related to the decay helicity amplitudes quantized along the moving directions of τ^+ and τ^- by nontrivial Wigner rotation. Let us first give the helicity amplitudes for the latter case. In the mass less approximation, the only nonzero helicity amplitudes are those with $\sigma_1 = -1$ for τ^- and $\sigma_2 = +1$ for τ^+ (note that the helicities σ_i are quantized along the moving directions of τ^+ and τ^- in the $\pi^+\pi^-$ rest frame), and the corresponding helicity amplitudes are

$$\widehat{\mathcal{M}}_{1,-} = 4\sqrt{2}G_F f_1 E_1 \sqrt{E_\pi}\sqrt{1-x_1}\sin\frac{\theta_1}{2}\sin\frac{\theta_\nu}{2}\,, \tag{3.39}$$

$$\widehat{\mathcal{M}}_{2,+} = 4\sqrt{2}G_F f_1 E_2 \sqrt{E_\pi}\sqrt{1-x_2}\cos\frac{\theta_1}{2}\cos\frac{\theta_{\bar\nu}}{2}\,. \tag{3.40}$$

The helicity amplitudes quantized along the z-axis in the $\pi^+\pi^-$ rest frame then can be obtained by using following Wigner rotations

$$\widehat{\mathcal{M}}'_{1,\lambda'_1} = \left[D^{1/2}_{-,\lambda'_1}(\theta_1,\phi_1)\right]^{-1}\widehat{\mathcal{M}}_{1,-} = \left[D^{1/2}_{\lambda'_1,-}(\theta_1,\phi_1)\right]^{*}\widehat{\mathcal{M}}_{1,-}\,, \tag{3.41}$$

$$\widehat{\mathcal{M}}'_{2,\lambda'_2} = \left[D^{1/2}_{+,\lambda'_2}(\theta_2,\phi_2)\right]^{-1}\widehat{\mathcal{M}}_{2,+} = \left[D^{1/2}_{\lambda'_2,+}(\theta_2,\phi_2)\right]^{*}\widehat{\mathcal{M}}_{2,+}\,. \tag{3.42}$$

The explicit expressions are

$$\widehat{\mathcal{M}}'_{1,+} = -N_1\sin\frac{\theta_1}{2}\sin\frac{\theta_1}{2}\sin\frac{\theta_\nu}{2}e^{i\phi_1}\,, \tag{3.43a}$$

$$\widehat{\mathcal{M}}'_{1,-} = N_1\cos\frac{\theta_1}{2}\sin\frac{\theta_1}{2}\sin\frac{\theta_\nu}{2}\,, \tag{3.43b}$$

$$\widehat{\mathcal{M}}'_{2,+} = N_2\cos\frac{\theta_2}{2}\cos\frac{\theta_2}{2}\cos\frac{\theta_{\bar\nu}}{2}\,, \tag{3.43c}$$

$$\widehat{\mathcal{M}}'_{2,-} = N_2\sin\frac{\theta_2}{2}\cos\frac{\theta_2}{2}\cos\frac{\theta_{\bar\nu}}{2}e^{-i\phi_2}\,. \tag{3.43d}$$

By definition, the helicity of τ^- in the Higgs rest frame λ_1 equals to its helicity quantized along the z-axis in the same frame, while there is a minus sign for τ^+. Therefore we have $\lambda'_1 = \lambda_1$ and $\lambda'_2 = \lambda_2$. Furthermore we have $\lambda_1 = \lambda_2$, *i.e.* $\lambda'_1 = -\lambda'_2$ for the spin conservation along the quantization axis. Therefore the total decay helicity amplitudes in terms of helicities λ_i are

$$\widehat{\mathcal{M}}_D(+,+) = -\frac{1}{4}N_1N_2\sin\theta_2(1-\cos\theta_1)\cos\frac{\theta_{\bar\nu}}{2}\sin\frac{\theta_\nu}{2}e^{i(\phi_1-\phi_2)}\,, \tag{3.44a}$$

$$\widehat{\mathcal{M}}_D(-,-) = \frac{1}{4}N_1N_2\sin\theta_1(1+\cos\theta_2)\cos\frac{\theta_{\bar\nu}}{2}\sin\frac{\theta_\nu}{2}\,. \tag{3.44b}$$

Then the decay density matrix can be written as

$$\widehat{\mathcal{D}}^{++}_{++} = \frac{1}{16} N_1^2 N_2^2 \sin^2\theta_2 (1-\cos\theta_1)^2 \cos^2\frac{\theta_{\bar{\nu}}}{2} \sin^2\frac{\theta_\nu}{2}\,, \tag{3.45}$$

$$\widehat{\mathcal{D}}^{--}_{--} = \frac{1}{16} N_1^2 N_2^2 \sin^2\theta_1 (1+\cos\theta_2)^2 \cos^2\frac{\theta_{\bar{\nu}}}{2} \sin^2\frac{\theta_\nu}{2}\,, \tag{3.46}$$

$$\widehat{\mathcal{D}}^{++}_{--} = -\frac{1}{16} N_1^2 N_2^2 \sin\theta_1 \sin\theta_2 (1-\cos\theta_1)(1+\cos\theta_2) \cos^2\frac{\theta_{\bar{\nu}}}{2} \sin^2\frac{\theta_\nu}{2} e^{i(\phi_1-\phi_2)} \tag{3.47}$$

Including the production density matrix we can see that there is a azimuthal angle correlation. The squared matrix element is

$$\begin{aligned} |\widehat{\mathcal{M}}|^2 \;\propto\; & (1+\cos\theta_{\bar{\nu}})(1-\cos\theta_\nu)\Bigg(\sin^2\theta_1 (1+\cos\theta_2)^2 + \sin^2\theta_2 (1-\cos\theta_1)^2 \\ & - \; 2\sin\theta_1 \sin\theta_2 (1-\cos\theta_1)(1+\cos\theta_2)\cos\left(\phi_1-\phi_2-2\xi_{h\tau\tau}\right)\Bigg)\,. \end{aligned} \tag{3.48}$$

The factor $(1+\cos\theta_{\bar{\nu}})(1-\cos\theta_\nu)$ indicate the correlation vanishes in the collinear limit, $\theta_\nu = 0, \theta_{\bar{\nu}} = \pi$ (also the decay rate is zero since massless tau can never decay). Comparing to the correlation in the Higgs rest frame, the angular dependence of the correlation is more complicated. However, in the most sensitive signal region where $\theta_1 = \theta_2 = \pi/2$, we have

$$|\widehat{\mathcal{M}}|^2 \propto 2 - 2\cos\left(\phi_1-\phi_2-2\xi_{h\tau\tau}\right), \tag{3.49}$$

which is identical to the case in the Higgs rest frame.

3.4 Reconstruction algorithm

Because of CP conserving dynamics, the quantum numbers of the $\tau^+\tau^-$ system are constrained by the CP parity of Higgs. That is represented by the spin correlation of τ^+ and τ^- which can be measured by studying the azimuthal angular correlation of their decay products. For a mixing Higgs (3.1), one of the observable with maximum sensitivity to the spin correlation is the azimuthal angle correlation in the Higgs rest frame, which has a distribution as follows

$$\frac{1}{\Gamma}\frac{d\Gamma}{d\phi} = \frac{1}{2\pi}\left(1 - \frac{\pi^2}{16\widetilde{\kappa}_\tau^2}\cos(\phi+2\xi_{h\tau\tau})\right), \tag{3.50}$$

where ϕ is the azimuthal angle of π^- measured by choosing the τ^- momentum along the z-axis and the momentum of π^+ having positive x-component, and $\widetilde{\kappa}_\tau^2 = (\beta_\tau^2 \cos^2\xi_{h\tau\tau} + \sin^2\xi_{h\tau\tau})$ stands for kinematical suppression factor. In the Higgs rest frame, the τ mass can be neglected safely. Therefore $\widetilde{\kappa}_\tau^2 = 1 + \cos^2\xi_{h\tau\tau}(\beta_\tau^2 - 1) \approx 1$ is an excellent approximation. On the other hand, the azimuthal angle of τ^- in the $\pi^+\pi^-$ rest frame, where the z-axis is defined by the momentum of π^- and the momentum of τ^+ has a positive x-component, also has the maximum sensitivity to the spin correlation with the same distribution as (3.50). The advantage of the latter frame is that the z-axis can be directly constructed by the measurable momenta of $\pi^+\pi^-$. However the x-axis is still not defined uniquely. Therefore in practice the azimuthal angle correlation mentioned above can never be measured, even through they have maximum sensitivity to the CP violation.

Fortunately, τ's from Higgs decay have relatively large decay lengths $|\vec{l}_{\tau^\pm}|$ because of the big Lorentz boost. Therefore the impact parameter vectors $\vec{b}_{\pi^\pm}$ of $\pi^\pm$, which provide additional important kinematical informations, can be measured with a significant efficiency. It has been pointed out that the impact parameter vectors along with momenta of $\pi^\pm$ can be used to construct new CP observables [75–78]. In this letter we propose to use the impactor parameter vectors to reconstruct all the kinematical informations such that CP violation can be observed with maximum sensitivity by measuring the azimuthal angle correlation (3.50).

For single tau decay, say τ^-, once the impact parameter vector $\vec{b}_{\tau^-}$ is measured, the system is underdetermined with only one free parameter. In principle we can chose any quantity in the system. Here we propose to use the magnitude of τ^- momentum $|\vec{p}_{\tau^-}|$. The advantage of this choice is that the relative orientation of τ^- and π^-, which has to be preserved to a sufficient accuracy for measuring the azimuthal angle correlation, can be unambiguously determined directly for a given $|\vec{p}_{\tau^-}|$ by using the on-shell condition of neutrino,

$$\cos\theta_{\tau^-\pi^-} = \frac{2E_{\tau^-}E_{\pi^-} - m_\tau^2 - m_{\pi^-}^2}{2|\vec{p}_{\tau^-}||\vec{p}_{\pi^-}|}\,. \tag{3.51}$$

As a result the direction of the τ^- momentum can be solved directly

$$\frac{\vec{p}_{\tau^-}}{|\vec{p}_{\tau^-}|} = \frac{\vec{b}_{\pi^-} + \frac{|\vec{b}_{\pi^-}|}{\tan\theta_{\tau^-\pi^-}}\frac{\vec{p}_{\pi^-}}{|\vec{p}_{\pi^-}|}}{\left|\vec{b}_{\pi^-} + \frac{|\vec{b}_{\pi^-}|}{\tan\theta_{\tau^-\pi^-}}\frac{\vec{p}_{\pi^-}}{|\vec{p}_{\pi^-}|}\right|}\,, \tag{3.52}$$

where we have used the condition $\vec{b}_{\pi^-} \cdot \vec{p}_{\pi^-} = 0$ to simplify the result, and the sign of the second term is fixed by the boundary condition

$$(\vec{p}_{\tau^-} \cdot \vec{p}_{\pi^-})\big|_{\theta_{\tau^-\pi^-}=0} > 0\,. \tag{3.53}$$

The same algorithm can be used equivalently for τ^+. Therefor there are free parameters $|\vec{p}_{\tau^-}|$ and $|\vec{p}_{\tau^+}|$ for the Higgs decay process. However, because the decay width of Higgs is very small so that the Breit-Wigner distribution,

$$\rho_{BW}(|\vec{p}_{\tau^\pm}|) = \frac{N_{BW} m_h^2 \Gamma_h^2}{(m_{\tau\tau}^2 - m_h^2)^2 + m_h^2 \Gamma_h^2} \tag{3.54}$$

(where N_{BW} is a normalization constant) is essentially a Dirac-δ function. Because of the very small width of Higgs, this distribution is really a δ function. Therefore only one parameter is left effectively. On the other hand, using of ρ_{BW} can introduce bias when we include the background events. Fortunately, almost all the backgrounds have flat azimuthal angle distribution. Therefore the bias cannot affect the experimental sensitivity to the CP violation measurement. We will show this latter by using the numerical simulations.

If missing transverse momentum $\not{p}_T$, which provide two additional observables, can be measured precisely, the system of the full decay process $h \to \tau^-\tau^+ \to (\pi^-\nu_\tau)(\pi^+\bar{\nu}_\tau)$ can be determined completely (even over determined). Unfortunately, on hadron collider, the missing transverse momentum $\not{p}_T$ have very large uncertainty. Therefore instead of solving the system, we maximize the probability density function of the reconstructed missing transverse momentum

$$\not{p}_T{}^{\text{Reco}} = \vec{p}_{\nu_\tau,T} + \vec{p}_{\bar{\nu}_\tau,T} \tag{3.55}$$

for given $|\vec{p}_{\tau^-}|$ and $\vec{p}_{\tau^+}$, which quantifies the compatibility of $\tau^\pm$ decays hypothesis with the measured missing transverse momentum $\not{p}_T$ event by event, assuming the neutrinos from the $\tau^\mp$ decays to be the only source of missing transverse energy, and defined as

$$\rho_{\not{p}_T}(|\vec{p}_{\tau^\mp}|) = \frac{1}{2\pi\sqrt{|V|}} \exp\left[-\frac{1}{2}(\Delta\not{p}_T)^T V^{-1} (\Delta\not{p}_T)\right] \tag{3.56}$$

where the pseudo-error of the reconstructed missing transverse energy for given $|\vec{p}_{\tau^-}|$ and $\vec{p}_{\tau^+}$ is

$$\Delta \not{p}_T = \not{p}_T - \not{p}_T{}^{\text{Reco}} \,. \tag{3.57}$$

The expected missing transverse moemtum resolution is represented by the covariance matrix V, which is estimated on an event-by-event basis using a missing transverse momentum significance algorithm [92]. $|V|$ is the determinant of this matrix. The probability density ρ_ν along with the probability density of the distance between neutrino and visible decay product, $\rho_{\Delta R}$ which can be parameterized by the Landau distribution function with an argument $x(|\vec{p}_\tau|) = (\Delta R - \overline{\Delta R}(|\vec{p}_\tau|))/\overline{\sigma}(|\vec{p}_\tau|)$ as

$$\rho_{\Delta R}(|\vec{p}_{\tau^\pm}|) = \frac{\overline{C}}{\sqrt{2\pi}} \exp\left[-\frac{1}{2}(x + e^{-x})\right] , \tag{3.58}$$

has been used by ATLAS to reconstruct the full kinematics in the measurement of the Higgs mass in the $h \to \tau^-\tau^+$ decay mode, and shown that it is powerful. The quantities $\overline{C}$, $\overline{\Delta R}$ and $\overline{\sigma}$ depend on the tau momentum $|\vec{p}_{\tau^\pm}|$.

Because for given $|\vec{p}_{\tau^-}|$ and $|\vec{p}_{\tau^+}|$, ΔRs are already determined. Therefore the density function $\rho_{\Delta R}$ can not improve the reconstruction efficiency. However, it can provide strong constrains on the backgrounds, particularly the QCD jets. In addition, if we allow more quantities, for instance the impact parameter vector free, then $\rho_{\Delta R}$ can provide strong constraint. So the total probability density function is

$$\rho(|\vec{p}_{\tau^\mp}|) = \rho_{BW} \cdot \rho_{\not{p}_T} \cdot \rho_{\Delta R_\tau} \cdot \rho_{\Delta R_{\bar{\tau}}} \tag{3.59}$$

The best estimate of $|\vec{p}_{\tau^\pm}|$ is taken to be the value of $|\vec{p}_{\tau^\mp}|$ that maximizes $\rho(|\vec{p}_{\tau^\pm}|)$.

3.5 Numerical results

Below we use our approach explained above to reconstruct the full kinematics for the process $pp \to h \to \tau^-\tau^+ \to (\pi^-\nu_\tau)(\pi^+\bar{\nu}_\tau)$. The events are generated at the LO with a center of mass energy $\sqrt{s} = 14$TeV by using MadGraph5 [62]. The azimuthal spin correlation is simulated by using the TauDecay package [88]. The generated events are then showered by using Pythia8 [66], and the detector effects are simulated by using

Delphes3 [67]. The jets are classified by using the FastJet package [68] with anti-k_T algorithm and a distance $\Delta R = 0.4$.

The $\tau^{\pm}$-jets are tagged by using the Delphes3 algorithm which has a reconstruction efficiency of tau candidate about 0.8. We mutiply this efficiency by the τ-identification efficiency which is about 0.6 for a medium tau-jet identification condition and has a fake rate about 1% from QCD jets [89, 91].

The directions of $\pi^{\pm}$ momenta are chosen as the exact values in first, and then smeared by using the current resolutions of tracks [61]. The magnitudes of $\pi^{\pm}$ momenta are smeared to be the corresponding $\tau^{\pm}$-tagged jets momentum. Using tracks inside of the τ-tagged jets (instead of the τ-tagged jets) is rather important because the soft particles inside of the $\tau^{\pm}$-tagged jets could completely wash out the relative orientation between $\tau^{\pm}$ and $\pi^{\pm}$, and then the correlation vanishes. We require $|\vec{p}_{\pi^{\pm},T}| > 10\text{GeV}$ and $\eta_{\pi^{\pm}} < 2.5$.

The impact parameters $\vec{b}_{\pi^{\mp}}$ are smeared according to Gaussian distribution with an resolution $\sigma_{b_T} = 20\mu m$ in the transverse plane, and an resolution $\sigma_{b_Z} = 40\mu m$ in the beam direction [61]. We also require $|\vec{b}_{\pi^{\mp}}| > 20\mu m$ to reject those events having larger uncertainty. The efficiency is about 0.8 at 14TeV.

Fig. 3.1 shows the correlation in the $\pi^+\pi^-$ rest frame between the true and reconstructed azimuthal angle for a maximum mixing configuration, i.e. $\xi_{h\tau\tau} = \pi/4$. We can see that a very good positive correlation exists. The events in the left-top and right-bottom corners indicate the $\hat{z}$ axis is misidentified in those events, and then the azimuthal angles have $\pm 2\pi$ differences. This kind of misidentification can happen when the total momentum of $\pi^{\pm}$ is smaller then the uncertainties of the momenta $\vec{p}_{\pi^{\pm}}$. Our simulation shows that the misidentification rate is higher in the $\tau^+\tau^-$ rest frame than the rate in the $\pi^+\pi^-$ rest frame. This is because the reconstructed $\tau^{\pm}$ momenta have larger error. Therefore we propose to use the $\pi^+\pi^-$ rest frame rather than the $\tau^+\tau^-$ rest frame to study the spin correlation. On the other hand This misidentification preserves the spin correlation because the correlation function is periodic in $\pm 2\pi$. This property can be understood by the observation that there are more (blue-circle) events in the left-upper corner than the one in the right-bottom corner in Fig. 3.1. The blue-solid and red-dashed histograms in Fig. 3.2 shows the distributions of the reconstructed azimuthal angle for $\xi_{h\tau\tau} = 0$ and $\xi_{h\tau\tau} = \pi/4$, respectively.

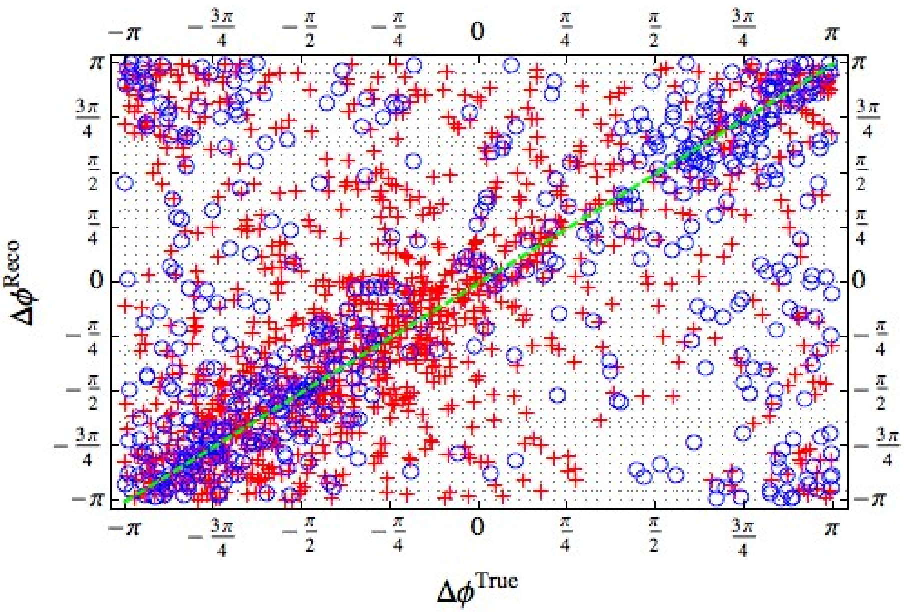

FIGURE 3.1: Correlation between the true and reconstructed azimuthal angle difference for a maximum mixing, i.e. $\xi_{h\tau\tau} = \pi/4$. The azimuthal angle is calculated in the $\pi^+\pi^-$ rest frame. The data points correspond to an integrated luminosity 1 ab^{-1}.

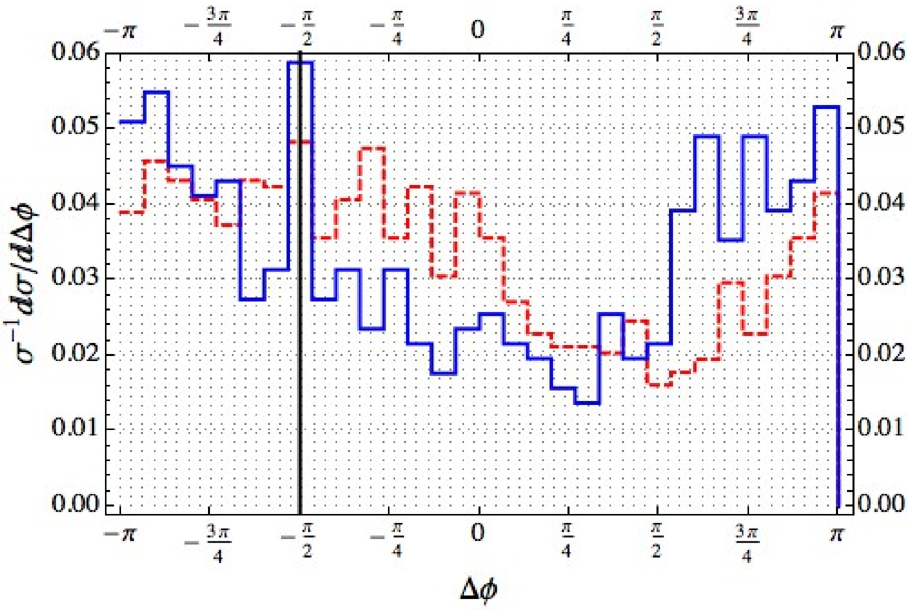

FIGURE 3.2: Distributions of the reconstructed azimuthal angle for $\xi_{h\tau\tau} = 0$ (blue-solid line) and $\xi_{h\tau\tau} = \pi/4$ (red-dashed line). The azimuthal angle is calculated in the $\pi^+\pi^-$ rest frame. The data points correspond to an integrated luminosity 1 ab^{-1}.

Now let us discuss the backgrounds. We consider only the background from $pp \to Z \to \tau^-\tau^+$. As we have mentioned the BW density function ρ_{BW} introduces positive bias in the Z events. However the correlation is not affected much because of the trivial correlation in the $pp \to Z \to \tau^-\tau^+$ process. Fig.3.3 shows the distribution of $\Delta\phi$ for Z. The flat distribution indicates that the bias because of ρ_{BW} is negligible. It is expected that this bias in other backgrounds are also negligible. On the other hand the kinematical cuts used to reduce the backgrounds, for instance $m_{\tau\tau}$ is certainly affected by this bias. So we need to classifies in first the events based on the standard techniques [89, 91], and then introduce the density function ρ_{BW}. Here we introduce a cut $m_{\tau\tau} > 100$GeV to select the events, where $m_{\tau\tau}$ could be reconstructed using the SVFIT [91] or MMC [89, 90] techniques. We assume the efficiencies are 0.8 for Higgs and 0.2 for Z.

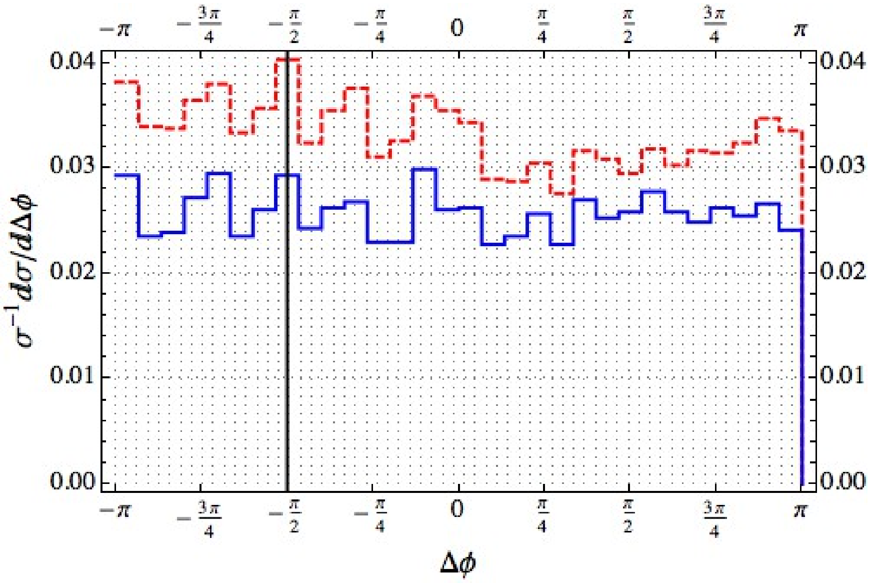

FIGURE 3.3: Distributions of reconstructed azimuthal angle differences for the major background process $pp \to Z \to \tau^-\tau^+$ (blue-solid), and the sum of signal and this background (red-dashed line) in the maximum mixing case $\xi_{h\tau\tau} = \pi/4$. The data points correspond to an integrated luminosity 1 ab^{-1}.

The efficiencies and number of events are summarized in Table 3.1. The tau-tag efficiency for the signal process is relatively higher than the efficiency for the background because of harder transverse momentum distribution in the signal process. The efficiency of impact parameters cut for Higgs decay is slightly lower than the one for Z decay because of the harder $\tau^{\mp}$ momenta. We use a set of relatively soft transverse momenta cuts to keep the signal events as many as possible, meanwhile the background events are also kept. However the naive discovery ability is high, $S/\sqrt{S+B} \approx 10.4$.

The experimental sensitivity is estimated by including the major $Z \to \tau^+\tau^-$ background. The 1σ error of $\xi_{h\tau\tau}$ is taken as the Gaussian width of the fitted mixing angles of 50 independent runs. We find $\sigma_{\xi_{h\tau\tau}} \approx 0.10$ with an integrated luminosity $3\,\text{ab}^{-1}$, which is better than the result in Ref. [74] by a factor of two.

Table 3.1: Efficiency and number of events of the processes $pp \to h/Z \to \tau^-\tau^+ \to (\pi^-\nu_\tau)(\pi^+\bar{\nu}_\tau)$ at 14TeV with an integrated luminosity 1ab^{-1}.

	Eff.	Evt.(h)	Eff.	Evt.(Z)
No cuts	1.000	3.60×10^4	1.000	1.89×10^7
tau-tag	0.225	8.10×10^3	0.140	2.65×10^6
$\lvert\vec{b}_{\pi^\mp}\rvert > 20\mu m$	0.823	6.67×10^3	0.822	2.18×10^6
$\eta_{\pi^\mp} < 2.5$ $\min(\lvert\vec{p}_{\pi^\mp,T}\rvert) > 15\text{GeV}$ $\max(\lvert\vec{p}_{\pi^\mp,T}\rvert) > 35\text{GeV}$ $\lvert\not{p}_T\rvert > 40\text{GeV}$	0.118	7.87×10^2	0.009	1.96×10^4
$m_{\tau\tau} > 100\text{GeV}$	0.900	7.08×10^2	0.200	3.92×10^3

Chapter 4

Probing CP violation in e^+e^- production of the Higgs boson and toponia

For the e^+e^- production of the Higgs boson and toponia at $\sqrt{s} = 500\text{GeV}$, $e^+ + e^- \to \gamma^*, Z^* \to t + \bar{t} + h$, the simplest CP-odd observable is,

$$\mathcal{O}_- \equiv \left\langle \vec{p}(\, e^-) \cdot \left[\vec{p}(t) \times \vec{p}(\bar{t})\right] \right\rangle . \tag{4.1}$$

However this observable requires the reconstruction of the t and $\bar{t}$ momenta from their decay products which is very hard even for electron-position collider. Furthermore, because of the property of near threshold production of $t\bar{t}$, the soft kinematics reduce the sensitivity of this observable. On the other hand, the t and $\bar{t}$ momenta can be replaced by the momenta of the b and $\bar{b}$ jets from the t and $\bar{t}$ decays, respectively. Then the observable

$$\mathcal{O}_-^b \equiv \left\langle \vec{p}(\, e^-) \cdot \left[\vec{p}(b) \times \vec{p}(\bar{b})\right] \right\rangle \tag{4.2}$$

can be used for observing the CP violation. However, the CP violation strength gets diluted in this partial reconstruction.

It has also been pointed out that the different phase space distributions for scalar and pseudo-scalar Higgs production can be used to determine the CP properties of the $t\bar{t}h$ coupling. In Ref. [79], the authors demonstrated that the CP properties of Higgs can be assessed by measuring just the total cross section and the top polarization. However, both these two observables are CP-even, hence only proportional to the square of CP-odd coupling. Furthermore the ratio of the production rates for pseudo-scalar and for scalar is very small unless $\sqrt{s} \gg 1$TeV where the chiral limit is recovered. Therefore the experimental sensitivity is not as good as enough to probe small CP-odd coupling. We really need CP-odd observables, which is linearly proportional to CP-odd coupling, to pin down the CP properties of Higgs. The up-down asymmetry of the anti-top quark with respect to the top-electron plane is an example of such an observable [80, 81]. However, the asymmetry is because of the interferences between the amplitudes involving $t\bar{t}h$ vertex and the amplitudes involving hZZ vertex. It has been shown that the latter contribution is very small, amounting for only a few percent for $\sqrt{s} \leq 1$TeV [79]. Therefore only about 5% asymmetry in maximum can be observed[80, 81].

We study the CP violation in the Higgs and toponia production process at the ILC on which toponia are produced near the threshold region. With the approximation that the production vertex of Higgs and toponia is contact, and neglecting the P-wave toponia, we analytically calculated the density matrix. We find that the production rate of singlet toponium is highly suppressed, which behaves just like the production of a P-wave toponia. This is because in the singlet case the Higgs can not affect anything except for carrying away some energy, and also the specialty of near threshold region. In case of triplet toponium, the CP property of Higgs can affect the physics significantly. This is because the S-wave triplet toponium can contribute even in the pseudo-scalar case, even through the contribution is still small. Three CP observables, azimuthal angles of lepton and anti-leptons in the toponium rest frame as well as their sum, are predicted based on our analytical results, and checked by using the tree-level event generator. The nontrivial correlations come from the longitudinal-transverse interference for azimuthal angles of leptons, and transverse-transverse interference for their sum. The azimuthal angle correlation of lepton is related to the azimuthal angle correlation by CP transformation. Compared to the up-down asymmetry observable in Refs. [79–81], our observables don't require the reconstruction of the top or anti-top momentum which is not an easy task. Furthermore, for all these three observables found in this paper the maximum asymmetries are about 32%, more than 6 times larger than the maximum asymmetry ($\approx 5\%$) in Refs. [79–81]. Most importantly, because only one lepton is needed in the longitudinal-transverse interference, the signal events are significantly enhanced.

These three observables are well defined at the ILC, because the rest frame of toponium can be reconstructed directly. Furthermore, the QCD-strong corrections, which are important at the near threshold region, are also studied with the approximation of spin-independent QCD-Coulomb potential at LO. It is found the total cross section is enhanced by a factor of about 3, while the spin correlation is not affected. It has been pointed out that the NLO corrections are important particularly in the large $t\bar{t}$ invariant mass region [85], and the overall enhancement factor is about 2. We will use this NLO factor in the overall normalization.

4.1 Effective $t-\bar{t}-h$ vertex

In this section we study how the $t\bar{t}h$ interactions affect the top-anti-top pair production near the threshold. We assume the Higgs(125) is a mixture of CP even (H) and CP odd (A) particles,

$$h = H\cos\xi + A\sin\xi = \frac{1}{\sqrt{1+|\epsilon|^2}}(H+\epsilon A)\,. \tag{4.3}$$

For simplicity, we assume that the Yukawa interactions are CP conserving

$$\mathcal{L}_{\text{int.}} = -g_{Hff}\bar{\psi}_f\psi_f H - ig_{Aff}\bar{\psi}_f\gamma^5\psi_f A\,, \tag{4.4}$$

such that the only source of CP violation is in the ϵ parameter (or the mixing angle ξ) in Eq. (4.3). The interactions between the mass eigenstate $h(125)$ and the fermion anti-fermion pair is then described by

$$\mathcal{L}_{int.} = -\Big(g_{Hff}\cos\xi\bar{\psi}_f\psi_f + ig_{Aff}\sin\xi\bar{\psi}_f\gamma^5\psi_f\Big)h = -g_{hff}\Big(\bar{\psi}_f\psi_f + i\epsilon_{hff}\bar{\psi}_f\gamma^5\psi_f\Big)h\,, \tag{4.5}$$

where

$$g_{hff} = g_{Hff}\cos\xi = \frac{g_{Hff}}{\sqrt{1+|\epsilon|^2}}\,, \tag{4.6a}$$

$$\epsilon_{hff} = \tan\xi_{hff} = \frac{g_{Aff}}{g_{Hff}}\tan\xi = \frac{g_{Aff}}{g_{Hff}}\epsilon\,. \tag{4.6b}$$

It is worth noting that the effective strengths of the CP-violating hff couplings can be different for each fermion, even if the origin of CP-violation is only in the mixing parameter $\epsilon = \tan\xi$. In this chpter, we study the htt coupling. This assumption is valid when the Higgs sector CP-violation is mediated mainly by the interactions with new heavy particles. It also makes the ϵ parameter (or the mixing parameter $\tan\xi$) approximately real, as in the $K^0 - \overline{K}^0$ mixing*.

For the s-channel production of $t\bar{t}$ in associated with a $h(125)$,

$$e^-(k_1, \sigma_e) + e^+(k_2, \sigma_{\bar{e}}) \to t(p_1, \sigma_t) + \bar{t}(p_2, \sigma_{\bar{t}}) + h(k) \tag{4.7}$$

the Higgs $h(125)$ is emitted by either a very virtual top or an anti-top as shown in Fig.4.1. Even through the Higgs can also be produced through the hBB' vertexes ($B = Z, \gamma$), but the contributions are negligible (a few percent for $\sqrt{s} \leq 1$TeV [79]) because of the very off-shell propagation of the vector bosons. In principle, CP violation can also appear in these operators. However these operators are induced at the 1-loop level, and hence are hugely suppressed compared to the CP-even operators. On the other hand, because the CP-even hBB' vertex are very simple, therefore we don't consider it when we simplify the vertex function in this section.

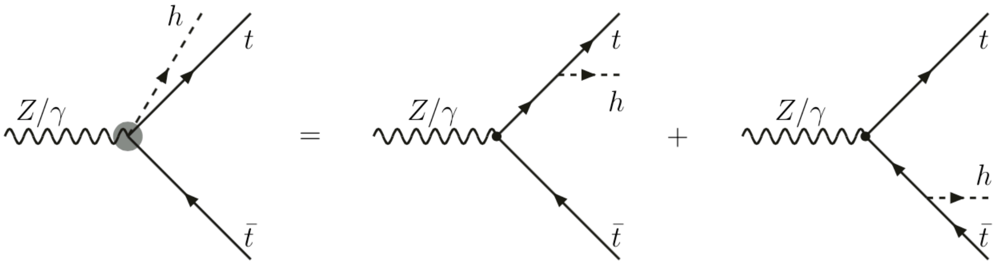

FIGURE 4.1: Feynman diagrams that contribute the $V - ht\bar{t}$ effective vertex (labeled by a big gray dot) in the threshold region. This approximation does not depend on the $V - t\bar{t}$ vertex, so V could be either Z or γ.

Near production threshold, $\sqrt{s} = 2m_t + m_h = 471$GeV, the $t\bar{t}h$ system is non-relativistic. According to the uncertainty principle, the virtual top and anti-top states can propagate only a distance $\sim 1/(\sqrt{s} - m_t)$, which is considerably shorter than the Columb radius $r_C \sim 1/(\alpha_s m_t)$, at which the QCD interactions bound top and anti-top to form bound states toponia. Therefore the approximation of local interaction should be excellent for the combination of the Higgs radiation channels. If denote the $t\bar{t}$ production vertex from

---

[*] Ulike in the $K^0 - \overline{K}^0$ system, which has just one CP-even and CP-odd state each, the two Higgs doublet models have two two CP-even and one CP odd states. Accordingly in general the mixing element $\cos\xi$ in Eq. (4.3) can be small than $\sqrt{1-\cos^2\xi}$.

virtual vector boson B ($B = \gamma, Z$) as $\Gamma_B^\mu = g_V^{Bt\bar{t}}\gamma^\mu + g_A^{Bt\bar{t}}\gamma^\mu\gamma^5$, the leading order effective Higgs radiation vertex is

$$V^\mu(p_1, p_2) = \frac{1}{Q^2 - 2Q\cdot p_2}\Gamma_h(\not{Q} - \not{p}_2 + m)\Gamma_V^\mu - \frac{1}{Q^2 - 2Q\cdot p_1}\Gamma_V^\mu(\not{Q} - \not{p}_1 - m)\Gamma_h, \quad (4.8)$$

where Γ_h is the abbreviation of the $t\bar{t}h$ vertex, and the kinematical variables are defined as in Fig.4.2; $Q = k_1 + k_2 = p_1 + p_2 + k$. Furthermore, the contribution from the hZZ vertex has been neglected, which amounts for only a few percent for $\sqrt{s} \leq 1$TeV [79]. Because both $t\bar{t}$ and $h(125)$ are non-relativistic, so the momentum components $\vec{p}_{1,2}$ could be neglected in the denominators, *i.e.* $p_{1,2}^\mu \approx (m_t, \vec{0})$. Then the two radiation channels can be combined into a compact form. For convenience, we expand the spinor structure of this vertex by using the Clifford algebra as follows

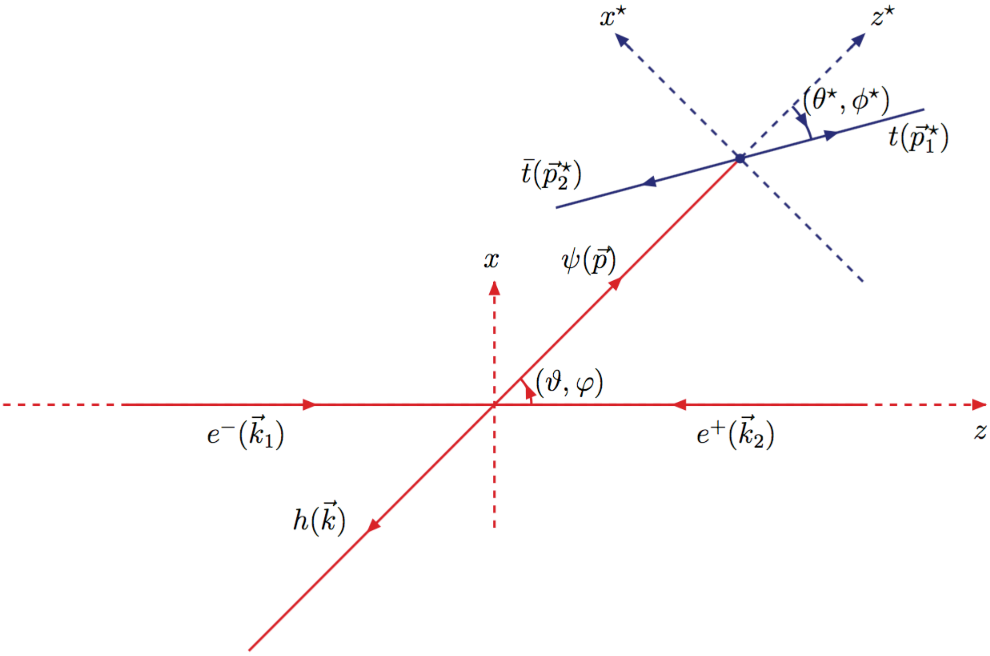

Figure 4.2: Definitions of the kinematical variables in the e^+e^- rest frame specified by the axises $x - y - z$, and the $t\bar{t}$ rest frame specified by the axises $x^* - y^* - z^*$. In the $e^- + e^+$ rest frame, the electron momentum is chosen along the z-axis and the $t\bar{t}$ momentum lies in the $x - z$ plane with positive x component. In the $t\bar{t}$ rest frame, the negative of the h momentum direction is chosen as the $z^\star$-axis, and the $y^\star$-axis has the same direction as the y-axis.

$$V^\mu(p_1, p_2) = \frac{1}{s - 2m_t\sqrt{s}}\left(c_S^\mu + c_P^\mu\gamma^5 + c_V^{\mu\nu}\gamma_\nu + c_A^{\mu\nu}\gamma_\nu\gamma^5 + \frac{1}{2}c_T^{\mu\alpha\beta}\sigma_{\alpha\beta}\right) \quad (4.9)$$

where the coefficients can be calculated easily for the scalar $\Gamma_h = g_h$ and for the pseudo-scalar $\Gamma_h = i\epsilon_h g_h \gamma_5$, as shown in Table 4.1. The production dynamics are described completely by this vertex function. Note that the coefficients of the (CP-even) hBB' vertexes are not included in Table 4.1 for the clarity and compactness of the table. On the other hand, these contributions are very small, a few percent for $\sqrt{s} \leq 1\text{TeV}$ [79]), and can be easily counted by modifying the coefficients $c_V^{\mu\nu}$ and $c_A^{\mu\nu}$. Furthermore, because the spin correlation, which can be used to measure the CP violation effects, doesn't depend on the coefficients of the operators, therefore below we always assume the contributions from the hBB' have been included. The magnitudes of these contributions will be discussed in the numerical simulation part, *i.e.* in Sec.4.4

Table 4.1: The Clifford expansion coefficients of the vertex Eq. (4.9). The $Bt\bar{t}$ ($B = \gamma, Z$) vertex is denoted as $\Gamma_B^\mu = g_V^{Bt\bar{t}}\gamma^\mu + g_A^{Bt\bar{t}}\gamma^\mu\gamma^5$. The momentum $q^\mu = p_1^\mu - p_2^\mu$ is the relative momentum between top and anti-top.

$\mathcal{O}_X$	Scalar ($\Gamma_h = g_h$)	Pseudo-Scalar ($\Gamma_h = \epsilon_h g_h \gamma_5$)
c_S^μ	$g_h\, g_V^{Bt\bar{t}}\, q^\mu$	$i\,\epsilon_h\, g_h\, g_A^{Bt\bar{t}}(Q^\mu + k^\mu)$
c_P^μ	$g_h\, g_A^{Bt\bar{t}}\,(Q^\mu + k^\mu)$	$i\epsilon_h\, g_h\, g_V^{Bt\bar{t}} q^\mu$
$c_V^{\mu\nu}$	$2m_t\, g_h\, g_V^{Bt\bar{t}}\, g^{\mu\nu}$	0
$c_A^{\mu\nu}$	$2m_t\, g_h\, g_A^{Bt\bar{t}}\, g^{\mu\nu}$	0
$c_T^{\mu\alpha\beta}$	$ig_h\, g_V^{Bt\bar{t}}\left[(Q^\beta + k^\beta)g^{\mu\alpha} - (Q^\alpha + k^\alpha)g^{\mu\beta}\right];$ $-g_h\, g_A^{Bt\bar{t}}\,\epsilon^{\alpha\beta\mu\nu}\, q_\nu$	$-i\epsilon_h\, g_h\, g_V^{Bt\bar{t}}\,\epsilon^{\alpha\beta\mu\nu}(Q_\nu + k_\nu)$; $\epsilon_h\, g_h\, g_A^{Bt\bar{t}}\,(q^\alpha g^{\mu\beta} - q^\beta g^{\mu\alpha})$

After the electroweak production of $t\bar{t}h$, the strong interaction between $t\bar{t}$ becomes important. In the threshold region, infinite number of Feynman diagrams that are proportional to the powers of $\alpha_s/\beta_t \sim \mathcal{O}(1)$ contribute, and their resummation is needed, see Fig.4.3. After the resummation, the vertex function satisfies an integral equation, the Bethe-Salpeter equation[82], which describes the formation of bound states in this region. We will discuss it carefully in Sec 4.3. Here we would like to classify the possible bound states that can be produced.

Table 4.2 lists the possible bound states up to P-wave in the spectrum notation for general bispinor vertex structures of spinors ψ and φ in the non-relativistic limit (see

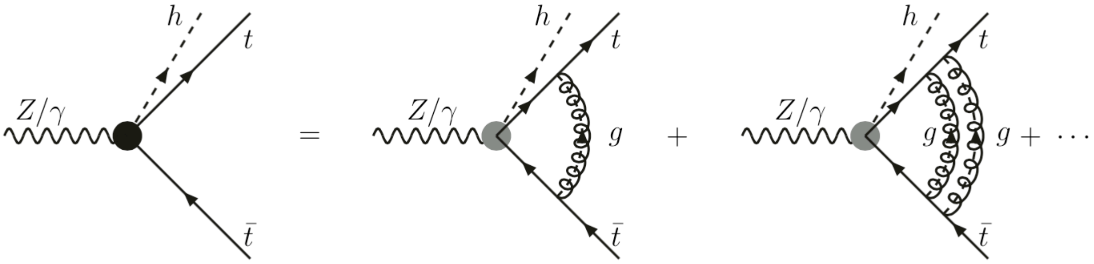

FIGURE 4.3: QCD corrections to the effective $V - ht\bar{t}$ vertex in the threshold region. In this region, summation of an infinite number of diagrams is needed. The big black dot indicates the exact vertex function after this summation.

TABLE 4.2: Quantum numbers of the standard bi-spinors formed by top and anti-top in the non-relativistic limit. The bi-spinors are evaluated in the rest frame of $t\bar{t}$.

Operators	Non-relativistic limit	Quantum state
$\bar{\psi}\varphi$	$\xi^\dagger\vec{q}\cdot\vec{\sigma}\eta$	${}^3P_0$
$\bar{\psi}\gamma^5\varphi$	$\xi^\dagger\eta$	${}^1S_0$
$\bar{\psi}\gamma^\mu\varphi$	$(0, \xi^\dagger\vec{\sigma}\eta)$	${}^3S_1$
$\bar{\psi}\gamma^\mu\gamma_5\varphi$	$(\xi^\dagger\eta\,,\ \xi^\dagger\vec{q}\times\vec{\sigma}\,\eta)$	$({}^1S_0\,,\ {}^3P_1)$
$\bar{\psi}\sigma^{0i}\varphi$	$\xi^\dagger\sigma^i\,\eta$	${}^3S_1$
$\bar{\psi}\sigma^{ij}\varphi$	$q^i\xi^\dagger\sigma^j\,\eta - q^j\xi^\dagger\sigma^i\,\eta$	${}^3P_1$

App.B.0.1 for our conventions of the spinor wave functions in the Dirac representation). The spin-singlet state can be produced only by the speudo-scalar operator, other operators can generate spin-triplet but with different orbital angular momentum. Those quantum numbers are also affected by the coefficients of these operators, which are tabled in Table 4.1. We show the possible bound states by combine the coefficients and operators in Table 4.3. For scalar production vertex operator $\mathcal{O}_S$, both the coefficient and bi-spinor are of P-wave for a CP-even Higgs, therefore the $t\bar{t}$ system is in D-wave state which can be ignored completely. In case of CP-odd Higgs, the $t\bar{t}$ system is a P-wave state because of the S-wave coefficient, so it is still negligible. For pseudo-scalar production vertex operator, single toponium can be produced in S-wave for scalar Higgs and in P-wave for pseudo-scalar Higgs. The vector and axial vector production vertexes are affected only by the scalar component of Higgs, and both can generate triplet toponium but of P-wave for axial vector vertex. In addition, the axial vector can also

TABLE 4.3: Quantum states of the total final system. The spin and angular momenta are summed by first combine the top and anti-top system, and then combine the toponim (ψ_t) and Higgs system.

Operators	Scalar Higgs		Pseudo-Scalar Higgs	
	$(t,\bar{t})$-System	(ψ_t,h)-System	$(t,\bar{t})$-System	(ψ_t,h)-System
$\mathcal{O}_S$	${}^3D_1$	${}^3S_1$	${}^3P_0$	${}^1P_1$
$\mathcal{O}_P$	${}^1S_0$	${}^1P_1$	${}^1P_1$	${}^3S_1$
$\mathcal{O}_V$	${}^3S_1$	${}^3S_1$	0	0
$\mathcal{O}_A$	${}^1S_0$	${}^1P_1$	0	0
	${}^3P_1$	${}^3S_1$	0	0
$\mathcal{O}_T$	${}^3S_1$	${}^3S_1$	${}^3S_1$	${}^3P_1$
	${}^3P_1$	${}^1S_1$	${}^3P_1$	${}^3S_1$
	${}^3P_1$	${}^3S_1$	${}^3P_1$	${}^3P_1$
	${}^3D_1$	${}^3S_1$	${}^3D_1$	${}^3S_1$

generate singlet toponium via its time-component. This contribution turns out to be very important, because it is deconstructive with the contribution of the pseudo-scalar vertex. Their sum makes the total production rate of singlet toponium highly suppressed near the threshold. Of particularly interesting is the production involving tensor vertex, where both the bi-spinor and the coefficients contain S-wave and P-wave $t\bar{t}$. Here we discuss only the S-wave contributions. For both scalar and pseudo-scalar Higgs, it is the "electric component" of the tensor vertex $\propto \sigma^{0i}$ generating S-wave toponia.

4.2 Helicity amplitudes

In this section we will give the full helicity amplitudes in terms of the toponium helicity. Near the threshold the QCD-strong interactions become important. Here we assume the QCD corrections are completely factorized out, i.e. the strong force is spin-independent. see Sec. 4.3. In this approximation the full physics could be modeled by using pure electroweak $ht\bar{t}$ production and their decays. In this model, the toponium helicity are obtained by spin projection. The spin projection becomes simple when the relative momentum q^μ between top and anti-top is neglected. Furthermore neglecting the relative momentum doesn't loss the essential physics as the top and anti-top have very large decay width. Therefore while we calculate the density matrix without the assumption $|q^\mu| \approx 0$, some important results are discussed under this simplification. In subsections 4.2.1 we will give our formalism about the factorization of QCD correction, as well as the spin projection method. In subsection 4.2.2 and 4.2.3 we will give the helicity amplitudes as well as density matrix elements for pure electroweak production and decays. The total helicity amplitude and density matrix elements as well as the CP observables are discussed in subsection 4.2.4.

4.2.1 Factorization and Projection of the helicity amplitudes

The total amplitude for the process $e^- + e^+ \to h + \bar{t}(\ell\nu_{\bar{\ell}}\bar{b}) + t(\bar{\ell}\nu_\ell b)$ can be written in general as follows

$$\mathcal{M} = \langle(\ell\nu_{\bar{\ell}}\bar{b})(\bar{\ell}\nu_\ell b)h|\mathcal{T}|e^-e^+\rangle\,. \tag{4.10}$$

Here we want to see the CP violation effects by the anormalous interaction between toponium and Higgs. This is done by inserting a complete basis of the $t\bar{t}$ resonance states ψ_t with quantum number $(J_{\psi_t}, \lambda_{\psi_t})$, then the total helicity amplitude could be written as the production and decay of the toponiym,

$$\mathcal{M} = \sum_{J_{\psi_t},\lambda_{\psi_t}} \langle(\ell\nu_{\bar{\ell}}\bar{b})(\bar{\ell}\nu_\ell b)|\mathcal{T}_D|\psi_t(J_{\psi_t},\lambda_{\psi_t})\rangle\langle\psi_t(J_{\psi_t},\lambda_{\psi_t})h|\mathcal{T}_P|e^-e^+\rangle\,. \tag{4.11}$$

Note that the phase space factor of toponium has been dropped here, it will be counted in the phase space part. Here and after we always drop the phase space factor whenever the amplitudes are expanded by the complete basis. However this amplitude cannot be calculated directly in perturbation theory because of the $t\bar{t}$ resonance ψ_t are composite states. We therefore expand the helicity amplitudes by using the fundamental fields t and $\bar{t}$, and the amplitudes take the following form

$$\mathcal{M} = \sum_{J_{\psi_t},\lambda_{\psi_t}} \sum_{\sigma'_t,\sigma'_{\bar{t}}} \sum_{\sigma_t,\sigma_{\bar{t}}} \mathcal{M}_{\psi_t}(J_{\psi_t},\lambda_{\psi_t};\sigma'_t,\sigma'_{\bar{t}};\sigma_t,\sigma_{\bar{t}})\mathcal{M}_D(\sigma'_t,\sigma'_{\bar{t}})\mathcal{M}_P(\sigma_t,\sigma_{\bar{t}})\,, \tag{4.12}$$

where the production, decay and resonance amplitudes are, respectively,

$$\mathcal{M}_P(\sigma_t,\sigma_{\bar{t}}) = \langle t(\sigma_t)\bar{t}(\sigma_{\bar{t}})h|\mathcal{T}_P|e^-e^+\rangle\,, \tag{4.13}$$

$$\mathcal{M}_D(\sigma'_t,\sigma'_{\bar{t}}) = \langle(\ell\nu_{\bar{\ell}}\bar{b})(\bar{\ell}\nu_\ell b)|\mathcal{T}_D|t(\sigma'_t)\bar{t}(\sigma'_{\bar{t}})\rangle\,, \tag{4.14}$$

$$\mathcal{M}_{\psi_t} = \langle t(\sigma'_t)\bar{t}(\sigma'_{\bar{t}})|\mathcal{T}^\dagger_{QCD}|\psi_t(J_{\psi_t},\lambda_{\psi_t})\rangle\langle\psi_t(J_{\psi_t},\lambda_{\psi_t})|\mathcal{T}_{QCD}|t(\sigma_t)\bar{t}(\sigma_{\bar{t}})\rangle \tag{4.15}$$

Here both the production and decay processes are electroweak, and the QCD corrections are accounted for the resonance amplitudes. In order to make our discussions more simple and clean, we use the free $t\bar{t}$ resonance states $\widetilde{\psi}_t(J'_\psi,\lambda'_{\psi_t})$ to separate out the spin degrees of freedom. Then the toponium formation amplitudes from top pair can be written as

$$\begin{aligned}&\langle\psi_t(J_{\psi_t},\lambda_{\psi_t})|\mathcal{T}_{QCD}|t(\sigma_t)\bar{t}(\sigma_{\bar{t}})\rangle\\ =&\sum_{J'_{\psi_t},\lambda'_{\psi_t}}\langle\psi_t(J_{\psi_t},\lambda_{\psi_t})|\mathcal{T}_{QCD}|\widetilde{\psi}_t(J'_{\psi_t},\lambda'_{\psi_t})\rangle\langle\widetilde{\psi}_t(J'_{\psi_t},\lambda'_{\psi_t})|\mathcal{O}^{J'_\psi}_{\lambda'_{\psi_t}}|t(\sigma_t)\bar{t}(\sigma_{\bar{t}})\rangle\,,\end{aligned} \tag{4.16}$$

where we have introduced an pure kinematical operator $\mathcal{O}^{J'_\psi}_{\lambda'_{\psi_t}}$ to account for the spin correlations of $t\bar{t}$ to $\widetilde{\psi}_t$. In general the quantum numbers $(J_{\psi_t},\lambda_{\psi_t})$ can be different from $(J'_{\psi_t},\lambda'_{\psi_t})$ by QCD corrections, for instance when we include the spin-orbital interactions, etc.. Here we neglect those spin-dependent corrections, i.e. we take $(J_{\psi_t},\lambda_{\psi_t})=(J'_{\psi_t},\lambda'_{\psi_t})$. Then the resonance amplitudes can be written as

$$\mathcal{M}_{\psi_t}(J_{\psi_t},\lambda_{\psi_t};\sigma'_t,\sigma'_{\bar{t}};\sigma_t,\sigma_{\bar{t}}) = (\mathcal{P}^{J_{\psi_t},\lambda_{\psi_t}}_{\sigma'_t,\sigma'_{\bar{t}}})^\dagger(\mathcal{P}^{J_{\psi_t},\lambda_{\psi_t}}_{\sigma_t,\sigma_{\bar{t}}})\mathcal{K}_{J_{\psi_t},\lambda_{\psi_t}}\,, \tag{4.17}$$

where the factor $\mathcal{K}_{J_{\psi_t},\lambda_{\psi_t}}$ is defined as the squared renormalization factor which gives the pure QCD corrections,

$$\mathcal{K}_{J_{\psi_t},\lambda_{\psi_t}} = |\langle\psi(J_{\psi_t},\lambda_{\psi_t})|\mathcal{T}_{QCD}|\widetilde{\psi}_t(J_{\psi_t},\lambda_{\psi_t})\rangle|^2\,, \tag{4.18}$$

and the spin projection operator $\mathcal{P}^{J_\psi,\lambda_{\psi_t}}_{\sigma_t,\sigma_{\bar{t}}}$ is defined as the matrix elements of $\mathcal{O}^{J_{\psi_t}}_{\lambda_{\psi_t}}$,

$$\mathcal{P}^{J_\psi,\lambda_{\psi_t}}_{\sigma_t,\sigma_{\bar{t}}} = \langle\widetilde{\psi}(J_\psi,\lambda_{\psi_t})|\mathcal{O}^{J_\psi}_{\lambda_{\psi_t}}|t(\sigma_t)\bar{t}(\sigma_{\bar{t}})\rangle\,. \tag{4.19}$$

The pure QCD correction will be discussed in Sec.4.3. Let us focus on the spin projection in first. In general J_{ψ_t} could be any integer. However the production rates of toponium states with higher angular momentum L are suppressed by β_t^L. Therefore we discuss only the S-wave resonance. Then ψ_t could be either a spin-singlet or a spin-triplet, i.e., $J_{\psi_t} = 0, 1$. The corresponding projection operators are defined as follows

$$\mathcal{O}_{\lambda_{\psi_t}}^{J_{\psi_t}=0} = \frac{1}{\sqrt{2s_{\psi_t}}\sqrt{1-\frac{(m_t^{\star 2}-\bar{m}_t^{\star 2})^2}{s_{\psi_t}^2}}}\widetilde{\psi}_t(\lambda_{\psi_t})\bar{t}\gamma^5 t\,, \tag{4.20}$$

$$\mathcal{O}_{\lambda_{\psi_t}}^{J_{\psi_t}=1} = \frac{1}{\sqrt{2s_{\psi_t}}\sqrt{1-\frac{(m_t^{\star 2}-\bar{m}_t^{\star 2})^2}{s_{\psi_t}^2}}}\widetilde{\psi}_t^{\mu}(\lambda_{\psi_t})\bar{t}\,\gamma_\mu t\,, \tag{4.21}$$

where $\sqrt{s_{\psi_t}}$, $m_t^\star$ and $\bar{m}_t^\star$ are the the mass of toponium, top and anti-top respectively. The normalization factor is chosen such that the spin projection operators are dimensionless (the overall normalization of $\mathcal{M}_{\psi_t}$ is fixed by the total QCD correction). With the help of spin projection operators the total helicity amplitude can be expressed in terms of the toponium production and decay helicity amplitudes as follows

$$\mathcal{M} = \sum_{J_{\psi_t},\lambda_{\psi_t}} \mathcal{K}_{J_{\psi_t},\lambda_{\psi_t}} \widetilde{\mathcal{M}}_P(J_{\psi_t},\lambda_{\psi_t})\widetilde{\mathcal{M}}_D(J_{\psi_t},\lambda_{\psi_t}) \tag{4.22}$$

where the projected production and decay helicity amplitudes are

$$\widetilde{\mathcal{M}}_P(J_{\psi_t},\lambda_{\psi_t}) = \sum_{\sigma_t,\sigma_{\bar{t}}} \mathcal{P}_{\sigma_t,\sigma_{\bar{t}}}^{J_{\psi_t},\lambda_{\psi_t}} \mathcal{M}_P(J_{\psi_t},\lambda_{\psi_t};\sigma_t,\sigma_{\bar{t}})\,, \tag{4.23}$$

$$\widetilde{\mathcal{M}}_D(J_{\psi_t},\lambda_{\psi_t}) = \sum_{\sigma'_t,\sigma'_{\bar{t}}} (\mathcal{P}_{\sigma'_t,\sigma'_{\bar{t}}}^{J_{\psi_t},\lambda_{\psi_t}})^\dagger \mathcal{M}_D(J_{\psi_t},\lambda_{\psi_t};\sigma'_t,\sigma'_{\bar{t}})\,. \tag{4.24}$$

We will study the these two helicity amplitudes in the next two subsections.

4.2.2 Production helicity amplitudes

In this subsection we give the helicity amplitudes for the production process of toponium in associated with the Higgs. The kinematical variables are defined as follows (see also the Fig. 4.2)

$$e^-(k_1,\sigma_e) + e^+(k_2,\sigma_{\bar{e}}) \to \widetilde{\psi}_t(p;J_{\psi_t},\lambda_{\psi_t}) + h(k) \to t(p_1,\sigma_t) + \bar{t}(p_2,\sigma_{\bar{t}}) + h(k) \tag{4.25}$$

The fermion helicity $\sigma_i = \pm 1/2$, $i = e, \bar{e}, t, \bar{t}$. For spin-singlet toponium $J_{\psi_t} = 0, \lambda_{\psi_t} = 0$, and $J_{\psi_t} = 1, \lambda_{\psi_t} = 0, \pm 1$ for spin-triplet toponium. In the rest frame of e^+e^- the momenta are given by

$$Q^\mu = \sqrt{s}(1,\, 0,\, 0,\, 0)\,, \tag{4.26a}$$

$$k_1^\mu = \frac{\sqrt{s}}{2}(1,\, 0,\, 0,\, 1)\,, \tag{4.26b}$$

$$k_2^\mu = \frac{\sqrt{s}}{2}(1,\, 0,\, 0,\, -1)\,, \tag{4.26c}$$

$$p^\mu = \frac{\sqrt{s}}{2}(1 + \frac{s_{\psi_t} - m_h^2}{s},\, \beta \sin\vartheta \cos\varphi,\, \beta \sin\vartheta \sin\varphi,\, \beta \cos\vartheta)\,, \tag{4.26d}$$

$$k^\mu = \frac{\sqrt{s}}{2}(1 - \frac{s_{\psi_t} - m_h^2}{s},\, -\beta \sin\vartheta \cos\varphi,\, -\beta \sin\vartheta \sin\varphi,\, -\beta \cos\vartheta)\,. \tag{4.26e}$$

Here we use $\sqrt{s}$ to denote the total energy, and $\sqrt{s}_{\psi_t}$ to denote the mass of the toponium. In this frame the leptonic current is give by

$$L_V^\mu(\lambda_e) = -\lambda_V g_{\lambda_V}^e \sqrt{2s}\, \varepsilon^\mu(\vec{Q} = \vec{0}, \lambda_V)\,, \tag{4.27}$$

where $\lambda_V = \sigma_e - \sigma_{\bar{e}} = \pm 1$ is the helicity of the virtual vector particle; the helicity dependent constant $g_{\lambda_V}^e$ is

$$g_{\lambda_V}^e = \frac{e}{Q^2} - \frac{1}{4}\frac{(1 - \lambda_V) + 4\sin^2\theta_W}{Q^2 - m_Z^2 + i m_Z \Gamma_Z}\,, \tag{4.28}$$

where the first term stands for the photon pole and the second term stands for the Z pole. The momenta of toponium, t and $\bar{t}$ in the rest frame of the toponium are given by

$$p^{\star\mu} = \sqrt{s_\psi}(1,\, 0,\, 0,\, 0)\,, \tag{4.29a}$$

$$p_1^{\star\mu} = \frac{\sqrt{s_\psi}}{2}(1 + \frac{m_t^{\star 2} - \bar{m}_t^{\star 2}}{s_\psi},\, \beta_t \sin\theta^\star \cos\phi^\star,\, \beta_t \sin\theta^\star \sin\phi^\star,\, \beta_t \cos\theta^\star)\,, \tag{4.29b}$$

$$p_2^{\star\mu} = \frac{\sqrt{s_\psi}}{2}(1 - \frac{m_t^{\star 2} - \bar{m}_t^{\star 2}}{s_\psi},\, -\beta_t \sin\theta^\star \cos\phi^\star,\, -\beta_t \sin\theta^\star \sin\phi^\star,\, -\beta_t \cos\theta^\star)\,, \tag{4.29c}$$

where

$$\beta_t = \sqrt{1 + \frac{m_t^{\star 4}}{s_\psi^2} + \frac{\bar{m}_t^{\star 4}}{s_\psi^2} - \frac{2 m_t^{\star 2} \bar{m}_t^{\star 2}}{s_\psi^2} - \frac{2\bar{m}_t^{\star 2}}{s_\psi} - \frac{2 m_t^{\star 2}}{s_\psi}}. \tag{4.30}$$

Let use first calculate the projection operators. Because we discuss here only the S-wave toponium production, so there are only two kinds of projection operators: spin-singlet and spin-triplet projection operators which are corresponding to the matrix element of operators $\mathcal{O}_P$ and $\mathcal{O}_V$. In the rest frame of toponium we have

$$\mathcal{P}^{J_{\psi_t}=0}_{\sigma_t,\sigma_{\bar{t}}} = -\frac{1}{\sqrt{2}}|\tilde{m}|e^{i\tilde{m}\phi^\star} \quad , \quad (\mathcal{P}^{J_{\psi_t}=0}_{\sigma_t,\sigma_{\bar{t}}})^\dagger = -\frac{1}{\sqrt{2}}|\tilde{m}|e^{-i\tilde{m}\phi^\star} \tag{4.31a}$$

$$\mathcal{P}^{J_{\psi_t}=1}_{\sigma_t,\sigma_{\bar{t}}} = f(\tilde{m},m)D^{J=1}_{\lambda_{\psi_t},m}(\theta^\star,\phi^\star) \ , \ (\mathcal{P}^{J_{\psi_t}=1}_{\sigma_t,\sigma_{\bar{t}}})^\dagger = f^*(\tilde{m},m)\widetilde{D}^{J=1}_{m,\lambda_{\psi_t}}(\theta^\star,\phi^\star) \tag{4.31b}$$

where the helicities $m = \sigma_t - \sigma_{\bar{t}}$ and $\tilde{m} = \sigma_t + \sigma_{\bar{t}}$ are defined along the top momentum direction, and they are related by the Wigner rotations to the helicity states of toponium along its moving direction. The function $f(\tilde{m},m)$ is defined as follows,

$$f(\tilde{m},m) = \left(\frac{1}{\sqrt{2}}\tilde{m}\sqrt{1-\beta_t^2}\, e^{i\tilde{m}\phi^\star} - m\right). \tag{4.32}$$

Here we use $\widetilde{D}$ to denote the complex conjugate transpose of the Wigner-D functions, see Appendix. As we have explained in the non-relativistic approximation, the relative momentum between tops is negligible, so the factor β_t in the spin-triplet projection operator can be neglected completely. Furthermore, the orientation can also be neglected because the QCD correction preserves spin. In this approximation the spin projection operators are reduced to following forms

$$\mathcal{P}^{J_{\psi_t}=0,\lambda_{\psi_t}}_{\sigma_t,\sigma_{\bar{t}}} = -\frac{1}{\sqrt{2}}|\tilde{m}|\,, \quad \mathcal{P}^{J_{\psi_t}=1,\lambda_{\psi_t}}_{\sigma_t,\sigma_{\bar{t}}} = \frac{1}{\sqrt{2}}\tilde{m} - m\,. \tag{4.33}$$

The helicity amplitudes of $t\bar{t}$ production are governed by the types of production vertex. Here we use the notation $\mathcal{M}_P(X;\sigma_t,\sigma_{\bar{t}})$, $X = S,P,A,V,T$ to denote their contributions, and use the subscript to distinguish the contributions of scalar and pseudo-scalar components of Higgs. The operators that can generate toponium in S-wave are listed in the Table 4.4. For the scalar operator, both the scalar and pseudo-scalar components of Higgs start to contribute at P-wave, so there is no relevant contributions. For the pseudo-scalar operator, only the scalar component of Higgs contributes, and the helicity amplitude is

$$\mathcal{M}_P(P;\sigma_t,\sigma_{\bar{t}}) = -\lambda_V g^e_{\lambda_V} g_h g_A s\sqrt{s_{\psi_t}} X_P |\tilde{m}| e^{-i\tilde{m}\phi^\star}\widetilde{D}^{J=1}_{0\lambda_V}(\vartheta,\varphi)\,, \tag{4.34}$$

TABLE 4.4: Operators generate toponium in S-wave

Operators	Scalar Higgs	Pseudo-Scalar Higgs
$\mathcal{O}_S$		
$\mathcal{O}_P$	√	
$\mathcal{O}_V$	√	
$\mathcal{O}_A$	√	
$\mathcal{O}_T$	√	√

where the kinematical factor

$$X_P = \frac{\beta}{\sqrt{2}}\sqrt{1 - \frac{(m_t^{\star 2} - \bar{m}_t^{\star 2})^2}{s_\psi^2}}\,. \tag{4.35}$$

As we have explained in Sec.4.1, the pseudo-scalar operator can only generate P-wave between a singlet toponium and Higgs. This is also true for the axial vector operator. The helicity is similar with $\mathcal{M}_P(P;\sigma_t,\sigma_{\bar{t}})$,

$$\mathcal{M}_P(A;\sigma_t,\sigma_{\bar{t}}) = \lambda_V g^e_{\lambda_V} g_h g_A s\sqrt{s_{\psi_t}} X_A |\tilde{m}| e^{-i\tilde{m}\phi^\star} \widetilde{D}^{J=1}_{m\lambda_V}(\vartheta,\varphi) \tag{4.36}$$

where the kinematical factor is

$$X_A = \frac{\beta}{\sqrt{2}}\sqrt{\frac{4m_t^2}{s_{\psi_t}}}\sqrt{1 - \frac{(m_t^{\star 2} - \bar{m}_t^{\star 2})^2}{s_{\psi_t}^2}}\,. \tag{4.37}$$

The most important thing is that the contributions of pseudo-scalar and axial vector operators are deconstructive. Because only the pseudo-scalar and axial vector operators generate singlet toponium, so the total helicity amplitude for singlet toponium production is just the sum of these two contributions which is proportional to $1 - \sqrt{4m_t^2/s_{\psi_t}}$ that vanishes near the threshold region. Therefore we will neglect the singlet toponium in the following calculations.

On the other hand, the transverse polarized states of toponium start to contribute through the vector operator interaction. The helicity amplitude is

$$\mathcal{M}_P(V;\sigma_t,\sigma_{\bar{t}}) = \sum_{\lambda'_{\psi_t}} \lambda_V g^e_{\lambda_V} g_h g_V s \sqrt{s_{\psi_t}} X_V \widetilde{D}^{J=1}_{\lambda'_{\psi_t}\lambda_V}(\vartheta,\varphi) f^*(\tilde{m},m) \widetilde{D}^{J=1}_{m\lambda'_{\psi_t}}(\theta^\star,\phi^\star)\,. \quad (4.38)$$

Here the helicity λ'_{ψ_t} is quantized along the moving direction of the toponium, after the projection it is related to λ_{ψ_t}. The kinematical factor is

$$X_V = 2\sqrt{\frac{4m_t^2}{s}}\sqrt{1-\frac{(m_t^{\star 2}-\bar{m}_t^{\star 2})^2}{s_\psi^2}}\,. \quad (4.39)$$

This is a S-wave production, corresponding to an effective operator $h\psi_t^\mu V_\mu$. The contribution from the tenser operator is also of S-wave production, but corresponding to an effective operator $hF_{\psi_t\mu\nu}F_V^{\mu\nu}$, where $F_B^{\mu\nu} = \partial^\mu B^\nu - \partial^\nu B^\mu$ is the strength tensor of field $B = \psi_t, \gamma, Z$. The corresponding helicity amplitude is

$$\mathcal{M}_P(T_S;\sigma_t,\sigma_{\bar{t}}) = \sum_{\lambda'_{\psi_t}} \lambda_V g^e_{\lambda_V} g_h g_V s \sqrt{s_{\psi_t}} X_{T_S} \widetilde{D}^{J=1}_{\lambda'_{\psi_t}\lambda_V}(\vartheta,\varphi) f^*(\tilde{m},m) \widetilde{D}^{J=1}_{m\lambda'_{\psi_t}}(\theta^\star,\phi^\star)\,, \quad (4.40)$$

where the kinematical factor

$$X_{T_S} = 2\sqrt{\frac{s}{s_\psi}}\left(1-\frac{m_h^2}{s}\right)\sqrt{1-\frac{(m_t^{\star 2}-\bar{m}_t^{\star 2})^2}{s_\psi^2}}\,. \quad (4.41)$$

In the above calculations we have neglected a contribution of D-wave in production which is proportional to β^2. Apart from this kinematical factor, the rest are completely the same as the one of vector operator contribution. The important thing is that they are constructive. On the other hand the pseudo-scalar component of Higgs also contributes the production via the tensor operator. The contribution is of P-wave production, and corresponding to an effective operator $h\widetilde{F}_{\psi_t\mu\nu}F_V^{\mu\nu}$, where $\widetilde{F}_B^{\mu\nu} = 1/2\epsilon_{\mu\nu\alpha\beta}F_B^{\alpha\beta}$ is the dual strength tensor of field B. The corresponding helicity amplitude is

$$\mathcal{M}_P(T_P;\sigma_t,\sigma_{\bar{t}}) = \sum_{\lambda'_{\psi_t}} i\lambda_V g^e_{\lambda_V} \epsilon_h g_V s \sqrt{s_\psi} X_{T_P} \widetilde{D}^{J=1}_{\lambda'_{\psi_t}\lambda_V}(\vartheta,\varphi) f^*(\tilde{m},m) \lambda'_{\psi_t} \widetilde{D}^{J=1}_{m\lambda'_{\psi_t}}(\theta^\star,\phi^\star)\,, \quad (4.42)$$

where the kinematical factor

$$X_{T_P} = 2\beta\sqrt{\frac{s}{s_\psi}}\sqrt{1-\frac{(m_t^{\star 2}-\bar{m}_t^{\star 2})^2}{s_\psi^2}}\,. \tag{4.43}$$

Now we can obtain the projected helicity amplitudes. For pseudo-scalar and axial vector operators the projected helicity amplitudes are similar

$$\widetilde{\mathcal{M}}_P(P, J_{\psi_t}=0, \lambda_{\psi_t}=0) \;=\; \lambda_V g^e_{\lambda_V} g_h g_A s\sqrt{s_{\psi_t}}\beta \widetilde{D}^{J=1}_{0\lambda_V}(\vartheta,\varphi)\,. \tag{4.44}$$

$$\widetilde{\mathcal{M}}_P(A, J_{\psi_t}=0, \lambda_{\psi_t}=0) \;=\; -\lambda_V g^e_{\lambda_V} g_h g_A s\sqrt{s_{\psi_t}}\beta\sqrt{\frac{4m_t^2}{s_{\psi_t}}}\widetilde{D}^{J=1}_{0\lambda_V}(\vartheta,\varphi)\,. \tag{4.45}$$

Becuase only these two operators contribute the singlet toponium production, so the total helicity amplitude for the singlet toponium production is

$$\widetilde{\mathcal{M}}_P(\lambda_V; J_{\psi_t}=0) = g^e_{\lambda_V} g_h g_A s\sqrt{s_{\psi_t}}\beta\left(1-\sqrt{\frac{4m_t^2}{s_{\psi_t}}}\right)e^{i\lambda_V\varphi}\sin\vartheta\,. \tag{4.46}$$

As expected this is the usual production helicity amplitude of two scalar particles in P-wave. Because it is strongly suppressed by the kinematical factor $1-\sqrt{4m_t^2/s_{\psi_t}}$ which vanishes near the threshold region. Therefore we will neglect the singlet toponium in the study of spin correlations.

The contributions from vector and tensor operators are the same apart from the kinematical factors, and the projected helicity amplitudes are proportional to the Wigner-D function as follows

$$\widetilde{\mathcal{M}}_P(V/T_S/T_P, J_\psi=1, \lambda_{\psi_t}) \propto \widetilde{D}^{J=1}_{\lambda_{\psi_t}\lambda_V}(\vartheta,\varphi)\,. \tag{4.47}$$

Here we have used a relation as follows

$$\sum_{\sigma_t,\sigma_{\bar{t}}} f^*(\tilde{m},m)f(\tilde{m},m)D^{J=1}_{\lambda_{\psi_t},m}\widetilde{D}^{J=1}_{m\lambda'_{\psi_t}} = 2\cdot\frac{1}{2}D^{J=1}_{\lambda_{\psi_t},0}\widetilde{D}^{J=1}_{0\lambda'_{\psi_t}} + \sum_{m=\pm 1} D^{J=1}_{\lambda_{\psi_t},m}\widetilde{D}^{J=1}_{m\lambda'_{\psi_t}} = \delta_{\lambda_{\psi_t},\lambda'_{\psi_t}}\,. \tag{4.48}$$

This is the usual production helicity amplitude of a vector particle. Because the structures of the helicity amplitudes for these three operators are the same, we can add them up directly. After the summation, the helicity amplitudes are given by

$$\widetilde{\mathcal{M}}_P(\lambda_V; J_\psi = 1, \lambda_{\psi_t} = 0) \;\propto\; -\frac{1}{\sqrt{2}}\sin\vartheta\,, \tag{4.49a}$$

$$\widetilde{\mathcal{M}}_P(\lambda_V; J_\psi = 1, \lambda_{\psi_t} = 1) \;\propto\; \frac{1}{2}e^{i\tilde{\xi}}(1+\lambda_V\cos\vartheta)\,, \tag{4.49b}$$

$$\widetilde{\mathcal{M}}_P(\lambda_V; J_\psi = 1, \lambda_{\psi_t} = -1) \;\propto\; \frac{1}{2}e^{-i\tilde{\xi}}(1-\lambda_V\cos\vartheta)\,, \tag{4.49c}$$

where the coupling constant $\tilde{g}_h$ and CP phase angle $\tilde{\xi}$ are defined as follows

$$\tilde{g}_h \;=\; g_h\left(1+\frac{2m_t\sqrt{s_\psi}-m_h^2}{s}\right)\sqrt{\frac{s}{s_\psi}\left(1+\epsilon_h^2\kappa^2\right)}\,, \tag{4.50}$$

$$\tan\tilde{\xi} \;=\; \epsilon_h\kappa\,, \tag{4.51}$$

$$\kappa \;=\; \beta\bigg/\left(1+\frac{2m_t\sqrt{s_\psi}-m_h^2}{s}\right). \tag{4.52}$$

The production density matrix is defined as

$$\rho_P(\lambda_{\psi_t},\lambda'_{\psi_t}) = \sum_{\lambda_V=\pm1}\widetilde{\mathcal{M}}_P(\lambda_V;\lambda_{\psi_t})\widetilde{\mathcal{M}}^\dagger_P(\lambda_V;\lambda'_{\psi_t}) = \sum_{\lambda_V=\pm1}\rho_P(\lambda_V;\lambda_{\psi_t},\lambda'_{\psi_t})\,. \tag{4.53}$$

Inserting the helicity amplitudes we get

$$\rho_P(\lambda_V;+,+) \;\propto\; \frac{1}{4}(1+\lambda_V\cos\vartheta)^2\,, \tag{4.54a}$$

$$\rho_P(\lambda_V;-,-) \;\propto\; \frac{1}{4}(1-\lambda_V\cos\vartheta)^2\,, \tag{4.54b}$$

$$\rho_P(\lambda_V;0,0) \;\propto\; \frac{1}{2}\sin^2\vartheta\,, \tag{4.54c}$$

$$\rho_P(\lambda_V;+,-) \;\propto\; \frac{1}{4}e^{i2\tilde{\xi}}\sin\vartheta^2\,, \tag{4.54d}$$

$$\rho_P(\lambda_V;0,+) \;\propto\; -\frac{e^{-i\tilde{\xi}}}{2\sqrt{2}}\sin\vartheta(1+\lambda_V\cos\vartheta)\,, \tag{4.54e}$$

$$\rho_P(\lambda_V;-,0) \;\propto\; -\frac{e^{i\tilde{\xi}}}{2\sqrt{2}}\sin\vartheta(1-\lambda_V\cos\vartheta)\,. \tag{4.54f}$$

Other relevant matrix elements can be obtained by complex conjugation.

Before we go on to discuss the decay helicity amplitude, let us first discuss the angular distribution of the production. The squared helicity amplitudes are

$$|\widetilde{\mathcal{M}}_P(\lambda_V; J_\psi = 0)|^2 \propto g^2_{\lambda_V} \sin\vartheta^2 \,, \tag{4.55}$$

$$|\widetilde{\mathcal{M}}_P(\lambda_V; J_\psi = 1)|^2 \propto g^2_{\lambda_V} \left(\frac{1}{2}(\lambda^2_{\psi_t} - 1)\sin^2\vartheta + \frac{\lambda^2_{\psi_t}}{4}(1 + \cos^2\vartheta + 2\lambda_V \lambda_{\psi_t} \cos\vartheta) \right) \tag{4.56}$$

We can see that the forward-backward asymmetry appears when the helicity of the toponium is fixed. This could be done by observing the helicity of t and $\bar{t}$. However, the pseudo-scalar component of the Higgs affects only the total rate, so it is very hard to extract the coupling ϵ_h by using only the production informations.

4.2.3 Helicity amplitudes of the toponium decay

In this subsection we give the helicity amplitude of the leptonic decay of toponium. The kinematical variables are defined as follows (see also the Fig.4.4)

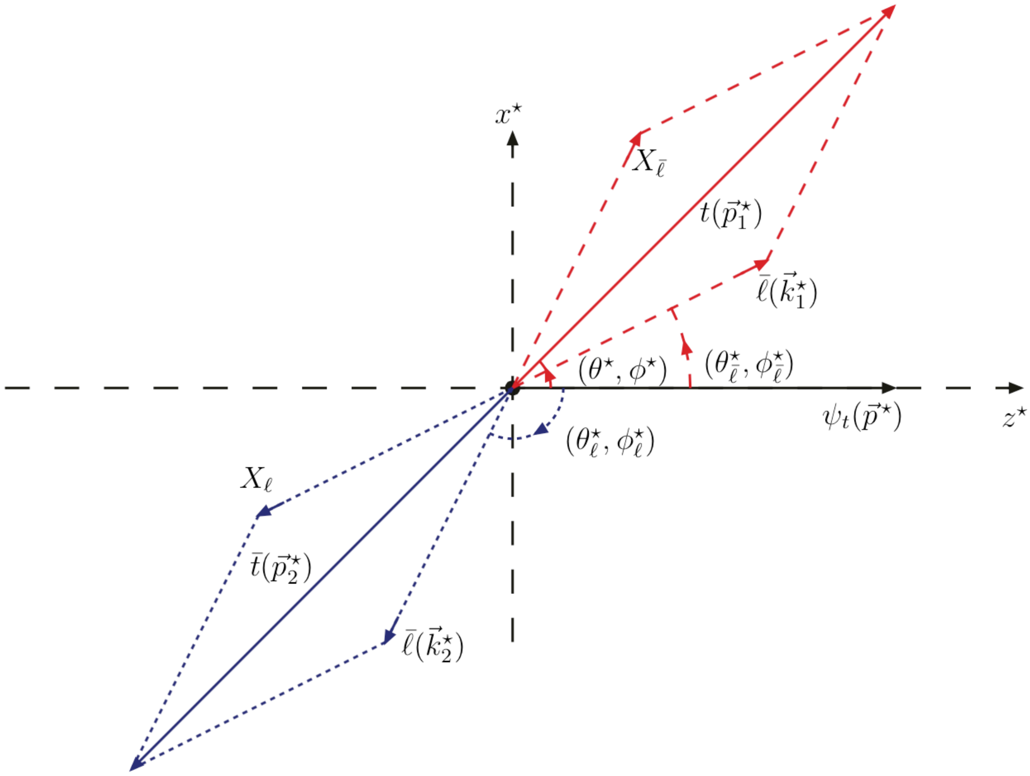

FIGURE 4.4: Definitions of the kinematical variables of tops and leptons in the toponium rest frame. The $z^\star$ and $x^\star$ axes are specified by the toponium moving direction and the scattering plane in the laboratory frame, respectively.

$$\widetilde{\psi}^{J_\psi}(p;\lambda_{\psi_t}) \to t(p_1,\sigma_t) + \bar{t}(p_2,\sigma_{\bar{t}}) \to \bar{\ell}(k_1) + X_{\bar{\ell}} + \ell(k_2) + X_\ell\,. \tag{4.57}$$

As we have mentioned the helicity amplitudes of toponium are obtained by using the spin projection of the helicity amplitudes of $t\bar{t}$ decay. The helicity amplitudes of $t\bar{t}$ decay can be separated into t and $\bar{t}$ decay amplitudes as follows

$$\mathcal{M}_D(\sigma_t,\sigma_{\bar{t}}) = \langle(\ell\nu_{\bar{\ell}}\bar{b})(\bar{\ell}\nu_\ell b)|\mathcal{T}_D|t(\sigma_t)\bar{t}(\sigma_{\bar{t}})\rangle = \mathcal{M}_t(\sigma_t)\mathcal{M}_{\bar{t}}(\sigma_{\bar{t}})\,. \tag{4.58}$$

The helicity amplitudes of t and $\bar{t}$ decays are well know. By using the Fierzt identities the amplitudes can be decomposed two parts which are separately Lorentz invariant. After integrating out the kinematical variables of $(b\nu)/(\bar{b}\bar{\nu}_\ell)$, t and $\bar{t}$ decays become just two two-body decays. The lepton/anti-lepton carries all the spin informations of t and $\bar{t}$. We use this technique to calculate the helicity amplitudes. Furthermore we will neglect the lepton mass in the following calculations. In the rest frame of toponium the kinematical variables are defined as follows,

$$p_1^{\star\mu} = \frac{\sqrt{s_\psi}}{2}(1+\frac{m_t^{\star 2}-\bar{m}_t^{\star 2}}{s_\psi},\ \beta_t\sin\theta^\star\cos\phi^\star,\ \beta_t\sin\theta^\star\sin\phi^\star,\ \beta_t\cos\theta^\star)\,, \tag{4.59a}$$

$$p_2^{\star\mu} = \frac{\sqrt{s_\psi}}{2}(1-\frac{m_t^{\star 2}-\bar{m}_t^{\star 2}}{s_\psi},\ -\beta_t\sin\theta^\star\cos\phi^\star,\ -\beta_t\sin\theta^\star\sin\phi^\star,\ -\beta_t\cos\theta^\star)\,, \tag{4.59b}$$

$$k_1^{\star\mu} = E_{\bar{\ell}}(1,\ \sin\theta_{\bar{\ell}}^\star\cos\phi_{\bar{\ell}}^\star,\ \sin\theta_{\bar{\ell}}^\star\sin\phi_{\bar{\ell}}^\star,\ \cos\theta_{\bar{\ell}}^\star)\,, \tag{4.59c}$$

$$k_2^{\star\mu} = E_\ell(1,\ \sin\theta_\ell^\star\cos\phi_\ell^\star,\ \sin\theta_\ell^\star\sin\phi_\ell^\star,\ \cos\theta_\ell^\star)\,. \tag{4.59d}$$

By using the Fierz transformations, the kinematical variables of $(b\nu)/(\bar{b}\bar{\nu}_\ell)$ can be factorized out completely. Then the helicity amplitudes of t and $\bar{t}$ decays can be written as,

$$\begin{aligned}
&\mathcal{M}_t(\sigma_t)\\
=\ & A_t\sqrt{E_t}\sqrt{E_{\bar{\ell}}}\,e^{i\sigma_t\phi^\star}\\
\times\ & \left(\cos\frac{\theta^\star}{2}\sqrt{1+2\sigma_t\cos\tilde{\theta}_{\bar{\ell}}}e^{i\sigma_t(\phi_{\bar{\ell}}^\star-\phi^\star)} + 2\sigma_t\sin\frac{\theta^\star}{2}\sqrt{1-2\sigma_t\cos\tilde{\theta}_{\bar{\ell}}}e^{-i\sigma_t(\phi_{\bar{\ell}}^\star-\phi^\star)}\right),
\end{aligned} \tag{4.60}$$

$$\begin{aligned}
& \mathcal{M}_{\bar{t}}(\sigma_{\bar{t}}) \\
= \;& A_t\sqrt{E_t}\sqrt{E_{\bar{\ell}}}\, e^{i\sigma_{\bar{t}}\phi^\star} \\
\times \;& \left(\cos\frac{\theta^\star}{2}\sqrt{1+2\sigma_{\bar{t}}\cos\tilde{\theta}_\ell}\, e^{-i\sigma_{\bar{t}}(\phi^\star_{\bar{\ell}}-\phi^\star)} + 2\sigma_{\bar{t}}\sin\frac{\theta^\star}{2}\sqrt{1-2\sigma_{\bar{t}}\cos\tilde{\theta}_\ell}\, e^{i\sigma_t(\phi^\star_{\bar{\ell}}-\phi^\star)}\right), \qquad (4.61)
\end{aligned}$$

where A_t and $A_{\bar{t}}$ stand for the rest of the helicity amplitude which are Lorentz invariant.

The $t\bar{t}$ decay helicity amplitudes $\mathcal{M}_D(\sigma_t,\sigma_{\bar{t}})$ can be obtained by using Eq. (4.58). In terms of helicity $(m,\tilde{m})$, $\mathcal{M}_D(\sigma_t,\sigma_{\bar{t}})$ can be written as follows

$$\mathcal{M}_D(m) \;\propto\; \cos^2\frac{\theta^\star}{2} f_{m,-m} - \sin^2\frac{\theta^\star}{2} f_{-m,m} - \frac{1}{2} m \sin\theta^\star\big(k_{m,m} - k_{-m,-m}\big) \qquad (4.62a)$$

$$\mathcal{M}_D(\tilde{m}) \;\propto\; e^{i\tilde{m}\phi^\star}\left(\cos^2\frac{\theta^\star}{2} k_{\tilde{m},\tilde{m}} + \sin^2\frac{\theta^\star}{2} k_{-\tilde{m},-\tilde{m}} + \frac{\tilde{m}}{2}\sin\theta^\star\big(f_{\tilde{m},-\tilde{m}} + f_{-\tilde{m},\tilde{m}}\big)\right), \qquad (4.62b)$$

where the functions $f_{m,m'}$ and $k_{m,m'}$ are defined as follows

$$f_{m,m'}(\phi^\star;\theta^\star_{\bar{\ell}},\phi^\star_{\bar{\ell}};\theta^\star_\ell,\phi^\star_\ell;) \;=\; g_{m,m'}(\theta^\star_{\bar{\ell}},\theta^\star_\ell)\, e^{im(\phi^\star_{\bar{\ell}}+\phi^\star_{\ell})/2} e^{im'\phi^\star} \qquad (4.63)$$

$$k_{m,m'}(\phi^\star;\theta^\star_{\bar{\ell}},\phi^\star_{\bar{\ell}};\theta^\star_\ell,\phi^\star_\ell;) \;=\; g_{m,m'}(\theta^\star_{\bar{\ell}},\theta^\star_\ell)\, e^{im(\phi^\star_{\bar{\ell}}-\phi^\star_{\ell})/2} \qquad (4.64)$$

$$g_{m,m'}(\theta^\star_{\bar{\ell}},\theta^\star_\ell) \;=\; \sqrt{1+m\cos\theta^\star_{\bar{\ell}}}\sqrt{1+m'\cos\theta^\star_\ell}\,. \qquad (4.65)$$

The projected helicity amplitudes can be obtained by using the projection operators in Eq. (4.31a) and Eq. (4.31b). As we have explained the production rate of singlet toponium is highly suppressed in the threshold region. Therefore we study only the decay of triplet toponium here. In terms of $(m,\tilde{m})$, the projected decay helicity for triplet toponium is

$$\widetilde{\mathcal{M}}_D(\lambda_{\psi_t}) = \sum_{m=\pm1,\,\tilde{m}=\pm1} f^*(\tilde{m},m)\tilde{D}^{J=1}_{m,\lambda_{\psi_t}}(\theta^\star,\phi^\star)\big(\mathcal{M}_D(m)+\mathcal{M}_D(\tilde{m})\big)\,. \qquad (4.66)$$

The explicit helicity amplitudes are

$$\widetilde{\mathcal{M}}_D(\lambda_{\psi_t}=0) \;\propto\; \sqrt{2}\Big(g_{1,1}(\theta^\star_{\bar{\ell}},\theta^\star_\ell)e^{i(\phi^\star_{\bar{\ell}}-\phi^\star_\ell)/2} - g_{-1,-1}(\theta^\star_{\bar{\ell}},\theta^\star_\ell)e^{-i(\phi^\star_{\bar{\ell}}-\phi^\star_\ell)/2}\Big), \qquad (4.67a)$$

$$\widetilde{\mathcal{M}}_D(\lambda_{\psi_t}=1) \;\propto\; -\,g_{1,-1}(\theta^\star_{\bar{\ell}},\theta^\star_\ell)e^{i(\phi^\star_{\bar{\ell}}+\phi^\star_\ell)/2}\,, \qquad (4.67b)$$

$$\widetilde{\mathcal{M}}_D(\lambda_{\psi_t}=-1) \;\propto\; g_{-1,1}(\theta^\star_{\bar{\ell}},\theta^\star_\ell)e^{-i(\phi^\star_{\bar{\ell}}+\phi^\star_\ell)/2}\,. \qquad (4.67c)$$

The corresponding decay density matrix is defined as

$$\rho_D(\lambda_{\psi_t}, \lambda'_{\psi_t}) = \int d\Phi(b\nu; b\bar{\nu}) \widetilde{\mathcal{M}}_D(\lambda_{\psi_t}) \widetilde{\mathcal{M}}^\dagger_D(\lambda'_{\psi_t}) \,, \tag{4.68}$$

with following matrix elements

$$\rho_D(0,0) \;\propto\; 2\left(4\cos^2\frac{\theta^\star_{\bar\ell}}{2}\cos^2\frac{\theta^\star_\ell}{2} + 4\sin^2\frac{\theta^\star_{\bar\ell}}{2}\sin^2\frac{\theta^\star_\ell}{2} - 2\sin\theta^\star_{\bar\ell}\sin\theta^\star_\ell\cos(\phi^\star_{\bar\ell} - \phi^\star_\ell)\right) \tag{4.69a}$$

$$\rho_D(+,+) \;\propto\; 4\cos^2\frac{\theta^\star_{\bar\ell}}{2}\sin^2\frac{\theta^\star_\ell}{2} \,, \tag{4.69b}$$

$$\rho_D(-,-) \;\propto\; 4\sin^2\frac{\theta^\star_{\bar\ell}}{2}\cos^2\frac{\theta^\star_\ell}{2} \,, \tag{4.69c}$$

$$\rho_D(0,+) \;\propto\; 2\sqrt{2}\left(\sin\theta^\star_{\bar\ell}\sin^2\frac{\theta^\star_\ell}{2}e^{-i\phi^\star_{\bar\ell}} - \sin\theta^\star_\ell\cos^2\frac{\theta^\star_{\bar\ell}}{2}e^{i\phi^\star_\ell}\right) \,, \tag{4.69d}$$

$$\rho_D(0,-) \;\propto\; 2\sqrt{2}\left(\sin\theta^\star_{\bar\ell}\cos^2\frac{\theta^\star_\ell}{2}e^{i\phi^\star_{\bar\ell}} - \sin\theta^\star_\ell\sin^2\frac{\theta^\star_{\bar\ell}}{2}e^{-i\phi^\star_\ell}\right) \,, \tag{4.69e}$$

$$\rho_D(+,-) \;\propto\; -\sin\theta^\star_{\bar\ell}\sin\theta^\star_\ell e^{i(\phi^\star_{\bar\ell}+\phi^\star_\ell)} \,. \tag{4.69f}$$

The spin correlations happens if the imaginary part of the decay density matrix is non-zero. The above results indicates that the spin correlations can appear in transverse-transverse and transverse-longitudinal interferences.

4.2.4 Total Helicity amplitudes and CP observables

In this subsection we discuss the interferences among the different helicity states of triplet toponium. The CP observables are obtained by study the spin correlations in the interferences. As we have mentioned there are two kinds of interference: transverse-transverse (TT) and transverse-longitudinal (LT) interferences, which are predicted by the total density matrix

$$\rho = \sum_{\lambda_V=\pm1} \rho(\lambda_V) = \sum_{\lambda_V=\pm1} \sum_{\lambda_{\psi_t}=0,\pm1} \sum_{\lambda'_{\psi_t}=0,\pm1} \rho(\lambda_V; \lambda_{\psi_t}, \lambda'_{\psi_t}) \tag{4.70}$$

where for convenience we have defined an intermediate density matrix as follows

$$\rho(\lambda_V; \lambda_{\psi_t}, \lambda'_{\psi_t}) = \rho_P(\lambda_V; \lambda_{\psi_t}, \lambda'_{\psi_t}) \rho_D(\lambda'_{\psi_t}, \lambda_{\psi_t}) \,. \tag{4.71}$$

For TT interference we have

$$\rho(\lambda_V;\lambda_{\psi_t},-\lambda_{\psi_t}) \propto -\frac{1}{4}\sin\vartheta^2\sin\theta^\star_{\bar\ell}\sin\theta^\star_\ell e^{i\lambda_{\psi_t}(\phi^\star_{\bar\ell}+\phi^\star_\ell+2\tilde\xi)}\,. \tag{4.72}$$

Therefore the total cross section has a following non-trivial distribution against the observable $\phi^\star_{\bar\ell}+\phi^\star_\ell$,

$$\frac{d\sigma}{d(\phi^\star_{\bar\ell}+\phi^\star_\ell)} = \frac{1}{2\pi}\sigma_0 - C_{TT}\cos(\phi^\star_{\bar\ell}+\phi^\star_\ell-2\tilde\xi)\,, \tag{4.73}$$

where σ_0 is the total cross section, and C_{TT} is the coefficient of the TT correlation.

For LT interference we have

$$\begin{aligned}&\rho(\lambda_V;0,+)\\ \propto\quad & -\sin\vartheta(1+\lambda_V\cos\vartheta)\left(\sin\theta^\star_{\bar\ell}\sin^2\frac{\theta^\star_\ell}{2}e^{-i(\phi^\star_{\bar\ell}-\tilde\xi)}-\sin\theta^\star_\ell\cos^2\frac{\theta^\star_{\bar\ell}}{2}e^{-i(\phi^\star_\ell-\tilde\xi)}\right), \qquad (4.74)\\ &\rho(\lambda_V;0,-)\\ \propto\quad & -\sin\vartheta(1-\lambda_V\cos\vartheta)\left(\sin\theta^\star_{\bar\ell}\cos^2\frac{\theta^\star_\ell}{2}e^{i(\phi^\star_{\bar\ell}-\tilde\xi)}-\sin\theta^\star_\ell\sin^2\frac{\theta^\star_{\bar\ell}}{2}e^{i(\phi^\star_\ell-\tilde\xi)}\right). \qquad (4.75)\end{aligned}$$

We can see that the azimuthal angles of lepton and anti-lepton have different $\tilde\xi$ dependences. For lepton, the total cross section has a following non-trivial distribution,

$$\frac{d\sigma}{d\phi^\star_\ell} = \frac{1}{2\pi}\sigma_0 + C_{LT}\cos(\phi^\star_\ell-\tilde\xi)\,, \tag{4.76}$$

where C_{LT} is the coefficient of the LT correlation. For anti-lepton we have,

$$\frac{d\sigma}{d\phi^\star_{\bar\ell}} = \frac{1}{2\pi}\sigma_0 - C_{LT}\cos(\phi^\star_{\bar\ell}-\tilde\xi)\,. \tag{4.77}$$

We can see that the correlations are different for lepton and anti-lepton. For lepton, the correlation is positive. For anti-lepton, the correlation is negative. However the phase shifts are negative for both lepton and anti-lepton. These tow correlations are related by the CP transformation. In the case of $\tilde\xi = 0$, *i.e.* CP is conserved, these two correlations are symmetric under the CP transformation $\phi^\star_{\bar\ell} \to \phi^\star_\ell + \pi$ and likewise for lepton. However, if $\tilde\xi \neq 0$, then the CP transformation of the parameter $\tilde\xi = 0$, $\xi \to -\xi$, violates this symmetry, and therefore indicates the violation of CP symmetry.

4.3 Radiative corrections near the threshold region

As we have explained in Sec.4.1, the virtual top is hugely off-shell. According to the uncertainty principle, it can propagate only a distance $\sim 1/(\sqrt{s} - m_t)$ which is considerably shorter than the Columb radius $r_C \sim 1/(\alpha_s m_t)$. Therefore, the near threshold production can be treated by a local source $\delta^4(y_t - y_{\bar{t}}) j^\mu(Q^2) e^{-iQ\cdot y_t}$. In this approximation, the higgs field decouple from the exact vertex function $\langle Th(z')\bar{t}_i(y_t) t_j(y_{\bar{t}}) V^\mu(z)\rangle$ by modifying the $t\bar{t}V$ vertex function which has been examined in Sec.4.1. The modified production vertex are then in turn to affect the quantum numbers of the generated toponium, which has been discussed in Sec.4.1. Here we examine how these vertexes are affected by the QCD radiative corrections. The corrections are described by the relativistic Salpeter-Bethe (SB) equation in general[82]. For a general production vertex Γ^μ_C the SB equation is

$$V^\mu_C(P,q) = \Gamma^\mu_C(P,q) + \int \frac{d^4k}{(2\pi)^4} \mathcal{U}_{\alpha\beta}(q-k)\gamma^\alpha S_F(P/2+k) V^\mu_C(P,k) S_F(-P/2+k)\gamma^\beta\,, \tag{4.78}$$

where $\mathcal{U}_{\alpha\beta}(q-k)$ is the potential in momentum space. This integral equation sum over all the contributions from the relevant ladder diagrams. Here we will consider only the instantaneous Coulomb-like potential, contributions from the transverse and rest gluons are suppressed by powers of β_t.

In the rest frame of $t\bar{t}$, the dominate contributions come from the region where $|\vec{k}| \ll m_t$, and the fermionic propagators are approximated by

$$S_F(P/2+k) = \frac{i(\gamma_+ - \vec{k}\cdot\vec{\gamma}/(2m_t))}{E/2 + k^0 - \vec{k}^2/(2m_t) + i\Gamma_t/2}\,, \tag{4.79a}$$

$$S_F(-P/2+k) = \frac{i(\gamma_- - \vec{k}\cdot\vec{\gamma}/(2m_t))}{E/2 - k^0 - \vec{k}^2/(2m_t) + i\Gamma_t/2}\,, \tag{4.79b}$$

where $\gamma_\pm = (1 \pm \gamma^0)/2$ are the non-relativistic projection operators for fermion and anti-fermion. Observing that the vertex function is independent on the energy q^0, then the variable k^0 could be integrated out and we get

$$V^\mu_C(E,\vec{q}) = \Gamma^\mu_C - \int \frac{d^3\vec{k}}{(2\pi)^3} U(\vec{q}-\vec{k})\gamma^0 \left(\gamma_+ - \frac{\vec{k}\cdot\vec{\gamma}}{2m_t}\right) \frac{V^\mu_C(E,\vec{k})}{E - \vec{k}^2/m_t + i\Gamma_t} \left(\gamma_- - \frac{\vec{k}\cdot\vec{\gamma}}{2m_t}\right)\gamma^0\,. \tag{4.80}$$

In our case the toponium system could be changed by the recoil of Higgs, therefore we express all the quantities in a Lorentz invariant way as follows

$$E = \frac{1}{2}\sqrt{(p_1+p_2)^2} = \frac{1}{2}\sqrt{p^2}\,, \tag{4.81a}$$

$$\gamma^0 = \frac{\not p_1 + \not p_2}{2E} = \frac{\not p}{2E} = \frac{\not p}{\sqrt{p^2}}\,, \tag{4.81b}$$

$$\gamma^i\gamma^0 = \frac{1}{2}[\gamma^\mu,\gamma^0] = \frac{1}{2\sqrt{p^2}}[\gamma^\mu,\not p] \equiv \widetilde{\gamma}^\mu\,. \tag{4.81c}$$

Then the integral equation can be rewritten in a covariant form,

$$V_C^\mu(E,\vec q) = \Gamma_C^\mu + \int \frac{d^3\vec k}{(2\pi)^3} U(\vec q - \vec k)\left(\gamma_+ - \frac{\widetilde{\not k}}{2m_t}\right)\frac{V_C^\mu(E,\vec k)}{E - \vec k^2/m_t + i\Gamma_t}\left(\gamma_- - \frac{\widetilde{\not k}}{2m_t}\right). \tag{4.82}$$

Define the non-relativestic projection opertators for fermion and anti-fermions as follows

$$\widetilde{\gamma}_+(\vec q) = \gamma_+ - \frac{\widetilde{\not q}}{2m_t} = \gamma_+(1 - \frac{\widetilde{\not q}}{2m_t}) - \gamma_-\frac{\widetilde{\not q}}{2m_t}\,, \tag{4.83a}$$

$$\widetilde{\gamma}_-(\vec q) = \gamma_- - \frac{\widetilde{\not q}}{2m_t} = (1 - \frac{\widetilde{\not q}}{2m_t})\gamma_- - \frac{\widetilde{\not q}}{2m_t}\gamma_+\,. \tag{4.83b}$$

The second terms in both $\widetilde{\gamma}_+(\vec q)$ and $\widetilde{\gamma}_-(\vec q)$ involve the small component of the Dirac spinor which are of P-wave and then suppressed by a further factor β_t. Therefore in the following calculations we will neglect them. In this approximation, an useful relation is

$$\gamma_+\widetilde{\not q} = \widetilde{\not q}\gamma_-\,. \tag{4.84}$$

Multiplying $\widetilde{\gamma}_+(\vec q)$ on the left-hand side and $\widetilde{\gamma}_-(\vec q)$ on the right-hand side of Eq. (4.82), we get

$$\widetilde{\gamma}_+(\vec q)V_C^\mu(E,\vec q)\widetilde{\gamma}_-(\vec q) \approx \widetilde{\gamma}_+(\vec q)\Gamma_C^\mu\widetilde{\gamma}_-(\vec q) + \int \frac{d^3\vec k}{(2\pi)^3} U(\vec q - \vec k)\frac{\widetilde{\gamma}_+(\vec k)V_C^\mu(E,\vec k)\widetilde{\gamma}_-(\vec k)}{E - \vec k^2/m_t + i\Gamma_t}\,. \tag{4.85}$$

Introducing the non-relativistic reduced vertex function

$$\widetilde{V}_C^\mu(E,\vec q) = \widetilde{\gamma}_+(\vec q)V_C^\mu(E,\vec q)\widetilde{\gamma}_-(\vec q) \quad , \quad \widetilde{\Gamma}_C^\mu = \widetilde{\gamma}_+(\vec q)\Gamma_C^\mu\widetilde{\gamma}_-(\vec q)\,, \tag{4.86}$$

the integral equation Eq. (4.85) reduces to

$$\widetilde{V}_C^\mu(E,\vec{q}) = \widetilde{\Gamma}_C^\mu(E,\vec{q}) + \int \frac{d^3\vec{k}}{(2\pi)^3} U(\vec{q}-\vec{k}) \frac{\widetilde{V}_C^\mu(E,\vec{k})}{E - \vec{k}^2/m_t + i\Gamma_t} . \tag{4.87}$$

This is a formal Lippmann-Schwinger (LS) equation [83]. Here we study only the corrections on production vertex up to tems linear in $\vec{q}$. Expanding the vertex $\widetilde{\Gamma}_C^\mu(E,\vec{q})$ by $\vec{q}$ we have,

$$\widetilde{\Gamma}_C^\mu(E,\vec{q}) = \mathcal{S}_C^\mu(E) - \mathcal{P}_C^{\mu\nu}(E) q_\nu , \tag{4.88}$$

where

$$\mathcal{S}_C^\mu(E) = \widetilde{\Gamma}_C^\mu(E,\vec{q}=0) , \tag{4.89a}$$
$$\mathcal{P}_C^{\mu\nu}(E) = \frac{\partial}{\partial q_\nu} \widetilde{\Gamma}_C^\mu(E,\vec{q}) \bigg|_{\vec{q}=0} , \tag{4.89b}$$

are the S- and P-wave components. The corrected vertex function $\widetilde{V}_C^\mu(E,\vec{q})$ can be expanded in the same way, and we get

$$\widetilde{V}_C^\mu(E,\vec{q}) = \mathcal{S}_C^\mu(E) \mathcal{K}_S(E,\vec{q}) + \vec{\mathcal{P}}_C^\mu(E) \cdot \vec{q}\, \mathcal{K}_P(E,\vec{q}) . \tag{4.90}$$

The expansion coefficients satisfy following integral equations

$$\mathcal{K}_S(E,\vec{q}) = 1 + \int \frac{d^3\vec{k}}{(2\pi)^3} U(\vec{q}-\vec{k}) \frac{\mathcal{K}_S(E,\vec{k})}{E - \vec{k}^2/m_t + i\Gamma_t} , \tag{4.91a}$$
$$\mathcal{K}_P(E,\vec{q}) = 1 + \int \frac{d^3\vec{k}}{(2\pi)^3} \frac{\vec{q}\cdot\vec{k}}{\vec{q}^2} U(\vec{q}-\vec{k}) \frac{\mathcal{K}_P(E,\vec{k})}{E - \vec{k}^2/m_t + i\Gamma_t} . \tag{4.91b}$$

These two integral equations are related to the Green function $G(\vec{r}_x, \vec{r}_x)$ which satisfies the Lippmann-Schwinger equation in the momentum space

$$\left(E - \frac{\vec{p}^2}{m_t} + i\Gamma_t\right) G(E;\vec{p},\vec{r}_y) = e^{i\vec{p}\cdot\vec{r}_y} + \int \frac{d^3\vec{k}}{(2\pi)^3} U(\vec{p}-\vec{k}) G(E;\vec{k},\vec{r}_y) . \tag{4.92}$$

As we have mentioned, the local interaction approximation is excellent in the production vertex, therefore the vertex functions are approximated by the condition $\vec{r}_y = 0$. Expanding the Green function $G(E;\vec{k},\vec{r}_y)$ by $\vec{r}_y$,

$$G(E;\vec{p},\vec{r}_y) = G_S(E;\vec{p},\vec{r}_y = 0) + (i\vec{r}_y \cdot \vec{p})\, G_P(E;\vec{p},\vec{r}_y = 0) , \tag{4.93}$$

and the plane wave factor $e^{i\vec{p}\cdot\vec{r}_y}$ we obtain following integral equations

$$\left(E-\frac{\vec{p}^2}{m_t}+i\Gamma_t\right)G_S(E;\vec{p}) \;=\; 1+\int\frac{d^3\vec{k}}{(2\pi)^3}U(\vec{p}-\vec{k})G_S(E;\vec{k})\,, \tag{4.94a}$$

$$\left(E-\frac{\vec{p}^2}{m_t}+i\Gamma_t\right)G_P(E;\vec{p}) \;=\; 1+\int\frac{d^3\vec{k}}{(2\pi)^3}\frac{\vec{p}\cdot\vec{k}}{\vec{p}^2}U(\vec{p}-\vec{k})G_P(E;\vec{k})\,. \tag{4.94b}$$

The solutions are

$$G_S(E;\vec{p}) \;=\; G_0(E;\vec{p})+G_0(E;\vec{p})\int\frac{d^3\vec{k}}{(2\pi)^3}U(\vec{p}-\vec{k})G_S(E;\vec{k})\,. \tag{4.95a}$$

$$G_P(E;\vec{p}) \;=\; G_0(E;\vec{p})+G_0(E;\vec{p})\int\frac{d^3\vec{k}}{(2\pi)^3}\frac{\vec{p}\cdot\vec{k}}{\vec{p}^2}U(\vec{p}-\vec{k})G_P(E;\vec{k})\,, \tag{4.95b}$$

where $G_0(E;\vec{p})$ is the Green function of the free toponium

$$G_0(E;\vec{p})=\frac{1}{E-\vec{p}^2/m_t+i\Gamma_t}\,. \tag{4.96}$$

The corrected Green functions are related to the correction factors $\mathcal{K}_S$ and $\mathcal{K}_P$ as follows

$$G_S(E;\vec{p}) \;=\; G_0(E;\vec{p})\mathcal{K}_S(E;\vec{p}) \tag{4.97a}$$

$$G_P(E;\vec{p}) \;=\; G_0(E;\vec{p})\mathcal{K}_P(E;\vec{p}) \tag{4.97b}$$

We will use the method give in Ref.[84] to solve the integral equation numerically. Fig. 4.5, 4.6, 4.7, 4.8 show the S- and P-wave Greens functions for binding energy $E = -2$GeV, 0GeV, 2GeV, 4GeV, respectively. We can see that at the ground state, the P-wave contribution is suppressed. However, the corrections on S- and P-wave are comparable for other states. Fig. 4.9, 4.10 show the counter lines of the absolute values of Green functions in the plane of binding enengy E and relative momentum $|\vec{q}|$.

4.4 Numerical results

Our numerical resuts are obtained by using MadGraph5[62] at the tree level, and then weighted by the QCD correction factor $\mathcal{K}_{S/p}(E,\vec{q})$ at LO. The LO QCD correction overestimated the non-relativistic effects by a constant factor of 0.843 in the whole phase space [85, 86], therefore our LO estimation can be safely used for studying the

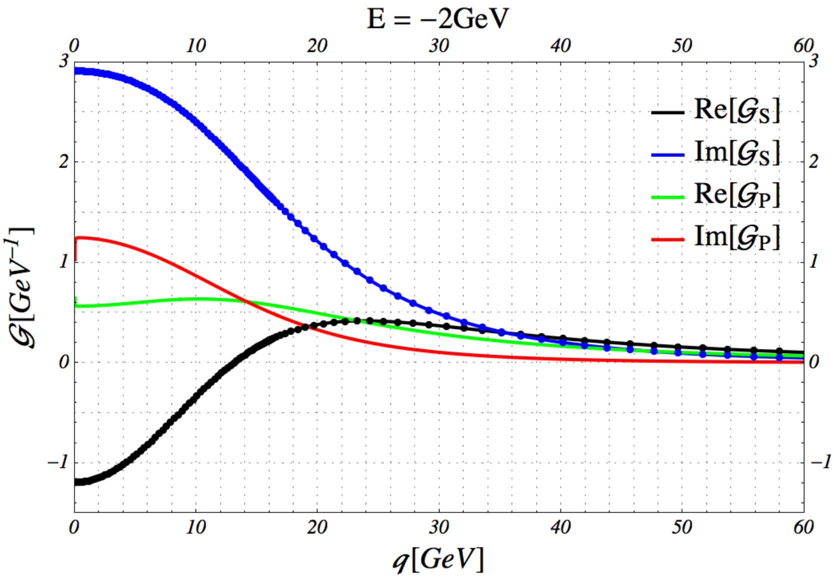

FIGURE 4.5: Green functions for binding energy $E = -2$GeV.

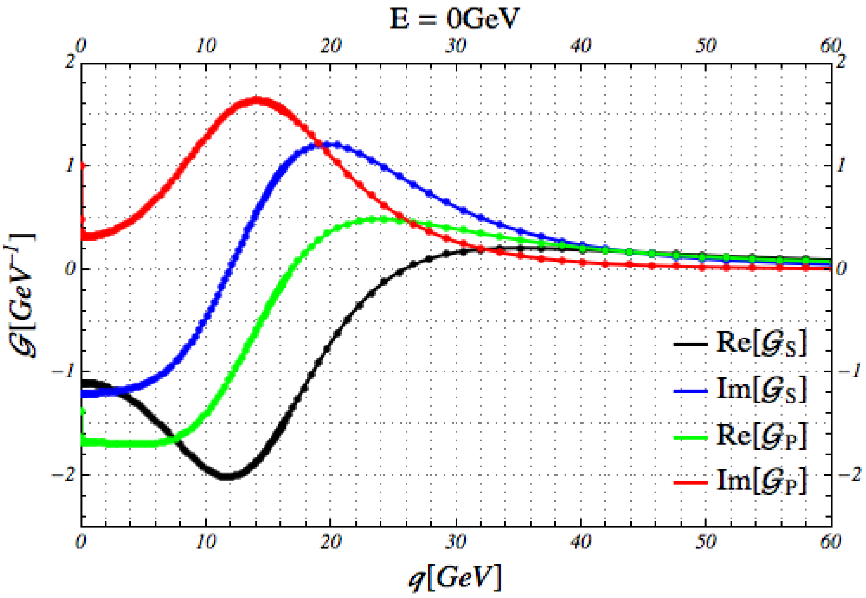

FIGURE 4.6: Green functions for binding energy $E = 0$GeV.

spin correlation. Fig. 4.11 and 4.12 show the production cross section of $ht\bar{t}$ with respect to the invariant mass of $t\bar{t}$ system for scalar Higgs and for pseudo-scalar Higgs, respectively. We can see the production cross section has a peak around the threshold energy. At the LO, the overall QCD enhancement factor is about 3. However, it has been pointed out that the NLO corrections are important particularly in the large $t\bar{t}$ invariant mass region [85], and the overall enhancement factor is about 2. The LO order $e^+e^- \to t\bar{t}h$ cross section is about $\sigma_{\mathrm{LO}} = 0.35\,\mathrm{fb}$ (we assume the electron and

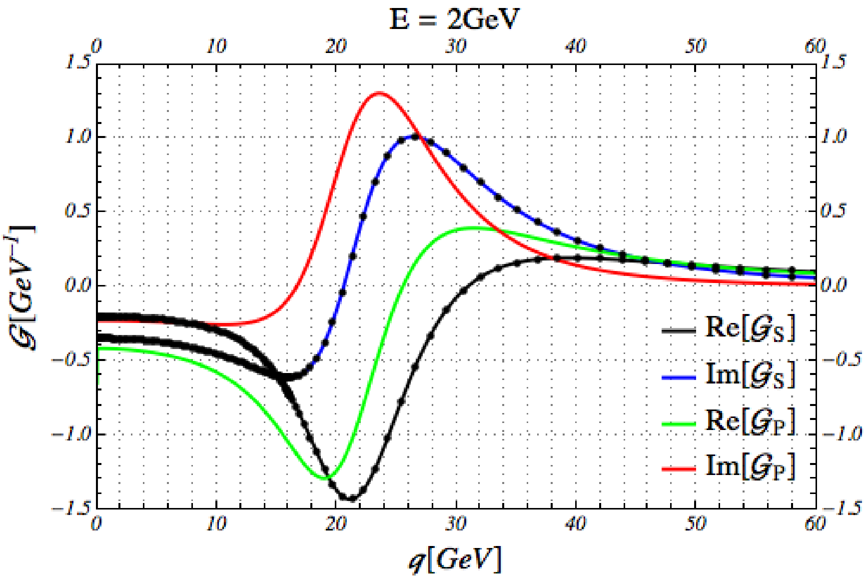

FIGURE 4.7: Green functions for binding energy 2GeV.

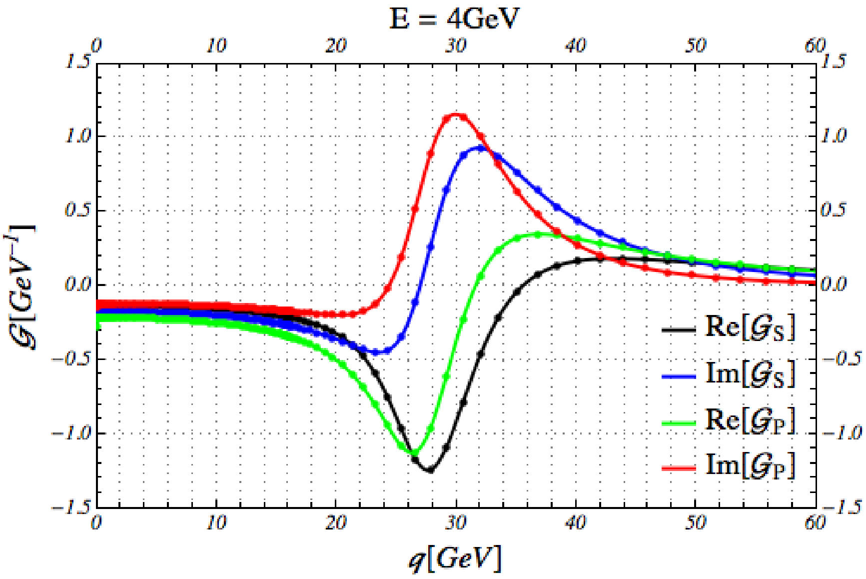

FIGURE 4.8: Green functions for binding energy $E = 4$GeV.

position beams are not polarized). Including the NLO correction the cross section is $\sigma_{\rm NLO} = 0.7\,{\rm fb}$. We will use this cross for the overall normalization.

With the approximation of only S-wave are dominate, we have calculated the azimuthal angle correlations of the leptons from taus decays. We have shown there are three independent CP observables. The first one is the sum of the azimuthal angles of leptons in the $t\bar{t}$ rest frame, which is because of the interference among ths transverse components of toponium. The correlation function has been given in Eq. (4.73). Fig.4.13 shows

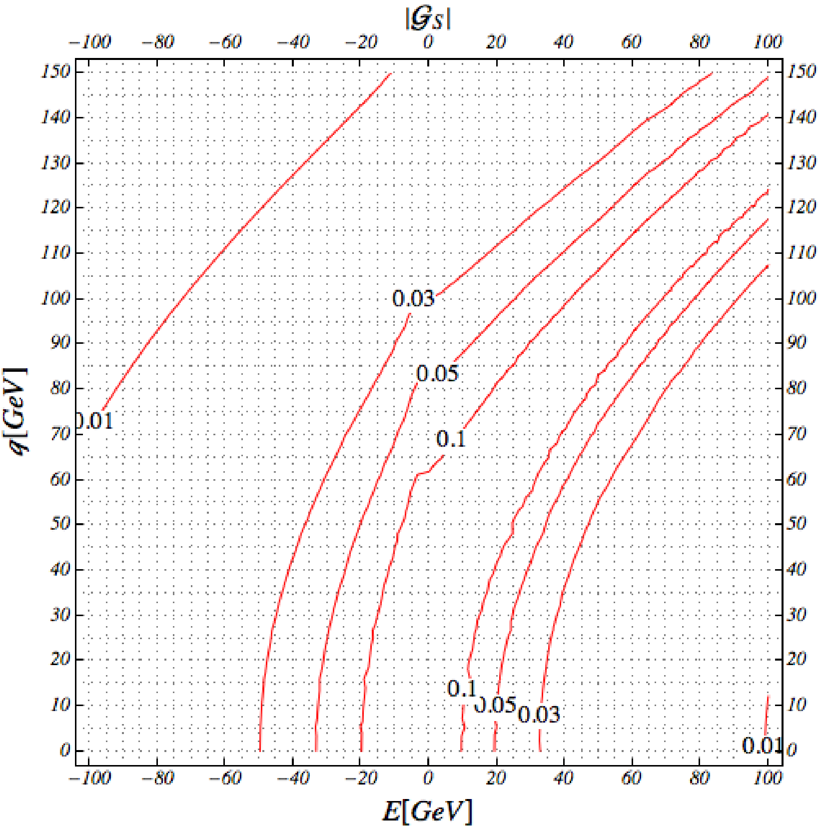

FIGURE 4.9: Contour plot of the absolute value of Green functions for S-wave.

the correlations for pure scalar Higgs (black-solid line) and for pure pseudo-scalar Higgs (red-dashed line). Both are symmetric about $\phi_{\bar{\ell}}^\star + \phi_\ell^\star = 0$ because of the CP conservation separately. However the distributions are completely different. In the case of scalar Higgs, the interference are constructive when the sum of azimuthal angles is $\pm\pi$. However it is constructive when the sum is 0 for a pseudo-scalar Higgs. Therefore the CP violation effect is sensitive to the sign of the parameter ϵ_h (or the mixing angle). Fig. 4.14 show three different cases: $\epsilon_h = 0$ (black-solid), $\epsilon_h = 5$ (red-dashed) and $\epsilon_h = -5$ (blue-dotted). Here in order to show the differences clearly we have chosen $|\epsilon_h| = 5$ which means an effectively maximum mixing because of a kinematical suppression factor $\kappa \approx 0.2$, see Eq. (4.51). Measuring the CP violation from transverse-transverse interference require the reconstruction of both lepton and anti-lepton. The branching ratio of top to leptons (e, μ) is $\text{Br}(t \to \ell X) = 19\%$. If we using the $h \to b\bar{b}$, which has a branching ratio 56.9%, to reconstruct the Higgs, then, for an projected integrated luminosity $4\,\text{ab}^{-1}$ at $\sqrt{s} = 500\text{GeV}$ [87], there are 60 signal events with 100% reconstruction efficiency. Simple estimation on the experimental sensitivity to $\Delta\xi_{htt} = 1.72$ is by assuming the kinematical suppression factor is 0.2. The sensitivity is rather low

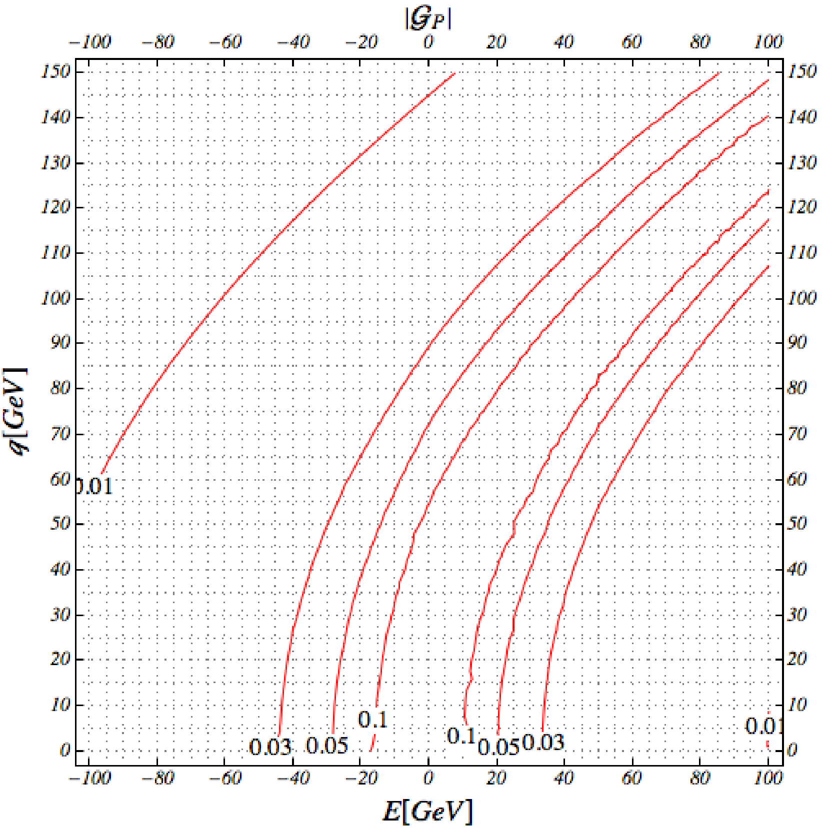

FIGURE 4.10: Contour plot of the absolute value of Green functions for P-wave.

because 1) the total production rate is low, 2) the strong kinematical suppression factor.

Apart from the interference among the transverse toponium, there are also interference between the longitudinal and transverse toponium which results in non-trivial azimuthal angle distributions of leptons in the $t\bar{t}$ rest frame. The correlation functions have been given in Eq. (4.76) and Eq. (4.77). The most important result is that lepton and anti-lepton have completely different interference distributions. It is constructive at the origin ($\phi^{\star}_{\ell,\bar{\ell}} = 0$) for lepton, however it is deconstructive for anti-lepton. For pure scalar Higgs, this feature is shown in Fig. 4.15. In the case of pure pseudo-scalar Higgs, because only the transverse toponium can be produced, there are no interference between longitudinal and transverse toponium. Therefore the azimuthal angle distributions are flat, which is shown in Fig. 4.16. Fig. 4.17 and 4.18 show the interferences in three cases: $\epsilon_h = 0$ (black-solid), $\epsilon_h = 5$ (red-dashed) and $\epsilon_h = -5$ (blue-dotted) for lepton and anti-lepton, respectively. We can see that both lepton and anti-lepton are sensitive to the sign of the CP violation parameter ϵ_h (or the mixing angle ξ). Most importantly, measuring

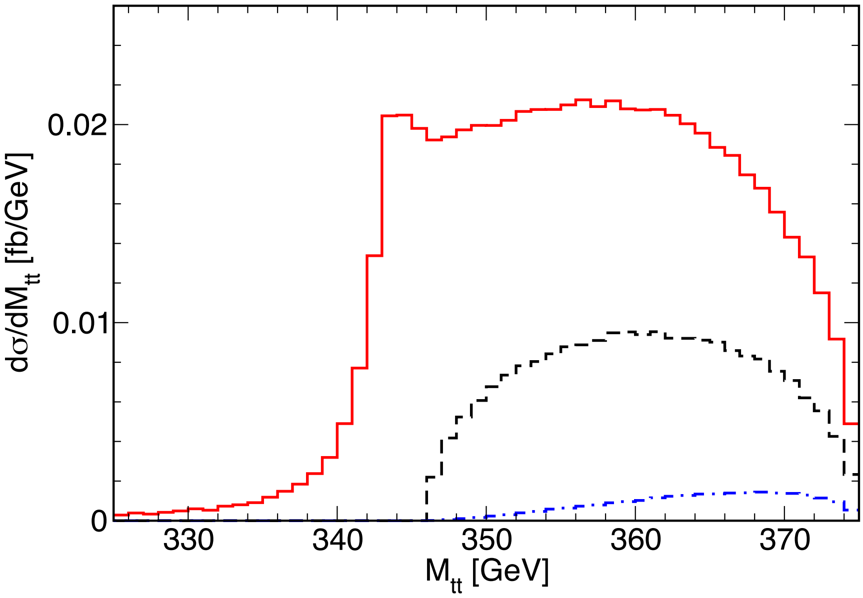

FIGURE 4.11: Production cross section for pure scalar Higgs with unpolarized beams at $\sqrt{s} = 500$GeV. The black-dashed line is the cross section of S-wave toponium at Born level. The blue-dash-dotted line shows the rest of the production cross section (which is essentially the P-wave contribution). The red-solid line shows the production cross section after the QCD-Coulomb corrections.

the CP violation from transverse-longitudinal interferences require only either lepton or anti-lepton is reconstructed. The branching ratio of top to leptons (e, μ) is $\mathrm{Br}(t \to \ell X) = 19\%$. If we using the $h \to b\bar{b}$, which has a branching ratio 56.9%, to reconstruct the Higgs, then for an projected integrated luminosity $4\,\mathrm{ab}^{-1}$ at $\sqrt{s} = 500$GeV [87], there are 298 signal events (for either lepton or anti-lepton) with 100% reconstruction efficiency. Combine the lepton and anti-leptons we have 595 signal events in total. Simple estimation on the experimental sensitivity to $\Delta\xi_{htt} = 0.5$ by assuming the kinematical suppression factor is 0.2.

In Ref. [79], the authors demonstrated that the CP properties of the Higgs can be assessed by measuring just the total cross section and the top polarization. However, both these two observables are CP-even, hence only proportional to the square of CP-odd coupling. Furthermore the ratio of the production rates pseudo-scalar and for scalar is small unless $\sqrt{s} \gg 1$TeV. Therefore the experimental sensitivity is not as good as enough to probe small CP-odd coupling. We really need CP-odd observables, which is linearly proportional to CP-odd coupling, to pin down the CP properties of Higgs. Here

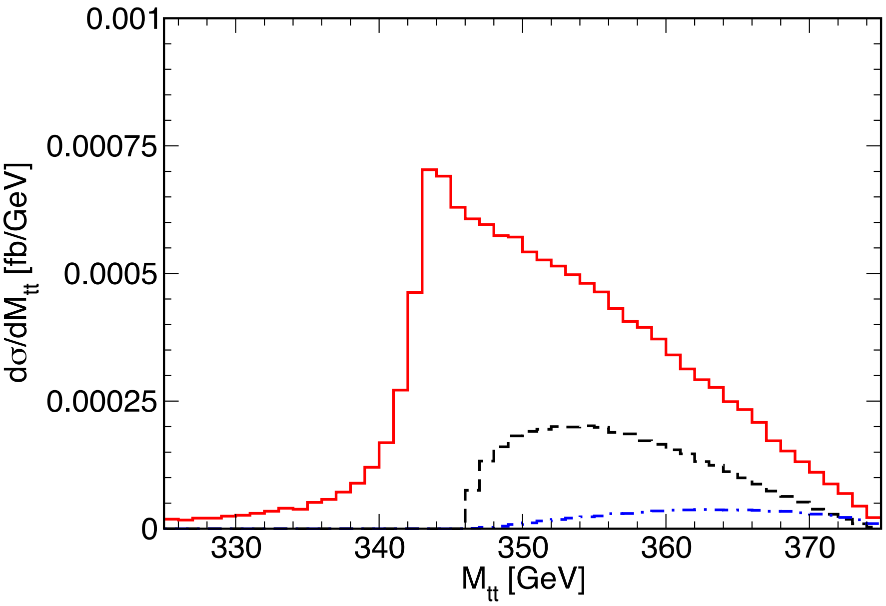

FIGURE 4.12: Production cross section for pure pseudo-scalar Higgs with unpolarized beams at $\sqrt{s} = 500\text{GeV}$, The black-dashed line is the cross section of S-wave toponium at Born level. The blue-dash-dotted line shows the rest of the production cross section (which is essentially the P-wave contribution). The red-solid line shows the production cross section after the QCD-Coulomb corrections.

based on our analytical results, we find three CP-odd observables, azimuthal angles of lepton and anti-leptons in the toponium rest frame as well as their sum. These three observables are well defined at the ILC, because the rest frame of toponium can be reconstructed directly. The nontrivial correlations come from the longitudinal-transverse interference for azimuthal angles of leptons, and transverse-transverse interference for their sum. Compared to the up-down asymmetry observable in Refs. [79–81] which requires the reconstruction of either top or anti-top momentum as well as the small hZZ interactions (a few percent for $\sqrt{s} \leq 1\text{TeV}$ [79]), our observables are purely from the dominate htt interactions, and don't require the reconstruction of the top or anti-top momentum. Furthermore, for all these three observables found in this paper have maximum asymmetries about 32%, more than 6 times larger than the maximum asymmetry (5%) in Refs. [80, 81]. Most importantly, for the longitudinal-transverse interference, because only one lepton is need, therefore the signal events are dramatically enhanced.

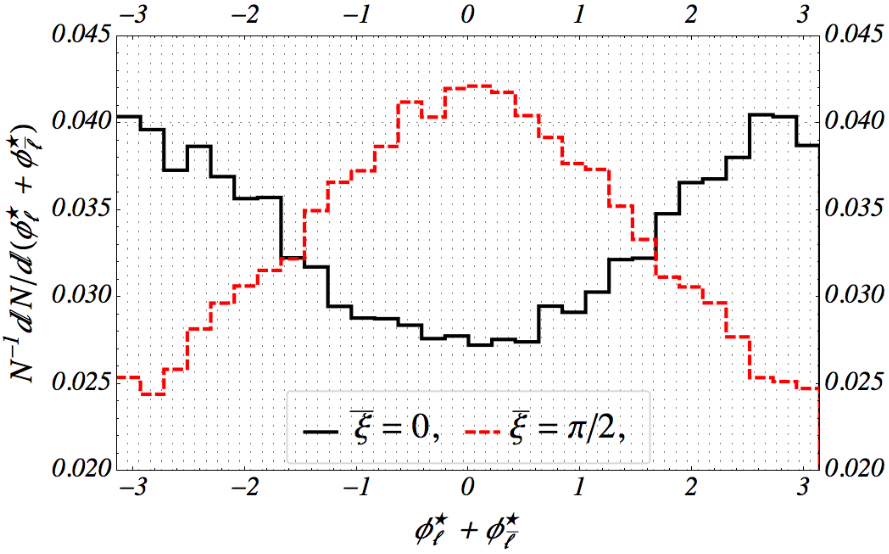

Figure 4.13: Azimuthal angle correlation for pure scalar (black-solid line) and pseudo-scalar (red-dahsed line).

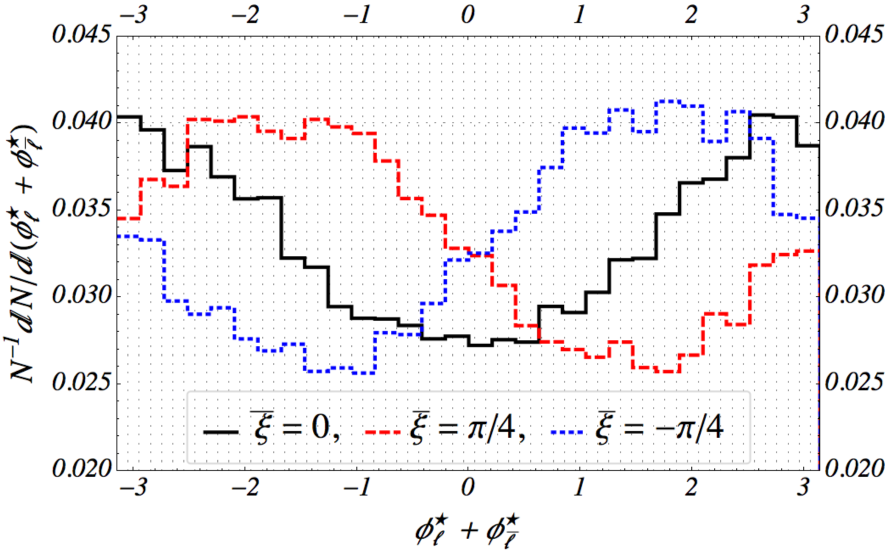

Figure 4.14: Azimuthal angle correlation for positive maximum mixing (red-dashed line), negative maximum mixing (blue-dotted line), and the reference case of pure scalar (black-solid line).

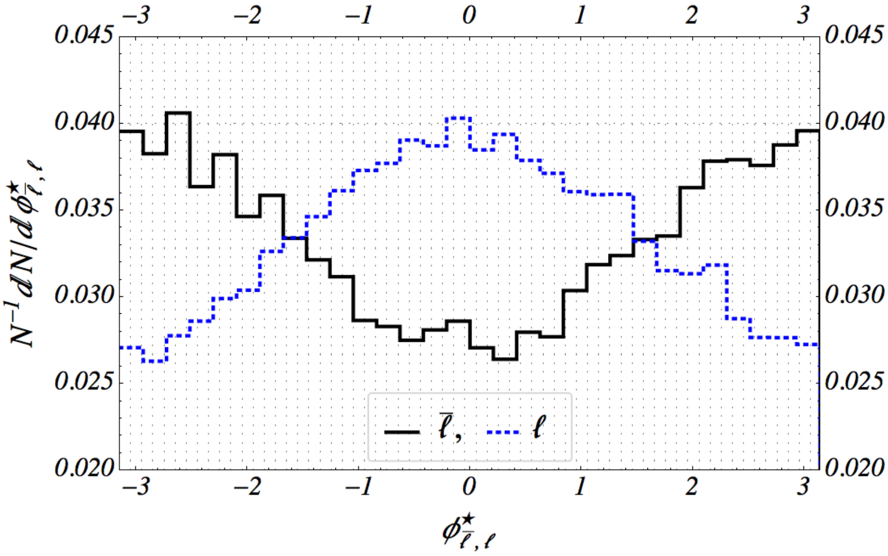

FIGURE 4.15: Azimuthal angle correlations of lepton and anti-leptons for pure scalar Higgs (black-solid line), pure pseudo-scalar (blue-dotted line).

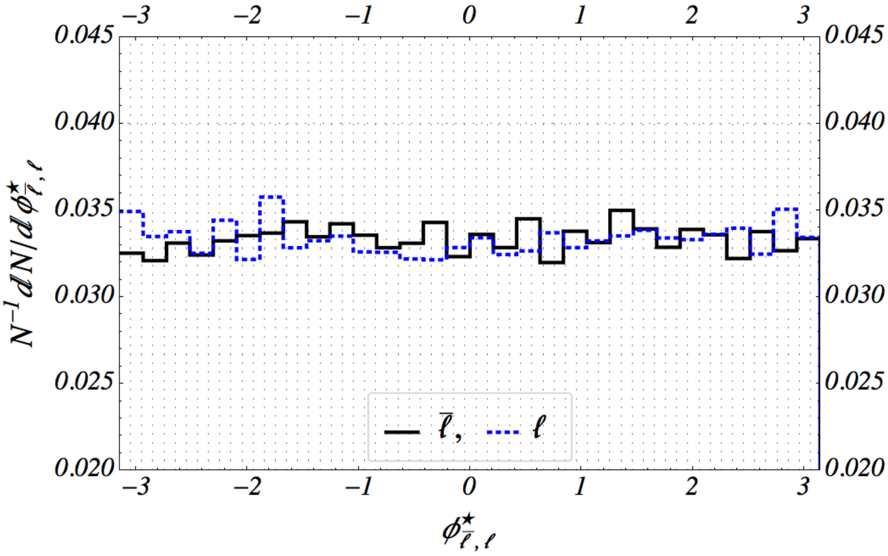

FIGURE 4.16: Azimuthal angle correlations of lepton and anti-leptons for pure scalar Higgs (black-solid line), pure pseudo-scalar (blue-dotted line).

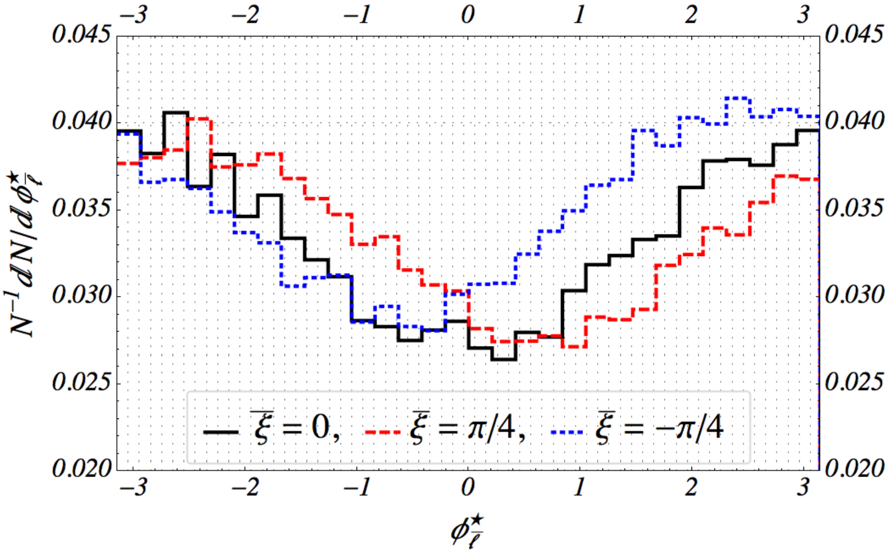

FIGURE 4.17: Azimuthal angle correlations of anti-leptons for mixing case.

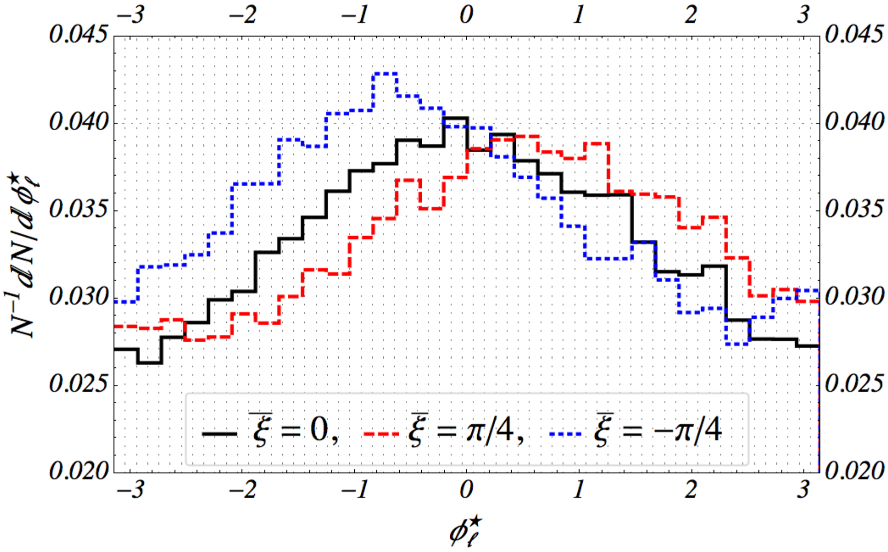

FIGURE 4.18: Azimuthal angle correlations of lepton for mixing case.

Chapter 5

Summary

We studied the CP violation effects in the Higgs sector via $h \to 4l$ channels at the LHC. Even through a pure CP odd Higgs is excluded experimentally based on the $h \to ZZ^\star \to 4l$. However, large mixing between CP even and CP odd scalars is still allowed. This is because the decay $h \to ZZ^\star \to 4l$ is proceed dominantly by the relevant CP even operator, however the CP odd scalar couples to Z pair only through the irrelevant CP odd operator at loop level.

However, it is promising to search for possible CP violation effects through the decay process $h \to Z(\gamma)\gamma \to 4l$, because both the CP even and CP odd operators appear at loop level. By investigating the analytical formulas, there are two kinds of correlations in which CP phase could come into play. The first one the azimuthal angle correlation between the two transverse polarized vector bosons. The correlation behaves like $\cos(2\phi)$. The second one is the azimuthal angle correlation between the longitudinal polarized Z and the transverse polarized photon, which behaves like $\cos(\phi)$. However we find there is tiny window to observe the correlation $\cos(\phi)$ since large backgrounds, it could not provide significant enhancement on the signal events. So the transverse-transverse correlation is the most important one.

For the process $h \to Z(\gamma)\gamma \to 4l$, the events are generated at tree level by using MadGraph5. And the nontrivial transverse momentum distribution of Higgs is included by using the Pythia6. For an integrated luminosity $3\,\text{ab}^{-1}$ at 14TeV, we find there are 60 events for $h \to \gamma\gamma \to 4l$, and 111 events for $h \to Z\gamma \to 4l$ for leptons with $p_T > 5$GeV and $|\eta| < 2.5$. The experiment sensitivity is estimated by assuming the CP violation is small and without backgrounds. For an integrated luminosity $3\,\mathrm{ab}^{-1}$ at 14TeV, a sensitivity 0.33 can be reached for $h \to \gamma\gamma$, and a sensitivity 0.25 can be reached for $h \to Z\gamma$.

On the other hand, even through the azimuthal angle of photon could be measured through the conversion process, and further about 60% the photons are converted to electrons in the ATLAS and CMS detectors, however we find the present angular resolution strongly suppresses the measuring efficiency. An improvement by a factor of 4 is need in order to have significant number of resolvable events.

The above results are obtained model independently. Here we discuss the implications on the MSSM model. In MSSM the interactions between the pseudo-scalar and down-type fermions are enhanced by $\tan\beta$, so apart from large CP violating coupling, a large nontrivial phase is also expected. Fig. 5.1 shows the $\tan\beta$ dependence of the magnitude of various loop induced couplings, and also the ratio of CP odd to CP even coupling. We can see that the CP even coupling $g_{HZ\gamma}$ is always larger then $g_{H\gamma\gamma}$, while the CP odd coupling $g_{AZ\gamma}$ is always smaller then $g_{A\gamma\gamma}$, and this results in a larger CP phase shift for $h-\gamma-\gamma$ interaction comparing to the $h-Z-\gamma$ interaction.

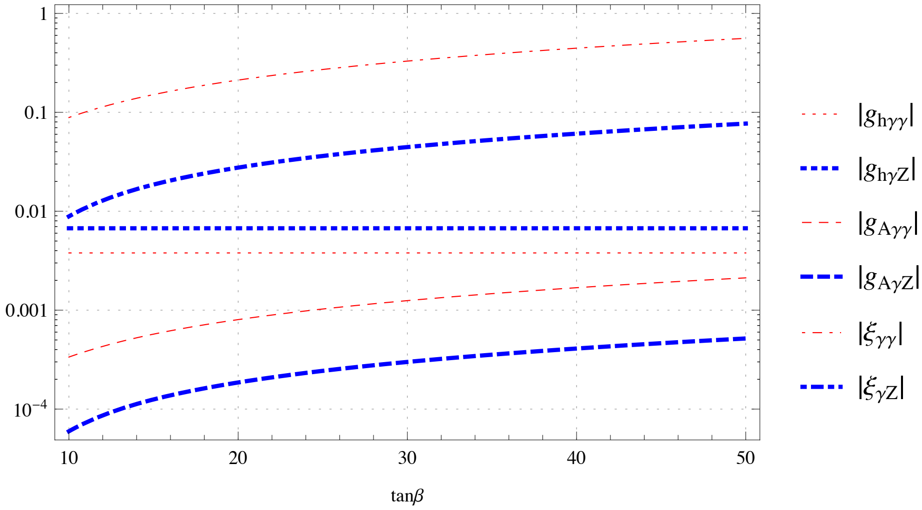

FIGURE 5.1: Magnitude of tffective HVV and AVV couplings as functions of $\tan(\beta)$ predicted in MSSM. (normalization is different from the definition in the first section).

On the other hand, both the couplings and phase shift depend on the relative phase in the couplings g_{HVV} and g_{AVV}. Fig. 5.2 shows the relative phase. For $\xi_{Z\gamma}$, the relative phase is about 0.86π for $\tan\beta > 30$, and then the sign of the CP phase shift is reversed, and the correlation coefficient is constructive. For $\xi_{\gamma\gamma}$, the relative phase is nearly 0.7π

for $\tan\beta > 30$, so the sign of CP phase shift is reversed and the magnitude also decreased a little, the correlation coefficient is destructive.

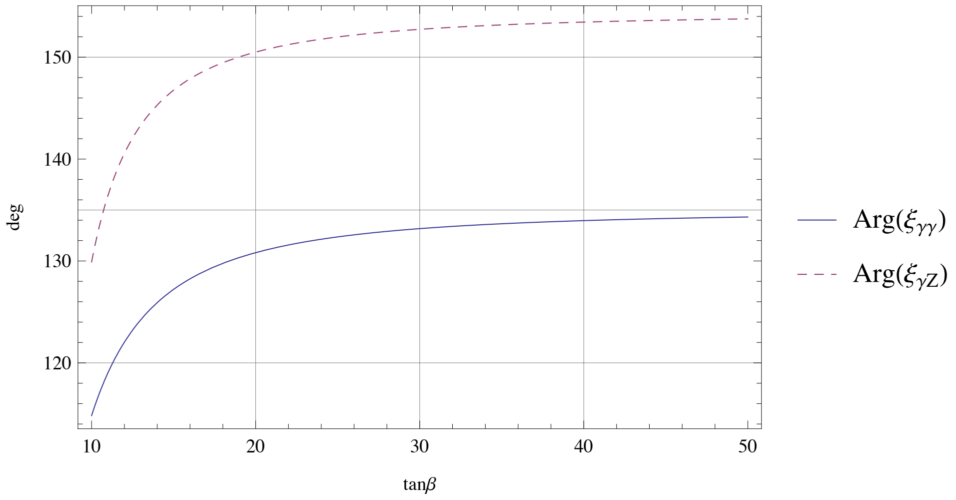

FIGURE 5.2: Relative phase of $\xi_{\gamma\gamma}$ and $\xi_{Z\gamma}$ as functions of $\tan(\beta)$ predicted in MSSM. (normalization is different from the definition in the first section).

Furthermore, the experimental sensitivity on the mixing parameter is $\Delta\bar{\epsilon}/|\xi_{VV}|$. Our results show that the process $h \to Z\gamma$ is more sensitive to the CP violation effects. However, the parameter $|\xi_{Z\gamma}|$ is smaller $|\xi_{\gamma\gamma}|$ by a factor of 10 in MSSM, see Fig. 5.1. So, in MSSM, the process $h \to \gamma\gamma$ provides a better experimental sensitivity on the mixing parameter.

For the process $pp \to h \to \tau^+\tau^-$ at LHC14 we study how well the CP property of the observed Higgs particle $h(125)$ could be measured by. The spin correlation in the $h \to \tau^+\tau^-$ decay is an ideal observable of measuring the CP composition of the Higgs particle. However the presence of at least two neutrinos in the final state makes the measurement challenge. We propose a novel method to reconstruct event by event the full kinematics of the $h \to \tau^+\tau^-$ decay proceses, that makes use of the impact parameter vectors of the τ^+ and τ^- decay pions and the probability distribution functions of the missing p_T vector and the angular separation ΔR between the charged π's. and the neutrinos. For the single charged π decay mode of both $\tau^+\tau^-$, we find an excellent agreement between the reconstructed and true kinematics in both the $\tau^+\tau^-(h)$ rest frame and $\pi^+\pi^-$ rest frames, by using the typical experimental resolutions of the LHC detectors. The sensitivity to the model independent mixing angle $\xi_{h\tau\tau}$ can reach 0.1 with an integrated luminosity $3\,\mathrm{ab}^{-1}$.

We also studied the CP violation effects in the production process of toponium in associated with the Higgs at ILC with $\sqrt{s} = 500\text{GeV}$. The Higgs particle can be produced by the emission of top or anti-top via the Yukawa interaction, or generated through the Gauge interactions between Higgs and vector bosons, Z or γ. CP violation effects can appear in both Yukawa and Gauge interactions. However observing the effects induced by Gauge interactions is rather hard. Because in one side, while the CP-even interaction between Higgs and Z appears at the tree-level (in SM), the CP-odd interaction between Higgs and Z and γ are induced at the 1-loop level, and hence suppressed by a factor of α_W. On the other hand, for the e^+e^- production with $\sqrt{s} = 500\text{GeV}$, the dominate contributions come from the emission processes, the contributions from the Gauge interactions can reach only a few percent [79]. Therefore, in our case the CP violation effects can be safely discussed without talking account of the gauge interactions.

Furthermore, at the center of mass energy $\sqrt{s} = 500\text{GeV}$, the toponia are produced at the near threshold region, therefore the P-wave toponia production rates are negligible. We analytically calculated the helicity amplitudes by neglecting contributions of this part. The eligibility of this approximation is proved by the numerical results based on the tree-level event generator. Furthermore by using the same approximation, the $ht\bar{t}$ production vertex from a virtual vector boson Z or γ can be modeled by a contact vertex operator, which is found to be an excellent approximation for understanding the physics. By assuming that the spins of top and anti-top are not altered by the QCD potential, *i.e.* the QCD potential is spin-independent, the possible toponium states that can be produced within above approximation are studied carefully. In our situation, the most important toponia are the ${}^1S_1$ and ${}^3S_3$ states. Either ${}^1S_1$ or ${}^3S_3$ state, the spin as well as the CP information are kept since the spin conservation, and then can be observed in principle by studying the subsequent decay products of toponia which in our paper are the lepton and anti-leptons.

However, the production rate of singlet toponium is found to be highly suppressed, and behaves just like the production of a P-wave toponia. This is because the radiation of a Higgs from a singlet toponium does not affect the dynamics, particularly in the spin degree of freedom, except for carrying away some energy. Therefore it is just like a production of a singlet toponium without Higgs, which must lie in the P-wave. This phenomena has also been check by using the tree-level event generator. In case of triplet toponium, the CP property of Higgs can affect the physics significantly. The pseudo-scalar component of Higgs can contribute the production rate of S-wave triplet toponium, but P-wave in the production of toponium and Higgs. Therefore it is suppressed by the factor β. Furthermore because it is P-wave between toponium and Higgs, the production of longitudinal polarized toponium is forbidden by the angular momentum conservation.

In order to avoid the reconstruction of top and/or anti-top rest frame for observing CP violation effects, we calculated the decay helicity amplitudes in the rest frame of the toponium which is directly accessible at ILC. Based on our analytical results, we find three completely independent CP observables, azimuthal angles of lepton and anti-leptons in the toponium rest frame as well as their sum, and checked by using the tree-level event generator. The nontrivial correlations come from the longitudinal-transverse interference for azimuthal angles of leptons, and transverse-transverse interference for their sum. These three observables are well defined at the ILC, because the rest frame of toponium can be reconstructed directly. The experimental sensitivities for these three observables are roughly estimated with an integrated luminosity $L = 4\ \text{ab}^{-1}$, and find to be small, roughly at the order of $\pi/2$. However the sensitivity can be enhanced by increasing the luminosity as the projected in Ref. [87]. The QCD-strong corrections, which are important at the near threshold region, are also studied with the approximation of spin-independent QCD-Coulomb potential. It is found the total cross section is enhanced by a factor of about 3, while the spin correlation is not affected.

Appendix A

MSSM Higgs sector with loop induced CP violation

A.1 The effective Lagrangian of $H \to \gamma\gamma$ and $H \to \gamma Z$ in the SM

The effective Lagrangian of $H \to \gamma\gamma$ and $H \to \gamma Z$ are given as follows:

$$\mathcal{L}_{\text{eff}} = -g^{\text{SM}}_{H\gamma\gamma} \frac{\alpha}{8\pi v} H F^{\mu\nu} F_{\mu\nu} - g^{\text{SM}}_{H\gamma Z} \frac{\alpha}{4\pi v} H F^{\mu\nu} Z_{\mu\nu}, \tag{A.1}$$

where $F_{\mu\nu}$ and $Z_{\mu\nu}$ are the fieldstrength of the photon and the Z boson and H is the CP-even Higgs field. The factor α is the fine-structure constant and v is vacuum expectation value (VEV) of the Higgs field. The effective couplings $g_{H\gamma\gamma}$, $g_{H\gamma Z}$ have no contributions from the tree-level diagram and the leading contribution comes from the one-loop diagrams mediated by the fermions and the W boson as follows:

$$g^{\text{SM}}_{H\gamma\gamma} = g^{(f)}_{H\gamma\gamma} + g^{(W)}_{H\gamma\gamma}, \tag{A.2}$$

$$g^{\text{SM}}_{H\gamma Z} = g^{(f)}_{H\gamma Z} + g^{(W)}_{H\gamma Z}, \tag{A.3}$$

where f's are the fermions of third generation. Here we assume the Yukawa couplings of the fermions in the first and second generation are zero because they are much smaller than the fermions in the third generation.

$$
\begin{aligned}
g^{(f)}_{H\gamma\gamma} &= -4 \sum_{f=t,b,\tau} Q_f^2 \frac{m_f^2}{m_H^2} \left[2 - \left(m_H^2 - 4m_f^2\right) C_0(0,0,m_H^2,m_f^2,m_f^2,m_f^2)\right], && \text{(A.4)}\\
g^{(W)}_{H\gamma\gamma} &= -12 \left(1 - \frac{2m_W^2}{m_H^2}\right) m_W^2 C_0(0,0,m_H^2,m_W^2,m_W^2,m_W^2) + \frac{12m_W^2}{m_H^2} + 2, && \text{(A.5)}\\
g^{(f)}_{H\gamma Z} &= -2 \sum_{f=t,b,\tau} \frac{N_c g_V^f Q_f}{c_W s_W} m_f^2 \Big[\frac{2m_Z^2}{(m_H^2 - m_Z^2)^2} \left[B_0(m_H^2,m_f^2,m_f^2) - B_0(m_Z^2,m_f^2,m_f^2)\right] \\
&\quad + \frac{1}{m_H^2 - m_Z^2} \left[(4m_f^2 - m_H^2 + m_Z^2) C_0(m_Z^2,0,m_H^2,m_f^2,m_f^2,m_f^2) + 2\right]\Big], && \text{(A.6)}\\
g^{(W)}_{H\gamma Z} &= \frac{1}{c_W s_W (m_H^2 - m_Z^2)^2} \Big[\left((2c_W^2 - 1)m_H^2 + 2(6c_W^2 - 1)c_W^2 m_Z^2\right) \\
&\quad \left((B_0(m_H^2,m_W^2,m_W^2) - B_0(m_Z^2,m_W^2,m_W^2) - 1)m_Z^2 + m_H^2\right) \\
&\quad + 2c_W^2 m_Z^2 \Big((1 - 6c_W^2)m_H^4 + 3(4c_W^4 + 4c_W^2 - 1)m_H^2 m_Z^2 \\
&\quad - 2(6c_W^4 + 3c_W^2 - 1)m_Z^4\Big) C_0(0,m_Z^2,m_H^2,m_W^2,m_W^2,m_W^2)\Big], && \text{(A.7)}
\end{aligned}
$$

where N_c is the color factor and $c_W = \cos(\theta_W)$, $s_W = \sin(\theta_W)$, where θ_W is the Weinberg angle. In our notation the Z-boson interaction with fermions ($f = t, b, \tau$) which have electric charge Q_f are given by

$$
\begin{aligned}
\mathcal{L}^Z_{\text{int}} &= g_Z \bar{f} \gamma^\mu \left[\frac{g_V^f + g_A^f}{2} P_R + \frac{g_V^f - g_A^f}{2} P_L\right] f Z_\mu, && \text{(A.8)}\\
g_V^f &= T^3 - 2\sin^2(\theta_W) Q_f, && \text{(A.9)}\\
g_A^f &= -T^3, && \text{(A.10)}
\end{aligned}
$$

where $T^3 = 1/2$ for up type quarks and $T^3 = -1/2$ for down type quarks and charged leptons.

The decay width of the Higgs boson into $\gamma\gamma$ and γZ are

$$
\begin{aligned}
\Gamma(H \to \gamma\gamma) &= \frac{\alpha^2 m_H^3}{256\pi^3 v^2} |g^{\text{SM}}_{H\gamma\gamma}|^2, && \text{(A.11)}\\
\Gamma(H \to \gamma Z) &= \frac{\alpha^2 m_H^3}{128\pi^3 v^2} \left(1 - \frac{m_Z^2}{m_H^2}\right)^3 |g^{\text{SM}}_{H\gamma Z}|^2. && \text{(A.12)}
\end{aligned}
$$

A.2 The effective Lagrangian of $H \to \gamma\gamma,\ H \to \gamma Z,\ A \to \gamma\gamma$ and $A \to \gamma Z$ in the two Higgs doublet model with decoupling limit

The effective Lagrangian in the two Higgs doublet model (2HDM) are given as follows:

$$\begin{aligned}\mathcal{L}_{\rm eff} &= -g^{\rm 2HDM}_{H\gamma\gamma}\frac{\alpha}{8\pi v}HF^{\mu\nu}F_{\mu\nu} - g^{\rm 2HDM}_{H\gamma Z}\frac{\alpha}{4\pi v}HF^{\mu\nu}Z_{\mu\nu} && (A.13)\\ &\quad -g^{\rm 2HDM}_{A\gamma\gamma}\frac{\alpha}{8\pi v}AF^{\mu\nu}\tilde{F}_{\mu\nu} - g^{\rm 2HDM}_{A\gamma Z}\frac{\alpha}{4\pi v}AF^{\mu\nu}\tilde{Z}_{\mu\nu}, && (A.14)\end{aligned}$$

where A is the CP-odd Higgs field and $\tilde{F}_{\mu\nu} = \epsilon_{\alpha\beta\mu\nu}F^{\alpha\beta}$, $\tilde{Z}_{\mu\nu} = \epsilon_{\mu\nu\rho\sigma}Z^{\rho\sigma}$. Here $\epsilon_{\mu\nu\rho\sigma}$ is the totally antisymmetric tensor which satisfies $\epsilon_{0123} = -1$. Assuming the decoupling limit, the effective couplings $g^{\rm 2HDM}_{H\gamma\gamma}$ and $g^{\rm 2HDM}_{H\gamma Z}$ are same as ones of the Standard Model.

$$\begin{aligned} g^{\rm 2HDM}_{H\gamma\gamma} &= g^{\rm SM}_{H\gamma\gamma}, && (A.15)\\ g^{\rm 2HDM}_{H\gamma Z} &= g^{\rm SM}_{H\gamma Z}. && (A.16)\end{aligned}$$

The effective couplings $g^{\rm 2HDM}_{A\gamma\gamma}$ and $g^{\rm 2HDM}_{A\gamma Z}$ have no contributions at the tree level and the leading contribution comes from the one-loop diagrams mediated by fermions.

$$\begin{aligned} g^{\rm 2HDM}_{A\gamma\gamma} &= g^{(f)}_{A\gamma\gamma}, && (A.17)\\ g^{\rm 2HDM}_{A\gamma Z} &= g^{(f)}_{A\gamma Z}, && (A.18)\end{aligned}$$

where f's are the fermions in the third generation. The effective couplings can be obtained as follows:

$$\begin{aligned} g^{(f)}_{A\gamma\gamma} &= 4\sum_f N_c Q_f^2 Y_\beta m_f^2 C_0(0,0,m_A^2,m_f^2,m_f^2,m_f^2), && (A.19)\\ g^{(f)}_{A\gamma Z} &= 2\sum_f N_c Q_f \frac{g_V^f}{c_W s_W} Y_\beta m_f^2 C_0(0,m_Z^2,m_A^2,m_f^2,m_f^2,m_f^2), && (A.20)\end{aligned}$$

where, in the type-II 2HDM, $Y_\beta = \cot\beta$ for up type quarks, $Y_\beta = \tan\beta$ for down type quarks and charged leptons.

The decay width of the processes $A \to \gamma\gamma$ and $A \to \gamma Z$ are

$$\Gamma(A \to \gamma\gamma) = \frac{\alpha^2 m_A^3}{256\pi^3 v^2}|g_{A\gamma\gamma}^{\mathrm{2HDM}}|^2, \tag{A.21}$$

$$\Gamma(A \to \gamma Z) = \frac{\alpha^2 m_A^3}{128\pi^3 v^2}\left(1 - \frac{m_Z^2}{m_A^2}\right)^3 |g_{A\gamma Z}^{\mathrm{2HDM}}|^2. \tag{A.22}$$

A.3 The effective Lagrangian of $H \to \gamma\gamma,\ H \to \gamma Z,\ A \to \gamma\gamma$ and $A \to \gamma Z$ in the MSSM with decoupling limit

The effective Lagrangian of in the MSSM are given as follows:

$$\mathcal{L}_{\mathrm{eff}} = -g_{H\gamma\gamma}^{\mathrm{MSSM}}\frac{\alpha}{8\pi v}HF^{\mu\nu}F_{\mu\nu} - g_{H\gamma Z}^{\mathrm{MSSM}}\frac{\alpha}{4\pi v}HF^{\mu\nu}Z_{\mu\nu} \tag{A.23}$$

$$-g_{A\gamma\gamma}^{\mathrm{MSSM}}\frac{\alpha}{8\pi v}AF^{\mu\nu}\tilde{F}_{\mu\nu} - g_{A\gamma Z}^{\mathrm{MSSM}}\frac{\alpha}{4\pi v}AF^{\mu\nu}\tilde{Z}_{\mu\nu}. \tag{A.24}$$

Assuming the decoupling limit, the effective couplings $g_{H\gamma\gamma}^{\mathrm{MSSM}}$ and $g_{H\gamma Z}^{\mathrm{MSSM}}$ are same as those in the Standard Model.

$$g_{H\gamma\gamma}^{\mathrm{MSSM}} = g_{H\gamma\gamma}^{\mathrm{SM}}, \tag{A.25}$$

$$g_{H\gamma Z}^{\mathrm{MSSM}} = g_{H\gamma Z}^{\mathrm{SM}}. \tag{A.26}$$

We have another contributions to the effective couplings $g_{A\gamma\gamma}$ and $g_{A\gamma Z}$ from one-loop diagrams of charginos other than one-loop diagrams of the fermions. Thus, the effective couplings are sum of the contributions induced by one-loop diagrams of the fermions and charginos as follows:

$$g_{A\gamma\gamma}^{\mathrm{MSSM}} = g_{A\gamma\gamma}^{(f)} + g_{A\gamma\gamma}^{(\tilde{\chi}^{\pm})}, \tag{A.27}$$

$$g_{A\gamma Z}^{\mathrm{MSSM}} = g_{A\gamma Z}^{(f)} + g_{A\gamma Z}^{(\tilde{\chi}^{\pm})}. \tag{A.28}$$

The effective couplings are given as follows:

$$\begin{aligned}
g^{(\tilde{\chi}^\pm)}_{A\gamma\gamma} &= 2gv\sum_{i=1,2} m_{\tilde{\chi}^\pm_i} C_0(0,0,m_A^2, m^2_{\tilde{\chi}^\pm_i}, m^2_{\tilde{\chi}^\pm_i}, m^2_{\tilde{\chi}^\pm_i})(g^L_{Aii} - g^R_{Aii}), && \text{(A.29)}\\
g^{(\tilde{\chi}^\pm)}_{A\gamma Z} &= \frac{gv}{c_W s_W (m_A^2 - m_Z^2)^2} \sum_{i,j=1,2} m_{\tilde{\chi}^\pm_i} G^{AZ}_{i,j} \Big[\\
&\left(m_A^2(m_A^2 - m_Z^2) + 2m_Z^2(m^2_{\tilde{\chi}^\pm_i} - m^2_{\tilde{\chi}^\pm_j}) \right) C_0(m_A^2, 0, m_Z^2, m^2_{\tilde{\chi}^\pm_i}, m^2_{\tilde{\chi}^\pm_j}, m^2_{\tilde{\chi}^\pm_i}) \\
&+ \left(m_Z^2(m_Z^2 - m_A^2) + 2m_Z^2(m^2_{\tilde{\chi}^\pm_i} - m^2_{\tilde{\chi}^\pm_j}) \right) C_0(m_A^2, 0, m_Z^2, m^2_{\tilde{\chi}^\pm_j}, m^2_{\tilde{\chi}^\pm_i}, m^2_{\tilde{\chi}^\pm_j}) \\
&+2m_Z^2 \left(B_0(m_Z^2, m^2_{\tilde{\chi}^\pm_j}, m^2_{\tilde{\chi}^\pm_j}) - B_0(m_Z^2, m^2_{\tilde{\chi}^\pm_i}, m^2_{\tilde{\chi}^\pm_i}) \right) \Big]. && \text{(A.30)}
\end{aligned}$$

The interaction Lagrangian in terms of A-$\tilde{\chi}^+$-$\tilde{\chi}^-$ and Z-$\tilde{\chi}^+$-$\tilde{\chi}^-$ are

$$\mathcal{L}_{\text{int}} = -igA\overline{\tilde{\chi}^+_i}\left[g^L_{Aji}P_L + g^R_{Aji}P_R\right]\tilde{\chi}^+_j - g_Z\overline{\tilde{\chi}^+_i}\gamma^\mu\left[g^R_{Zij}P_L + g^L_{Zij}P_R\right]\tilde{\chi}_j Z_\mu + \text{H.c.} \qquad \text{(A.31)}$$

Here, we use the following abbriviations:

$$\begin{aligned}
G^{AZ}_{i,j} &= -g^L_{Aji}g^L_{Zji} - g^L_{Aij}g^R_{Zij} + g^R_{Aij}g^L_{Zij} + g^R_{Aji}g^R_{Zji}, && \text{(A.32)}\\
G^{ZZ}_{i,j,k} &= g^L_{Aji}g^Z_{Zki}g^L_{Zjk} + g^L_{Aij}g^R_{Zik}g^R_{Zkj} - g^R_{Aij}g^L_{Zik}g^L_{Zkj} - g^R_{Aji}g^R_{Zki}g^R_{Zjk}, && \text{(A.33)}\\
g^L_{Aij} &= -Q^*_{j,i}s_\beta - S^*_{j,i}c_\beta, && \text{(A.34)}\\
g^R_{Aij} &= Q_{i,j}s_\beta + S_{i,j}c_\beta, && \text{(A.35)}\\
-g^R_{Zji} &= U_{i,1}U^*_{j,1} + \frac{1}{2}U_{i,2}U^*_{j,2} - \delta_{i,j}s_W^2, && \text{(A.36)}\\
-g^L_{Zij} &= V_{i,1}V^*_{j,1} + \frac{1}{2}V_{i,2}V^*_{j,2} - \delta_{i,j}s_W^2, && \text{(A.37)}\\
Q_{i,j} &= \frac{1}{\sqrt{2}}U_{i,2}V_{j,1}, && \text{(A.38)}\\
S_{i,j} &= \frac{1}{\sqrt{2}}U_{i,1}V_{j,2}, && \text{(A.39)}
\end{aligned}$$

where $U_{i,j}, V_{i,j}$ $(i,j = 1,2)$ are the elements of unitary matrices which diagonalize the mass matrices of charginos.

Appendix B

Spinor and vector wave functions

B.0.1 Spinor wave functions in Dirac Representation

For completeness we give our convientions for the Spinor wave functions in the Dirac Representation. In the Dirac representation, the Dirac matrix are given as follows

$$\gamma_D^0 = \begin{pmatrix} 1 & 0 \\ 0 & -1 \end{pmatrix} \,, \quad \vec{\gamma}_D = \begin{pmatrix} 0 & \vec{\sigma} \\ -\vec{\sigma} & 0 \end{pmatrix} \,. \tag{B.1}$$

The free solutions of the Dirac equation in the Dirac represention are

$$u_D(\vec{p}_1, s) = \begin{pmatrix} \xi_s \\ \dfrac{\vec{\sigma}\cdot\vec{p}_1}{E+m}\xi_s \end{pmatrix} \,, \quad v_D(\vec{p}_2, r) = \begin{pmatrix} r\dfrac{\vec{\sigma}\cdot\vec{p}_2}{E+m}\eta_{-r} \\ r\eta_{-r} \end{pmatrix} \,, \tag{B.2}$$

where ξ_s and η_r are eigenstates of the helicity operators $\vec{\sigma}\cdot\hat{\vec{p}}_1$ and $\vec{\sigma}\cdot\hat{\vec{p}}_2$, respectively. For completeness we also give the helicity eigenstates as follows

$$\xi_+ = \begin{pmatrix} \cos(\theta/2) \\ e^{i\phi}\sin(\theta/2) \end{pmatrix} \,, \quad \xi_- = \begin{pmatrix} -e^{-i\phi}\sin(\theta/2) \\ \cos(\theta/2) \end{pmatrix} \,. \tag{B.3}$$

The spinor wave functions and Dirac matrix in the Dirac representation are related to the ones in the Chiral representation by following unitary transformation

$$\psi_D = U_D \psi U_D^{-1} \,, \quad \gamma_D^\mu = U_D \gamma_C^\mu U_D^{-1} \,, \quad U_D = \frac{1}{\sqrt{2}} \begin{pmatrix} 1 & 1 \\ -1 & 1 \end{pmatrix} \,. \tag{B.4}$$

B.0.2 Vector wave functions and Wigner-D functions

The helicity wave functions polarized along the direction $\vec{n} = (\sin\theta\cos\phi,\, \sin\theta\sin\phi,\, \cos\theta)$ for vector particles in the rest frame are defined as follows

$$\epsilon(\vec{n}, \lambda = \pm 1) = \frac{1}{\sqrt{2}}(0,\, -\lambda\cos\theta\cos\phi + i\sin\phi,\, -\lambda\cos\theta\sin\phi - i\cos\phi,\, \lambda\sin\theta), \tag{B.5}$$

$$\epsilon(\vec{n}, \lambda = 0) = (0,\, \sin\theta\cos\phi,\, \sin\theta\sin\phi,\, \cos\theta) \tag{B.6}$$

The Wigner-D functions for spin-1 particle is defined as follows

$$\vec{\epsilon}(\vec{n}, \lambda') = \sum_{\lambda=0,\pm1} D^{J=1}_{\lambda\lambda'}(\theta,\phi)\, \vec{\epsilon}(\vec{0}, \lambda) \tag{B.7}$$

and it's inverse

$$\vec{\epsilon}(\vec{0}, \lambda) = \sum_{\lambda''=0,\pm1} \widetilde{D}^{J=1}_{\lambda''\lambda}(\theta,\phi)\, \vec{\epsilon}(\vec{n}, \lambda'') \tag{B.8}$$

and following relation holds

$$\widetilde{D}^{J=1}_{\lambda'\lambda}(\theta,\phi) = (D^{J=1}_{\lambda\lambda'}(\theta,\phi))^* \tag{B.9}$$

Based on these definitions we also have

$$\vec{\epsilon}^{\,*}(\vec{n}, \lambda') \cdot \vec{\epsilon}(\vec{0}, \lambda) = \widetilde{D}^{J=1}_{\lambda'\lambda}(\theta,\phi) \tag{B.10}$$

$$\vec{\epsilon}^{\,*}(\vec{0}, \lambda) \cdot \vec{\epsilon}(\vec{n}, \lambda') = D^{J=1}_{\lambda\lambda'}(\theta,\phi) \tag{B.11}$$

Bibliography

[1] E. Noether, *Invariante Variationsprobleme*, Nachr. D. König. Gesellsch. D. Wiss. Zu Göttingen, Math-phys. Klasse 235(1918).

[2] W. Pauli, *Relativistic Field Theories of Elementary Particles*, Rev. Mod. Phys. **13**, 203(1941).

[3] C. N. Yang, R. L. Mills, *Conservation of Isotopic Spin and Isotopic Gauge Invariance*, Phys. Rev. **96**, 191(1954).

[4] L. Cooper, *Bound Electron Pairs in a Degenerate Fermi Gas*, Phys. Rev. **104**, 1189(1956).

[5] J. Bardeen, L. N. Cooper, and J. R. Schrieffer, *Microscopic Theory of Superconductivity*, Phys. Rev. **106**, 162(1957).

[6] J. Bardeen, L. N. Cooper, and J. R. Schrieffer, *Theory of Superconductivity*, Phys. Rev. **108**, 1175(1957).

[7] F. Englert and R. Brout, *Broken Symmetry and the Mass of Gauge Vector Mesons* , Phys. Rev. Lett. **13**, 321(1964).

[8] P. W. Higgs, *Broken Symmetries and the Masses of Gauge Bosons*, Phys. Rev. Lett. **13**, 508(1964).

[9] G. S. Guralnik, C. R. Hagen, and T. W. B. Kibble, *Global Conservation Laws and Massless Particles*, Phys. Rev. Lett. *13*, 585(1964).

[10] T. D. Lee and C. N. Yang, *Question of Parity Conservation in Weak Interactions*, Phys. Rev. **104**, 254(1957); Erratum Phys. Rev. **106**, 1371 (1957).

[11] C. S. Wu, E. Ambler, R. W. Hayward, D. D. Hoppes, and R. P. Hudson, *Experimental Test of Parity Conservation in Beta Decay*, Phys. Rev. **105**, 1413(1957).

[12] W. A. Bardeen, *Anomalous Ward Identities in Spinor Field Theories*, Phys. Rev. **184**, 1848(1969).

[13] M. Kobayashi and T. Maskawa, *CP-Violation in the Renormalizable Theory of Weak Interaction*, Prog. Theor. Phys. **49**, 652(1973).

[14] A. D. Sakharov, *Violation of CP invariance, C asymmetry, and baryon asymmetry of the universe*, JETP, **5**, 24(1967).

[15] J. Schwinger, *The Theory of Quantized Fields. I*, Phys. Rev. **82**, 914(1951).

[16] G. Aad *et al.*. (ATLAS Collaboration), *Observation of a new particle in the search for the Standard Model Higgs boson with the ATLAS detector at the LHC*, Phys. Lett. **B716**, 1(2012).

[17] S. Chatrchyan *et al.*(CMS Collaboration), *Observation of a new boson at a mass of 125 GeV with the CMS experiment at the LHC*, Phys. Lett. **B716**, 30 (2012).

[18] S. Bolognesi, Y. Gao, A. V. Gritsan, K. Melnikov, M. Schulze, *et al.*, *On the spin and parity of a single-produced resonance at the LHC*, Phys. Rev. **D86**, 095031(2012).

[19] G. Aad *et al.*. (ATLAS Collaboration), *Evidence for the spin-0 nature of the Higgs boson using ATLAS data*, Phys. Lett. **B726**, 120(2013).

[20] S. Chatrchyan *et al.*(CMS Collaboration), *Study of the Mass and Spin-Parity of the Higgs Boson Candidate via Its Decays to Z Boson Pairs*, Phys. Rev. Lett. **110**, 081803(2013); Erratum Phys. Rev. Lett. **110**, 189901(2013).

[21] S. Chatrchyan *et al.*(CMS Collaboration), *Measurement of the properties of a Higgs boson in the four-lepton final state*, Phys. Rev. **D89**, 092007(2014).

[22] E. Accomando *et al.*, *CP Studies and Non-Standard Higgs Physics*, arXiv:hep-ph/0608079.

[23] Y. Chen, A. Falkowski, I. Low, R. V.-Morales, *New Observables for CP Violation in Higgs Decays*, Phys. Rev. **D90**, 113006(2014).

[24] Y. Chen, R. Harnik, R. V.-Morales, *Probing the Higgs Couplings to Photons in* $h \to 4\ell$ *at the LHC*, Phys. Rev. Lett. **113**, 191801 (2014).

[25] W. Bernreuther, P. Gonzalez, M. Wiebusch, *Pseudoscalar Higgs Bosons at the LHC: Production and Decays into Electroweak Gauge Bosons Revisited*, Eur. Phys. J. **C69**, 31(2010).

[26] T. Plehn, D. Rainwater, and D. Zeppenfeld, *Determining the Structure of Higgs Couplings at the CERN Large Hadron Collider*, Phys. Rev. Lett. **88**, 051801(2002).

[27] K. Odagiri, J. High Energy Phys. **03**, 009(2003).

[28] T. Figy and D. Zeppenfeld, Phys. Lett. **B519**, 297(2004).

[29] C. Englert, D. Goncalves-Netto, K. Mawatari, and T. Plehn, J. High Energy Phys. **01**, 148(2013).

[30] P. Artoisenet *et al.*, J. High Energy Phys. **11**, 043(2013).

[31] B. Grzadkowski and J. Gunion, *Using Decay Angle Correlations to Detect CP Violation in the Neutral Higgs Sector*, Phys. Lett. **B350**, 218 (1995).

[32] M. J. Dolan, P. Harris, M. Jankowiak, M. Spannowsky, *Constraining CP-violating Higgs Sectors at the LHC using gluon fusion*, Phys. Rev. **D90**, 073008 (2014).

[33] F. Campanario, M. Kubocz, and D. Zeppenfeld, Phys.Rev. **D84**, 095025 (2011).

[34] F. Campanario and M. Kubocz, *Higgs boson CP-properties of the gluonic contributions in Higgs plus three jet production via gluon fusion at the LHC*, arXiv:1402.1154.

[35] M. Voloshin, *CP Violation in Higgs Diphoton Decay in Models with Vectorlike Heavy Fermions*, Phys. Rev. **D86**, 093016 (2012).

[36] F. Bishara, Y. Grossman, R. Harnik, D. J. Robinson, J. Shu and J. Zupan, *Probing CP Violation in $h \to \gamma\gamma$ with Converted Photons*, J. High Energy Phys. **04**, 084(2014).

[37] M. A. Shifman, A. I. Vainshtein, M. B. Voloshin, V. I. Zakharov, *Low-Energy Theorems for Higgs Boson Couplings to Photons*, Sov. J. Nucl.Phys. **30**, 711(1979).

[38] L. Bergström, G. Hulth, *Induced Higgs couplings to neutral bosons in e^+e^- collisions*, Nucl. Phys. **B259**, 137(1985).

[39] J. F. Gunion, G. L. Kane, Jose Wudka, *Search techniques for charged and neutral intermediate-mass Higgs bosons*, Nucl. Phys. **B299**, 231(1988).

[40] A. Y. Korchin, V. A. Kovalchuk, *Polarization effects in the Higgs boson decay to gamma Z and test of CP and CPT symmetries*, Phys. Rev. **D88**, 036009(2013).

[41] G. Aad *et al.*(ATLAS Collaboration), *Search for the Standard Model Higgs boson in the diphoton decay channel with* $4.9fb^{-1}$ *of pp collisions at* $\sqrt{s} = 7\text{TeV}$ *with ATLAS*, Phys. Rev. Lett. **108**, 111803 (2012).

[42] S. Chatrchyan *et al.*(CMS Collaboration), *Search for the standard model Higgs boson decaying into two photons in pp collisions at* $\sqrt{s} = 7\text{TeV}$, Phys.Lett. **B710**, 403 (2012).

[43] W. N. Cottingham and I. B. Whittingham, *Signals of Higgs sector CP violation in neutral Higgs boson decays*, Phys. Rev. **D52**, 539 (1995).

[44] ATLAS Collaboration, *Measurements of the properties of the Higgs-like boson in the four lepton decay channel with the ATLAS detector*, Tech. Rep. **ATLAS-CONF-2013-013** (CERN, 2013).

[45] S. Chatrchyan *et al.*(CMS Collaboration), *Study of the Mass and Spin-Parity of the Higgs Boson Candidate via Its Decays to Z Boson Pairs*, Phys. Rev. Lett. **110**, 081803 (2013).

[46] H. Murayama, I. Watanabe and K. Hagiwara, *HELAS: HELicity Amplitude Subroutines for Feynman diagram evaluations*, KEK Report No. 91-11, 1992.

[47] D. McKeen, M. Pospelov, and A. Ritz, *Modified Higgs branching ratios versus CP and lepton flavor violation*, Phys.Rev. **D86**, 113004 (2012).

[48] J. Shu and Y. Zhang, *Impact of a CP-Violating Higgs Sector: From LHC to Baryogenesis*, Phys. Rev. Lett. **111**, 091801 (2013).

[49] W.-Y. Keung, I. Low, and J. Shu, *Landau-Yang Theorem and Decays of a Z' Boson into Two Z Bosons*, Phys. Rev. Lett. **101**, 091802 (2008).

[50] Q.-H. Cao, C. Jackson, W.-Y. Keung, I. Low, *The Higgs Mechanism and Loop-induced Decays of a Scalar into Two Z Bosons*, Phys. Rev. **D81**, 015010 (2010).

[51] Y.-S. Tsai, *Pair production and bremsstrahlung of charged leptons*, Rev. Mod. Phys. **46**, 815 (1974); Erratum: *Pair production and bremsstrahlung of charged leptons*, Rev. Mod. Phys. **49**, 421 (1977).

[52] S. Drell and J. Walecka, Ann. Phys. **28**, 18(1964).

[53] ATLAS Collaboration, *CSC NOTE - PHOTON CONVERSIONS IN ATLAS*, ATLAS NOTE. (CERN, Geneva, 2008).

[54] ATLAS Collaboration, *Expected photon performance in the ATLAS experiment*, Tech. Rep. ATL-PHYS-PUB-2011-007 (CERN, Geneva, 2011).

[55] ATLAS Collaboration, *Measurements of the properties of the Higgs-like boson in the two photon decay channel with the ATLAS detector using* $25\,\mathrm{fb}^{-1}$ *of proton-proton collision data*, Tech. Rep. ATLAS-CONF-2013-012 (CERN, Geneva, 2013).

[56] CMS Collaboration, *Updated measurements of the Higgs boson at 125 GeV in the two photon decay channel*, Tech. Rep. CMS-PAS-HIG-13-001 (CERN, Geneva, 2013).

[57] J. C. Slater, *Atomic Radii in Crystals*, J. Chem. Phys. **41**, 3199 (1964).

[58] C. N. Yang, *Selection Rules for the Dematerialization of a Particle into Two Photons*, Phys. Rev. **77**, 242 (1950).

[59] C. N. Yang, *Possible Experimental Determination of Whether the Neutral Meson is Scalar or Pseudoscalar*, Phys. Rev. **77**, 722 (1950).

[60] N. M. Kroll and W. Wada, *Internal Pair Production Associated with the Emission of High-Energy Gamma Rays*, Phys. Rev. **98**, 1355 (1955).

[61] G. Aad *et al.*(ATLAS Collaboration), *The ATLAS Inner Detector commissioning and calibration*, Eur. Phys. J. **C70**, 787(2010).

[62] J. Alwall, M. Herquet, F. Maltoni, O. Mattelaer, and T. Stelzer, *MadGraph 5 : Going Beyond*, J. High Energy Phys. **06**, 128(2011).

[63] P. Artoisenet, P. Artoisenet, P. de Aquino, F. Demartin, R. Frederix *et al.*, A framework for Higgs characterisation, J. High Energy Phys. **11**, 043(2013).

[64] J. Pumplin, D. Stump, J. Huston, H. Lai, P. M. Nadolsky, *et al.*., *New Generation of Parton Distributions with Uncertainties from Global QCD Analysis*, J. High Energy Phys. **07**, 012(2002).

[65] T. Sjostrand, S. Mrenna, and P. Z. Skands, *PYTHIA 6.4 Physics and Manual*, J. High Energy Phys. **05**, 026(2006) .

[66] T. Sjöstrand, S. Mrenna and P. Skands, J. High Energy Phys., **05**, 026(2006), Comput. Phys. Comm. **178**, 852(2008).

[67] J. de Favereau, *et al.*, *DELPHES3, A modular framework for fast simulation of a generic collider experiment*, J. High Energy Phys., **02**, 057(2014).

[68] M. Cacciari, G. P. Salam and G. Soyez, *FastJet user manual*, Eur. Phys. J. C **72**, 1896(2012).

[69] J. Brod, U. Haisch, and J. Zupan, *Constraints on CP-violating Higgs couplings to the third generation*, JHEP **1311**, 180 (2013).

[70] J. R. Dell'Aquila and C. A. Nelson, *Use of the $\bar{\tau}\tau$ or $t\bar{t}$ decay mode to distinguish an intermediate mass Higgs boson from a technipion*, Nucl. Phys. **B320**, 86 (1989).

[71] J. R. Dell'Aquila and C. A. Nelson, *CP determination for new spin zero mesons by the $\bar{\tau}\tau$ decay mode*, Nucl. Phys. **B320**, 61 (1989).

[72] G. Bower, T. Pierzchala, Z. Was, and M. Worek, *Measuring the Higgs boson's parity using $\tau \to \rho\nu$*, Phys. Lett. **B543**, 227 (2002).

[73] K. Desch, Z. Was, and M. Worek, Measuring the Higgs boson parity at a Linear Collider using the tau impact parameter and $\tau \to \rho\nu$ decay, Eur. Phys. J. **C29**, 491 (2003).

[74] R. Harnik, A. Martin, T. Okui, R. Primulando, and F. Yu, *Measuring CP Violation in $h \to \tau^+\tau^-$ at Colliders*, Phys. Rev. **D88**, 076009 (2013).

[75] S. Berge, W. Bernreuther, and J. Ziethe, *Determining the CP Parity of Higgs Bosons via Their τ Decay Channels at the Large Hadron Collider*, Phys. Rev. Lett. **100**, 171605 (2008).

[76] S. Berge and W. Bernreuther, *Determining the CP parity of Higgs bosons at the LHC in the τ to 1-prong decay channels*, Phys. Lett. **B671**, 470 (2009).

[77] S. Berge, W. Bernreuther, B. Niepelt, and H. Spiesberger, *How to pin down the CP quantum numbers of a Higgs boson in its tau decays at the LHC*, Phys. Rev. **D84**, 116003 (2011).

[78] S. Berge, W. Bernreuther, and H. Spiesberger, *Higgs CP properties using the tau decay modes at the ILC*, Phys. Lett. **B727**, 488(2013).

[79] P. S. Bhupal Dev, A. Djouadi, R. M. Godbole, M. M. Mühlleitner, and S. D. Rindani, *Determining the CP Properties of the Higgs Boson*, Phys. Rev. Lett. **100**, 051801(2008).

[80] R. M. Godbole, P.S. Bhupal Dev, A. Djouadi, M. M. Mühlleitner, S.D. Rindani, *Probing CP properties of the Higgs Boson via* $e^+e^- \to t\bar{t}\Phi$, arXiv:0710.2669, ECONF C0705302:TOP08,2007.

[81] R. M. Godbole, C. Hangst, M. Mühlleitner, S. D. Rindani, P. Sharma, *Model-independent analysis of Higgs spin and CP properties in the process* $e^+e^- \to t\bar{t}\Phi$, Eur. Phys. J. **C 71**, 1681(2011).

[82] E. E. Salpeter and H. A. Bethe, *A Relativistic Equation for Bound-State Problems*, Phys. Rev. **84**, 1232.(1951).

[83] B. A. Lippmann and J. Schwinger, *Variational Principles for Scattering Processes*, Phys. Rev. **79**, 469(1950).

[84] M. Jeżabek, J. H. Kühn and T. Teubner, *Momentum distributions in* $t\bar{t}$ *production and decay near threshold*, Z. Phy. **C56**, 653(1992).

[85] C. Farrell and A. H. Hoang, *Next-to-leading-logarithmic QCD corrections to the cross section* $\sigma(e^+e^- \to t\bar{t}H)$ *at* 500GeV, Phys. Rev. **D74**, 014008(2006).

[86] R. Yonamine, K. Ikematsu, T. Tanabe, K. Fujii, Y. Kiyo, Y. Sumino, and H. Yokoya *Measuring the top Yukawa coupling at the ILC at* $\sqrt{s} = 500$GeV, Phys. Rev. **D 84**, 014033(2011).

[87] T. Barklow, J. Brau, K. Fujii, J. Gao, J. List, N. Walker, K. Yokoya, *ILC Operating Scenarios*, arXiv:1506.07830.

[88] K. Hagiwara, T. Li, K. Mawatari, and J. Nakamura, *TauDecay: a library to simulate polarized tau decays via FeynRules and MadGraph5*, Eur. Phys. J. **C73**, 2489(2013).

[89] ATLAS Collaboration, *Evidence for the Higgs-boson Yukawa coupling to tau leptons with the ATLAS detector*, J. High Energy Phys. **04**, 117(2015).

[90] A. Elagin *et al.*, *A new mass reconstruction technique for resonances decaying to di-tau*, Nucl. Instrum. Meth. **A 654**, 481(2011).

[91] CMS Collaboration, *Evidence for the 125 GeV Higgs boson decaying to a pair of tau leptons*, J. High Energy Phys. **05**, 104(2014).

[92] CMS Collaboration, *Missing transverse energy performance of the CMS detector*, JINST, **6**, 09001(2011).

[93] M. R. Buckley and D, Goncalves, *Boosting the Direct CP Measurement of the Higgs-Top Coupling*, arXiv:1507.07926

[94] K. A. Olive *et al.* (Particle Data Group), Chin. Phys. **C38**, 090001(2014).